A Collaborative Optimization Approach to Improve the Design and Deployment of Satellite Constellations

A Thesis

Presented to the Academic Faculty

By

Irene Arianti Budianto

In Partial Fulfillment of the Requirements for the Degree of Doctor of Philosophy in the School of Aerospace Engineering

Georgia Institute of Technology

September 2000

For from Him, and through Him, and to Him are all things.
To Him be the glory forever.
Amen.

Romans 11:36

ACKNOWLEDGEMENTS

I am blessed to have many to thank for helping me through my journey up to this point. I begin with my advisor, Dr. John R. Olds, who helped make my career at Georgia Tech an interesting and fruitful one. I will always be grateful for all the learning opportunities he has provided me. I would like to recognize my mentor from the U.S. Air Force Research Laboratory, Dr. Patrick McDaniel, for the support and encouragement he has shown me in the past five years that I have known him. Thanks for believing in me! I would add Prof. Panagiotis Tsiotras for his insights as a member of my thesis committee and Dr. Amy Pritchett for making time for me in the midst of her busy schedule. I also appreciate all the guidance, inspirations, and enthusiasms I've received from Dr. Todd Mosher. I couldn't have made it without all of your help!

This research work would not be possible without the following: the U. S. Air Force Research Laboratory's Palace Knight program's financial support; the valuable and pertinent experiences of Thomas Lang and Christopher Kobel, which they generously shared with me.

I'm grateful for the extended SSDL family. I really have enjoyed working with you guys! Laura Ledsinger, my cubicle-mate for 3 years, thanks for putting up with me (I know how hard that can be sometimes). I really cherish our friendship. Thanks also to John Bradford, Dave McCormick, and Dave Way. We've been through a lot together, and I don't know what I would've done without you guys. I've really enjoyed getting to know y'all, and Heather, Danielle, Lilian, and Lucy, too! To the other SSDL members, past and present, there are too many of you to name, but hopefully you know my appreciation for your friendships and encouragement.

To my housemates and friends, Ann Campbell and Jill Hardin, the past 3 years' journey would've been so much more difficult without your help and support. Thank you for being there for me! I can only hope that I was there for you also. My high school friends, Barbara and Curtis Cady, Cindy Chung, Lily Ngo, and Teresa Wooden, thanks for having faith in me.

To my family, I'm always thankful for you! Aunt and uncle Raharja and Kelvin, thanks for taking care of me and for treating me as your own. My sisters, Oky and Ivonne, and my brother, Frank, I love you all. To my parents, Adolph and Maria Budianto, you are the best inspirations in my life. I will be forever grateful for the sacrifices you made so that us kids can have a better chance at life. But more than anything, thank you for loving us unconditionally!

TABLE OF CONTENTS

LIST OF ACRONYMS

AAO	All-At-Once
AS	Acquisition Sensor
BMD	Ballistic Missile Defense
CDC	Concept Design Center
CLIPS	C Language Integrated Production System
CPU	Computer Processing Unit
CO	Collaborative Optimization
CER	Cost Estimating Relationship
DER	Design Estimating Relationship
DMSP	Defense Meteorological Satellite Program
DSM	Design Structure Matrix
FOR	Field-of-Regard
FOV	Field-of-View
FPA	Focal Plane Array
GA	Genetic Algorithm
GCE	Geocentric Equatorial
GEO	Geo-synchronous Earth Orbit
GPS	Global Positioning System
HEO	Highly Elliptical Orbit
IP	Integer Programming
IR	Infrared
LCC	Life-Cycle Cost
LEO	Low Earth Orbit
LOS	Line of Sight
LWIR	Long Wavelength Infrared
MDO	Multidisciplinary Design Optimization
MEO	Medium Earth Orbit
MER	Mass Estimating Relationship
MTF	Modulation Transfer Function
NASA	National Aeronautics and Space Administration

NLMIP	Nonlinear Mixed-Integer Programming
RDT&E	Research, Design, Testing, and Evaluation
SBIRS	Space-Based Infrared Systems
SNR	Signal-to-Noise Ratio
SQP	Sequential Quadratic Programming
SWIR	Short Wavelength Infrared
TS	Tracking Sensor
VBA	Visual Basic for Applications

LIST OF SYMBOLS

A_i	available number of flights for vehicle i
c	speed of light
c_i	price per flight for vehicle i
D	sensor aperture diameter
D_{AS}	acquisition sensor aperture diameter
D_{MODIS}	MODIS aperture diameter
D_{TS}	tracking sensor aperture diameter
D_λ^*	spectral specific detectivity of the detector material
e_x	scan overlap efficiency along the width of the focal plane
e_y	scan overlap efficiency along the length of the focal plane
E_λ	blackbody spectral irradiance
F	sensor F-stop
f	sensor effective focal length
f_{AS}	acquisition sensor effective focal length
f_{MODIS}	MODIS effective focal length
f_{TS}	tracking sensor effective focal length
$F(\bar{x})$	the original objective function (cost through deployment)
$\bar{g}(\bar{x})$	vector of inequality constraints
h	altitude
h_{BO}	burnout altitude
h_p	Planck's constant
$\bar{h}(\bar{x})$	vector of equality constraints
ϖ	inclination
I_{TS}	moment of inertia for the tracking sensor optics
J_1	CO subspace objective function for the constellation & orbit design
J_2	CO subspace objective function for the spacecraft design
J_3	CO subspace objective function for the launch manifest

k_B	Boltzmann's constant
L	total launch cost
L_0	target total launch cost
L_λ	blackbody spectral radiance
M_{AS}	acquisition sensor total mass
M_{bus}	spacecraft bus total mass
M_{MODIS}	MODIS total mass
M_p	spacecraft propellant mass
$M_{s/c}$	spacecraft total mass
M_{TS}	tracking sensor total mass
m_{TS}	mass of tracking sensor optics
n_p	number of planes in the constellation
n_s	relative spacing of the Walker delta pattern
n_t	number of targets to be monitored by the tracking sensor
$n_{x,AS}$	width of the focal plane
$n_{y,AS}$	length of the focal plane
P	spacecraft orbital period
P_{AS}	acquisition sensor power requirement
P_{MODIS}	MODIS power requirement
P_{TS}	tracking sensor power requirement
p_x	pixel size
p_p	pixel pitch
R_0	target spacecraft RDT&E cost
r_0	longitudinal grid resolution at the equator
R_{bus}	spacecraft bus RDT&E cost
R_E	Earth radius
r_k	penalty function multiplier
$R_{\max}$	distance from the acquisition sensor to the limb
R_{sensor}	sensor RDT&E cost
r_Γ	longitudinal grid resolution at latitude Γ
s_{ij}	launch vehicle i's payload capability to plane j
T	blackbody absolute temperature

T_0	target spacecraft TFU cost
t	time
T_{bus}	spacecraft bus TFU cost
t_d	available detector dwell time
$t_{d,\,AS}$	available dwell time of the acquisition sensor detector
$t_{d,TS}$	available dwell time of the tracking sensor detector
t_f	available slew-and-target time for the tracking sensor
t_s	constellation size (total number of satellites)
T_{sensor}	sensor TFU cost
u_0	spacecraft argument of latitude
x	spatial ground resolution
$\overline{x}$	system-level variable vector in the AAO formulation
$\overline{x}^c$	continuous components of $\overline{x}$ $(\overline{x}^c \in \overline{x})$
$\overline{x}^d$	discrete components of $\overline{x}$ $(\overline{x}^d \in \overline{x})$
$\overline{y}_i$	local versions of $\overline{z}_i$, $i = \{1,2,3\}$
$\overline{z}$	system-level variable vector in the CO formulation
$\overline{z}_1$	CO system-level target variable vector for the constellation & orbit design $(\overline{z}_1 \in \overline{z})$
$\overline{z}_2$	CO system-level target variable vector for the spacecraft design $(\overline{z}_2 \in \overline{z})$
$\overline{z}_3$	CO system-level target variable vector for the launch manifest $(\overline{z}_3 \in \overline{z})$
Z_j	the required number of satellites to be deployed to plane j
α_{ij}	flight rate of vehicle i to plane j
α_{res}	angular resolution
β_{DL}	diffraction limit
β_{ij}	spacecraft i's viewing angle of grid point j
β_{SA}	spherical aberration
ΔT	change in temperature to be detected
$\Delta\phi$	phase difference in the Walker delta pattern
$\Delta\theta_{\max}$	maximum angular change in tracking sensor line-of-sight
$\Delta\upsilon$	in-plane node spacing in the Walker delta pattern
ε	elevation (grazing) angle

$\Phi(\bar{z})$	the penalty function objective
Γ	geodetic latitude
$\Gamma_{\max}$	upper geodetic bound of coverage zone
$\Gamma_{\min}$	lower geodetic bound of coverage zone
η	beam size of acquisition sensor
$\eta_{\max}$	maximum beam size (at zero elevation angle)
Λ	Earth central half-angle
$\Lambda_{\max}$	maximum Earth central half-angle
λ	sensor design wavelength
$\ddot{\theta}_{LOS}$	angular acceleration of the tracking sensor line-of-sight
$\ddot{\theta}_{\max}$	maximum angular acceleration
Ω_d^n	the set of discrete n-dimensional vectors
τ_a	transmission losses due to the atmosphere
$\tau_{\det}$	detector's inherent time constant
$\tau_{\det,AS}$	time constant of the acquisition sensor's detector
$\tau_{\det,TS}$	time constant of the tracking sensor's detector
τ_o	transmission losses due to the optics
τ_{TS}	torque required for the tracking sensor
$\overline{\psi}_1$	local variable vector for the constellation & orbit design
$\overline{\psi}_2$	local variable vector for the spacecraft design
$\overline{\psi}_3$	local variable vector for the launch manifest
$\Re^n$	the set of n-dimensional real vectors

LIST OF FIGURES

LIST OF TABLES

SUMMARY

This thesis introduces a systematic, multivariable, multidisciplinary method for the conceptual design of satellite constellations. The overall system consisted of three separate, but coupled, contributing analyses. The configuration and orbit design module performed coverage analysis for different orbit parameters and constellation patterns. The spacecraft design tool estimated mass, power, and costs for the payload and spacecraft bus that satisfy the resolution and sensitivity requirements. The launch manifest model found the best strategy, in terms of total launch cost, to deploy the given constellation system at the specified orbit.

Collaborative Optimization (CO) has been previously implemented successfully by others as a design architecture for large-scale, highly-constrained, multidisciplinary optimization problems related to aircraft and space vehicle studies. It is a distributed design architecture that allows its subsystems flexibility with regards to computing platforms and programming environment and, as its name suggests, many opportunities for collaboration. It is thus well suited to a team-oriented design environment, such as found in the constellation design process, and was implemented in this research. The design and deployment problem of a space-based infrared system to provide early missile warning was the application example.

Successful convergence in a preliminary study proved the feasibility of the CO architecture for solving the satellite constellation design problem. The constellation configuration was fixed as a Walker delta pattern of four planes and seven satellites per plane with relative phasing of two. The mission orbit (altitude and inclination), the spacecraft design, and the deployment strategy were varied to determine the optimal system (one with minimum cost to

deployment). To verify the result and validate the CO method for this type of problem, a large All-at-Once (AAO) optimization approach was also implemented.

A final more complex problem in which the configuration of the constellation was allowed to vary also converged successfully with the CO method. This study demonstrated several advantages of this approach over the standard practice used currently for designing a satellite constellation system. Specifically, the CO method explored the design space more systematically and more extensively; CO improved subsystem flexibility; CO formulation was more scalable to growth in problem complexity. However, the intensive computational requirement of this method, even with automation and parallel processing of the subsystem tasks, reduced its competitiveness versus the current practice given today's computing limitations.

Through these numerical experiments, this thesis further contributed to the current knowledge of the collaborative optimization method. To date, CO has been used exclusively with gradient-based optimization scheme, specifically Sequential Quadratic Programming (SQP). This research demonstrated the feasibility of zero-order methods as both system and sub-system optimizers. Also, the successful convergence of the final problem incorporating the integer variables needed to determine constellation configurations showed the flexibility of the architecture for handling mixed-discrete nonlinear problems.

CHAPTER I

INTRODUCTION

The advantages of satellite constellations have long been appreciated, principally for their coverage capabilities. Many missions have global observation requirements that simply cannot be met by single-spacecraft systems. Multi-satellite systems can tolerate limited failures in individual spacecraft in the constellation and still accomplish all or most of the mission objectives. Further benefits include increased mission robustness and survivability. Only recently, however, has there been a surge in the number of proposed concepts employing satellite constellations.

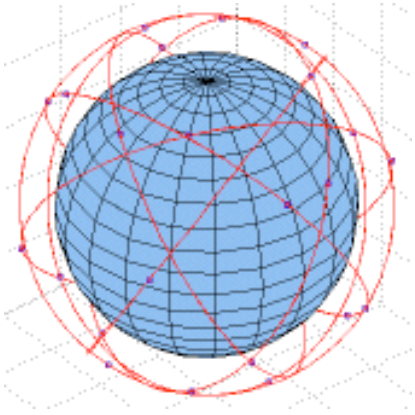

Figure 1. An illustration of a constellation.

In 1945, Arthur C. Clarke originally suggested that three satellites in geostationary orbit could provide instantaneous almost-global communication [1]. Two decades passed, however, before the first multi-satellite system flew in 1965. The mission was the Defense Meteorological Satellite Program (DMSP), operated in pairs by the US Air Force in Low Earth Orbit (LEO) for worldwide

weather monitoring [2]. Since then, the military and intelligence communities had deployed larger constellations for different applications, such as communication (DSCS [3]), early warning system (DSP [4]), and navigation (GPS [5]), using a variety of orbits. Today, they have several satellite constellation concepts under development for surveillance [10] and missile defense systems (Space Based Laser [11], Space Based Radar [12], and Space Based Infrared System [13]).

John R. Pierce first evaluated the financial prospects of Clarke's idea for space-based global real-time communication systems in 1955 [14] and predicted its billion-dollar potential. However, the commercial utilization of satellite constellations took even longer to materialize than the military systems. Iridium led the way in 1998 with its network of 66 satellites placed in LEO, offering global wireless voice and data transmissions. Other companies quickly followed suit to fill the growing demand for communication services (Table 1). LEO (Low Earth Orbit) and MEO (Medium Earth Orbit) were especially popular for telephony due to reduced time delays and better efficiency with regards to signal loss as compared to Geo-synchronous Orbits (GEO).

The deployment of Iridium marked another important milestone in a new era of space race. This time, however, it is not fueled by the pursuit of national eminence as in the days of the Cold War. Rather, its major driver is the desire to profit from the ever-increasing commercialization of space, as evidenced by the larger number of launches of commercial systems over those for government missions [16].

A paradigm shift forced by this development resulted, switching the emphasis to economic viability from the performance-focused tradition that started during the Apollo era. Especially with the high investment these spacecraft demand, no longer is *the best system at any cost* an acceptable philosophy. Instead, *faster, better, cheaper* is today's motto, pushing for minimum cost systems that can meet the performance, technology, and

schedule constraints. This movement towards affordability is further felt in the non-commercial sector, made necessary by tighter budgets and heavy scrutiny of government expenditures [30].

Table 1. A sample list of current constellation concepts [6], [7].

SYSTEM	SERVICE TYPES	ORBIT	CONSTELLATION SIZE	INITIAL OPERATION
Aster	broadband communication	GEO	5	2005
Astrolink	data, video, voice	GEO	4	2002
Cyberstar	broadband communication	GEO	3	1999
Eco-8	voice, data, paging	LEO	11	TBD
Ellipso	internet, voice, messaging, positioning	GEO + HEO	17	2002
FAISat	wireless data services	LEO	32	2003
Galileo (GNSS)	positioning	MEO	36	2005
Globalstar	voice, data, fax, paging, position location	LEO	48	1999
Glonass	positioning	MEO	21	1996
ICO	voice, data, fax, short message	MEO	10	2000
Inmarsat	internet, video, voice, fax, data	GEO	5	1998
Iridium	voice, data, fax, paging, messaging, positioning	LEO	66	1998
Leo One	messaging	LEO	48	2002
Orbcomm	data, messaging	LEO	36	1999
Orblink	internet, video, data	MEO	7	2002
SkyBridge	internet, video, voice, data	LEO	80	2002
Spaceway	broadband services	GEO	8	2004
Teledesic	voice, data, fax, paging, video	LEO	288	2003

1.1 Research Motivations

The growing emergence of satellite constellation concepts, coupled with the costly development these systems require, led to the question motivating this study. That is, "how best to attain an affordable constellation that meets all mission requirements" has significance both presently and in the future, as necessitated by the increased emphasis on cost or profitability. The key to this question, and therefore the focus of this research, lies in the early phases of the system design.

Concept development is the first of a sequence of steps that transform ideas into products. Within this initial design phase, mission objectives and requirements are more concretely defined and several possible concepts are generated. These options are then explored in greater details, their feasibility assessed, and the preferred concept is selected before the project can progress to the next stage of its design cycle.

The decisions made during the initial phases of design therefore have major impacts on the final product and its cost [18]. As shown in Figure 2, while most of the contribution to the accumulated life-cycle cost (LCC) typically occurs at the later phases of a product's life, it is during concept development that the design is largely determined and its cost committed. Thus, in today's design-for-cost environment, the significance of these early stages of the process, which are typically allowed shorter duration than the rest, must not be underestimated, especially for complex and costly systems such as satellite constellations.

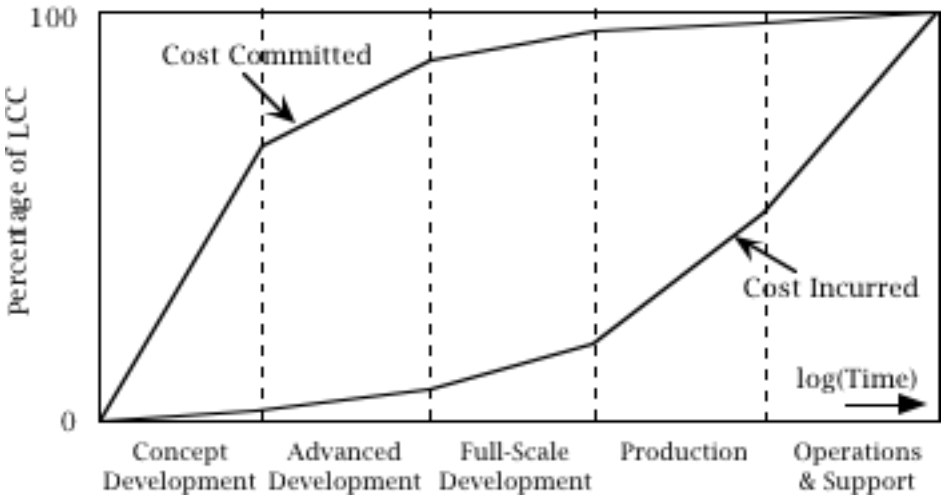

Figure 2. Cost commitment and cost incurred over design phases.

To aid engineers in making the decisions that can ultimately determine the success or failure of the end product, analysis tools and methodologies that are appropriate to the conceptual design environment are needed. Due to often-compressed design schedules, the tools must be capable of rapid turn-around analyses without compromising accuracy. The methodologies must enable engineers to explore the design space efficiently to help them make "smart" decisions quickly. That is, the methods must provide ways of analyzing system-level effects caused by changes in design variables so that the best design can be found. This is exactly the process of optimization and its importance must be especially emphasized within this stage of design where the concept is least defined and the greatest amount of design freedom is available.

The conceptual design of a satellite constellation, however, is a complex problem that involves a mix of discrete and continuous parameters and variables. Several of the constraints are non-smooth because they are functions of these same variables. The multidisciplinary nature, the amount of interdisciplinary couplings, and the inherent nonlinearities of the problem further add to the complexity. Finally, there are subsystem optimizations,

which can cause difficulties for system integration and, more importantly, for the overall system optimization.

The standard practice used currently for designing satellite constellations is a manual unstructured sequential process that heavily relies on engineers' expertise and intuition. This considerable involvement of design experts, which tends to be expensive (both computationally and in terms of man-hours), is required to efficiently resolve system integration issues and to guide the system-level trades. However, it has greater potential to yield designs that are similar to known or existing systems.

In addition, with the short time allowed for design, the scope of the problem must be kept at a manageable level, possibly limiting the level of detail allowed for the subsystems, and some narrowing of the design space (i.e., elimination of options) may be necessary within the current process. Also, the loosely coupled design environment, where the disciplinary experts use varied methods and models, have different objectives, use separate computing platforms, and perhaps even are remotely located from each other, creates difficulties for a structured system optimization. Thus, the main focus often becomes more of attaining feasibility and less effort is spent on exploring the design space in search of optimality. These shortcomings, which are perceived necessary due to the complexity of the problem and the constrained design schedules, helped establish the need for a new method to improve the satellite constellation design process that formed the research problem for this thesis work.

1.2 Research Goal

Given the motivating factors discussed in Section 1.1, the ultimate goal of this research is to formulate, demonstrate, and evaluate a new approach for the synthesis and optimization of multi-satellite systems. This new method is to have the following characteristics:

- *Subsystem Flexibility:* It comprises a distributed, team-oriented architecture that fits into the multidisciplinary design organization such that the disciplines retain control of their analysis methods and freedom to select their computing platforms and programming environments.
- *Optimality:* It includes an optimization procedure that systematically searches the multivariable design space so that greater confidence on the "goodness" of the solution is achieved.
- *Scalability:* It can easily handle greater problem complexity (more details or increased breadth), which would result in greater number of design variables and constraints at the discipline level, than can be accommodated by the current method.
- *Efficiency:* It produces solutions with reasonable computational requirements.

A secondary goal of this research aims to extend and improve an emerging design methodology. The contribution will be in the implementation and demonstration of the specific method on the satellite constellation design problem.

1.3 Research Approach

A literature review was first conducted to identify the important engineering characteristics and the dynamics of the satellite constellation design and deployment problem so that it can be modeled numerically. Many discussions can be found in the public domain, allowing for good general definition of the problem and its contributing factors. This background research also included characterization of the current design process, identifying its strengths and several areas in need of improvement.

The literature review further investigated Multidisciplinary Design Optimization (MDO) methods [18]. MDO was established to improve the conceptual design process of complex aerospace systems. It embodies many

optimization techniques that have been proven on various complex multidisciplinary design problems [39]. Optimization allows systematic search of the alternatives to better support the decision-making during the design process. It was thus hypothesized that MDO can improve this satellite constellation design process.

The next step was to develop the required discipline-level analysis tools that can model subsystem responses to system and subsystem-level changes. These tools were designed to be of appropriate fidelity and to be capable of rapid evaluations to ensure computational efficiency for the overall process. Various computing platforms and programming environments were utilized to demonstrate subsystem flexibility. The mission example used throughout this thesis was to design and deploy a LEO space-based infrared multi-satellite system for ballistic missile defense. Thus, the mission requirements were defined and the disciplinary analyses were programmed with this specific application in mind.

From the literature search, the distributed analysis architecture [39], another key concept in MDO, was found to have desirable characteristics (i.e., subsystem flexibility that allows a diverse set of analysis programs executed on different computing platforms) to support the goal of this research. It was thus implemented, allowing decomposition of the complex system analysis, into several smaller and more manageable subsystems that coincide with disciplinary tasks. Many multi-level optimization strategies are available that are suitable for this type of architecture. Collaborative Optimization (CO, [28]), in particular, has promising applicability to the constellation design problem.

CO, a distributed design architecture, further extends subsystem flexibility by giving control of local variables and constraints to the disciplines. It decomposes the system optimization problem into discipline-oriented sub-problems, yielding a highly scalable method. Its implementation involved problem reformulation and the development of optimization schemes for solving

the disciplinary sub-problems and the system-level coordination problem. Furthermore, the CO architecture removes dependencies between the disciplines, allowing for concurrent processing of these subsystem analyses and optimizations to ensure an efficient overall process.

A preliminary study was conducted to demonstrate the feasibility of the CO approach for this type of problem. For validation and verification, the All-at-Once (AAO) method was also applied. In addition to a quantitative comparison of optimization results, a qualitative evaluation of the two techniques was conducted in terms of computational efficiencies, organizational advantages, and method scalability, which are the basic characteristics desired of the proposed approach.

The preliminary study involved a simplified problem in which major variables of the constellation configuration were fixed so that it consisted of only continuous variables. Nevertheless, its results were significant to this research. First, it would provide evaluation of the analysis tools. Second, it would demonstrate the viability of the CO architecture to this type of problem and verify the optimization techniques implemented. Third, thus far CO has been demonstrated almost exclusively with gradient-based methods, such as Sequential Quadratic Programming (SQP). The preliminary study would contribute to the knowledge of CO methodology by successfully employing zero-order optimization algorithms at both system and subsystem levels, as recommended in [28].

To better represent the constellation design problem, a more difficult problem was investigated. Two of the previously fixed discrete parameters that determine the configuration of the constellation were turned into design variables, yielding a mixed-integer nonlinear problem. The main purpose of this final demonstration example was to provide a stronger validation for the applicability of CO architecture to the constellation design problem. Showing a capability to handle greater level of complexity would further prove the

scalability of this method. Also, solving this final problem would further extend the domain of CO application by demonstrating a capacity for dealing with integer variables.

The final step was to document the method formulation, implementation, and demonstration process used in this research work. From the results attained, conclusions were drawn as to the overall effectiveness of the proposed approach for solving the constellation design problem. Comparisons to the standard practice used currently and recommendations for future work were made.

1.4 Thesis Organization

The structure of this thesis corresponds for the most part with the steps described in Section 1.3. Chapter II provides reviews on MDO, distributed architectures, and collaborative optimization. A description of the space-based infrared application example used throughout this thesis is first presented in Chapter III, followed by characterization and definition of the constellation design problem. Description and evaluation of the integration and optimization process used currently in the industry can be found in the last section of this chapter. Chapter IV and VI present details on the original and modified versions of the analyses, respectively. The implementation and the preliminary results using both CO and AAO are given in Chapter V, in which validation of the CO method with respect to AAO is also found. Chapter VII describes the system and subsystem optimization schemes used in solving the final design and deployment problem within the CO architecture. The final results of the mixed-integer problem optimization are presented in Chapter VIII. Finally, conclusions and recommendations for future studies can be found in Chapter IX.

CHAPTER II

PROBLEM AND PROCESS DEFINITIONS

2.1 The Application Example

The U.S. Air Force Space-Based Infrared Systems (SBIRS) is to replace the DSP system in providing global and theater missile warning, national and theater missile defense, technical intelligence and battle-space characterization [13]. The overall architecture consists of GEO and LEO satellite constellations, as well as sensors mounted on satellites placed in Highly Elliptical Orbits (HEO). The application selected as the demonstration problem in this research is similar to the LEO components, also commonly referred to as SBIRS Low.

SBIRS Low complements the SBIRS High (SBIRS GEO and HEO satellites) in providing high-confidence missile launch identification. However, the major task of SBIRS Low is to acquire accurate post-boost state vector data of the target. This precision midcourse tracking capability is required for effective Ballistic Missile Defense (BMD). Off-line post-processing of infrared data obtained by the SBIRS Low system will also be very useful, not only to enhance target detection and characterization, but also for other applications, such as cataloging the space debris population [41].

The current SBIRS Low design is still not definitive, planning for 20-30 satellites of approximately 700 kg each that orbit below the inner Van Allen belt with design life of 10 years [8], [9], [41]. Each platform carries two sets of electro-optic systems. The first is a high resolution, wide field-of-view (FOV)

acquisition sensor. FOV, defined as the total solid angle visible by the sensor, accounts for mechanical or electronic scanning by the system and is also referred to as swath width (Figure 3). The acquisition sensor scans from horizon to horizon (plus a few degrees above the horizon to allow full coverage of up to 30 km above the surface of the Earth) to search, detect and track missiles during their boost phase. Thus, it operates in the Short Wavelength Infrared (SWIR) band (Figure 4) to detect the high-temperature plume of the rockets.

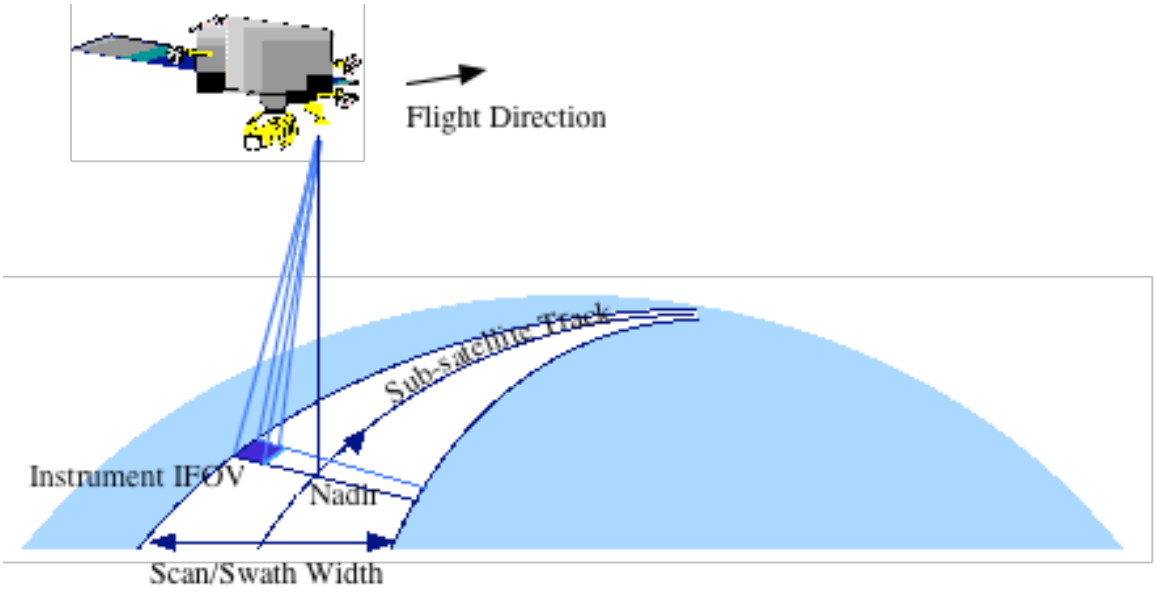

Figure 3. Illustration of terms used for acquisition sensor design.

When a target is detected, the acquisition sensor performs a handoff to the second system mounted on each SBIRS Low spacecraft, called the tracking sensor, to continue monitor of the missiles' trajectories through post-boost and reentry. The tracking sensor is a slew-and-stare multi-spectral infrared system (ranging from visible to Long Wavelength IR) with a narrow FOV but a large field of regard, resulting in a high agility requirement. The field of regard, or the total area to be covered by the tracking sensor, is the cylindrical field extending from the surface of the Earth to the orbit altitude and encircling the spacecraft 360° (Figure 5).

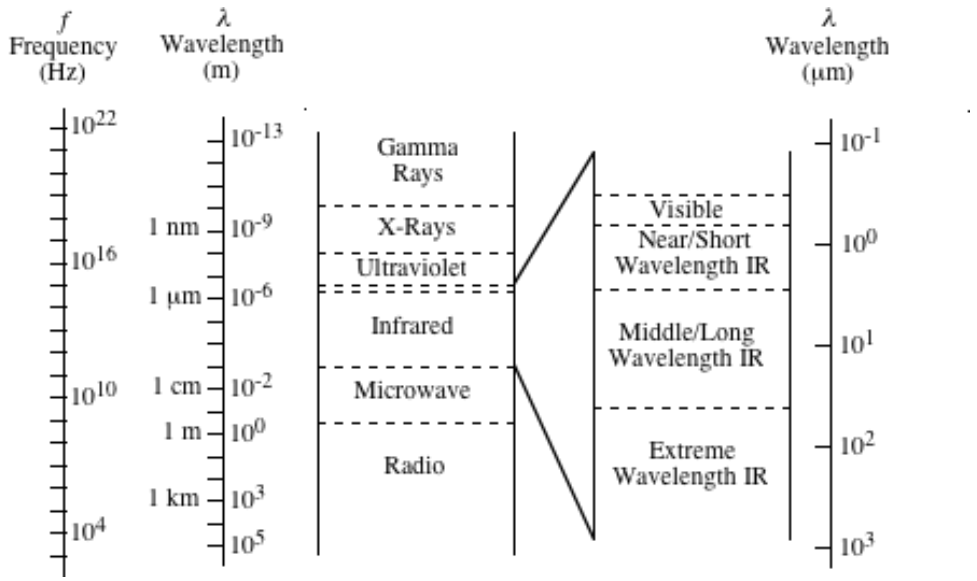

Figure 4. The electromagnetic spectrum.

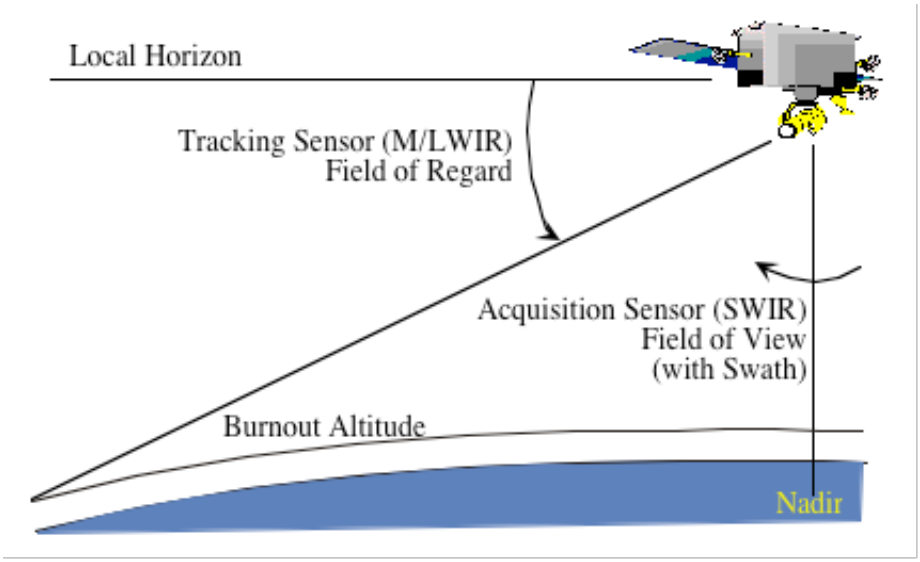

Figure 5. Illustration of the two sensors aboard SBIRS Low.

The application example used throughout this thesis was to design and deploy a system similar to the SBIRS Low. The overall objective was to find the

mission orbit (altitude and inclination) and the spacecraft design (sensor size and spacecraft mass) with the minimum cost through deployment, consisting of RDT&E (Research, Design, Testing and Development), production and launch costs. For this detection system, the spatial (ground) resolution requirements (x), defined as the minimum distance within which two target points can be resolved, were fixed at 0.4 km and 0.3 km for the acquisition and tracking sensors, respectively. Sensitivity was measured by the Signal-to-Noise ratio (SNR). For this type of mission, SNR of at least 10 dB was needed.

2.2 The Constellation Design Problem

The design of a satellite constellation is a highly constrained, multidisciplinary problem. Several variables and parameters act as interdisciplinary dependencies, which greatly influence not only the final system design and cost, but the responses of the disciplinary modules as well. The literature review provided information on the various factors that can influence the design of a satellite constellation and, applied to the mission example, yielded the DSM (Design Structure Matrix, [19]) representation shown in Figure 6. DSM is a graphical tool to aid the systems engineer in organizing and structuring the design synthesis process, showing the relationships between the various disciplines involved in this design problem. Engineering knowledge and experience of the important variables and contributing analyses is required in forming the DSM.

Each block is a subsystem module, while the horizontal and vertical lines represent outputs and inputs, respectively, for each block. The nodes connecting the blocks symbolize interdisciplinary couplings, or dependencies of the subsystems' inputs on the others' outputs. The existence of feedback loops (nodes below the diagonal of the matrix) implies an iterative process is needed for convergence.

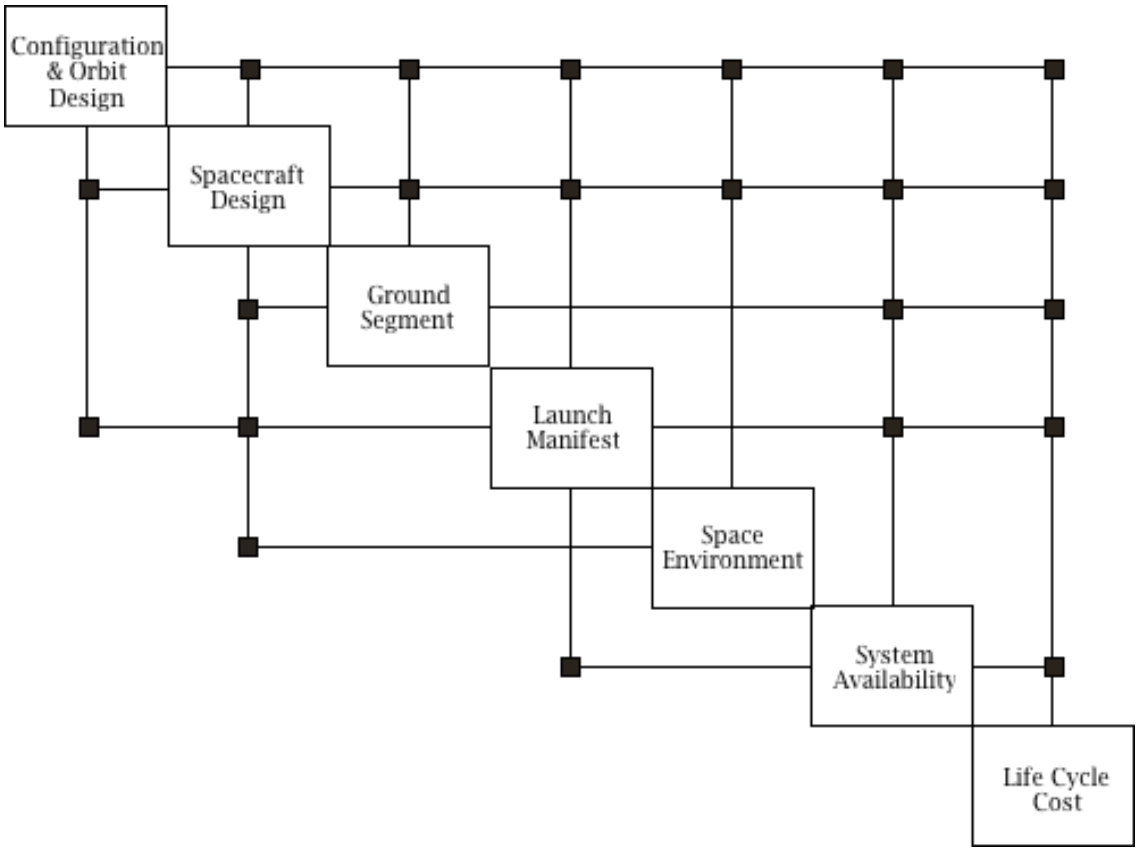

Figure 6. DSM representation of the satellite constellation design problem.

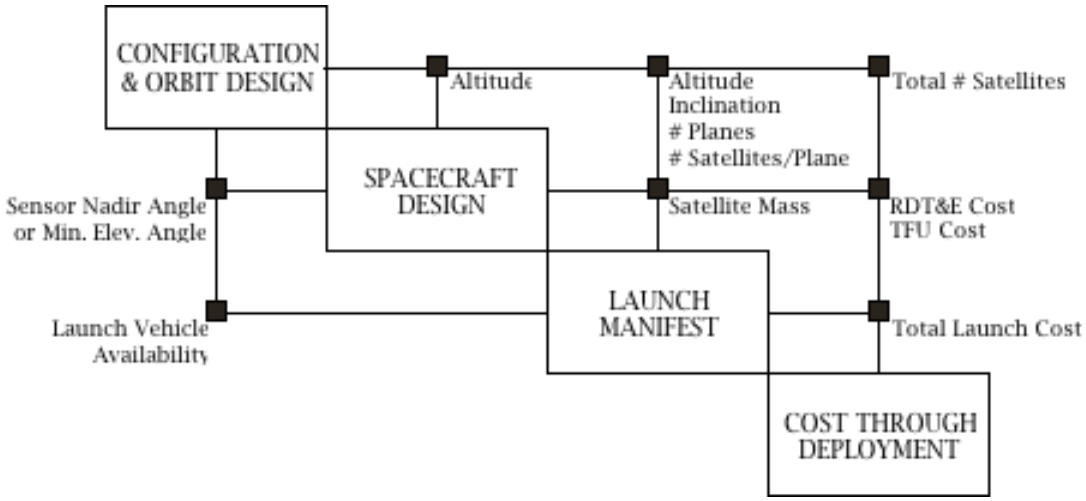

Figure 7. A simplified satellite constellation design problem.

For this thesis work, a simplified model of the multi-satellite system design problem (Figure 7) was used, based on the discussions found in [22] and [26]. The specifics of the application example also shaped the details of the problem. This model aimed to retain the first-order effects, choosing the variables and modules with the greatest influence on the overall space-based infrared system.

The simplified problem is mainly characterized by four contributing analyses. Within the configuration and orbit design module, trade studies are conducted to find the best orbital parameters and constellation configuration to provide the coverage required for the given sensor capability. The task of the spacecraft model is to design the payload and spacecraft bus that satisfies the resolution and sensitivity requirements at the specified altitude. The launch manifest block finds the best (i.e., lowest cost) strategy to deploy the entire constellation to the selected orbit, according to vehicle availability and capacity. Finally, the cost module simply sums up the individual cost components from development through deployment of the constellation system.

The "dynamics" of this design problem, even for the simplified version in Figure 7, is interesting and makes its optimization a challenging task. Altitude, for example, is an important decision variable because it has opposing effects for the different disciplines. At higher orbits, the coverage requirement can be satisfied with fewer satellites (Figure 8). However, since launch vehicle payload capability decreases with altitude, a larger and more expensive option may be needed to deploy the constellation. In addition, larger sensors and communication subsystems are needed at higher orbits to meet a fixed resolution requirement, resulting in heavier, higher powered, and more expensive satellite units. Thus, the decision on altitude will have major effects on system cost.

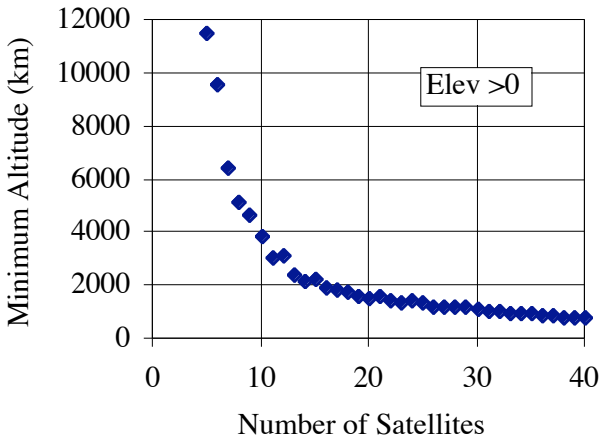

Figure 8. Minimum altitude (0° elevation angle) vs. Walker constellation size [22].

Inclination and minimum elevation angle are other key coupling variables in the design of satellite constellations. Inclination not only affects launch vehicle capabilities but the coverage provided by a given constellation configuration as well. Higher inclination orbits tend to result in broader coverage of the Earth's surface, but may reduce the closest approach distance between the satellites, increasing the chance for collision. Also, for a given vehicle and launch site, payload will be maximized for insertion into inclinations corresponding to the launch site latitude (Figure 9). As minimum elevation angle approaches zero, the resulting coverage characteristic tends to improve, while the instruments must grow in size to satisfy resolution requirements.

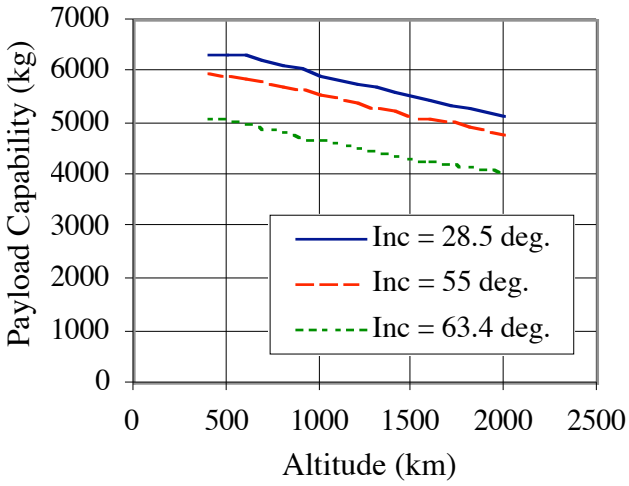

Figure 9. Payload capability of Atlas IIA launched from the Eastern Range (Cape Canaveral) for 2-burn direct injection to various inclinations [55].

Constellation configuration parameters (number of orbital planes and number of satellites per plane) also have different effects on the disciplines. Adding more orbital planes tends to improve performance (i.e. coverage) at the cost of requiring more launch vehicles to deploy the constellation. Placing more satellites per orbit typically leads to smaller swath width for each spacecraft and consequently allows smaller instruments and cheaper platforms so as to meet the overall coverage requirement. However, production cost increases with the number of total spacecraft in the constellation.

Table 2. Trade issues for satellite constellation designs (arrows signifying directions of improved subsystem performance).

VARIABLES	CONFIGURATION & ORBIT DESIGN	SPACECRAFT DESIGN	LAUNCH MANIFEST
Altitude	↑	↓	↓
Inclination	↑	—	↓
Minimum Elevation Angle	↓	↑	—
Number of Planes	↑	—	↓
Number of Satellites per Plane	↑	—	↓

Not only do these variables produce opposing effects on the different disciplines, but their interactions with each other also have varied results on the evaluation criterion (i.e., objective function) and the constraints satisfaction (or violation). Optimizing the overall system is therefore not a straightforward task. For certain missions, the best constellation (e.g. the constellation with the minimum life-cycle cost) may be the one that requires the fewest number of satellites to provide the specified total coverage. For others, launch vehicle capabilities may favor a constellation configuration with more (perhaps smaller) satellites at lower altitudes. When considerations such as fold of coverage (coverage overlap), cross-linking between satellites (connectivity requirements for passing information), replacement strategy, or end-of-life policy is taken into account, the solution may look different yet [22], [23].

Finally, the optimization of a mixed-integer nonlinear problem is fundamentally difficult [68]. Thus, the discrete nature of the configuration parameters, which have major influence on the overall design, adds to the already complex problem of optimizing constellation systems.

2.3 The Current Conceptual Design Process

The current state-of-practice for integrating and optimizing a multi-satellite system [15] has been used for designing several technically challenging systems that have achieved operational reality, such as Iridium, Globalstar, and Orbcomm. It begins by establishing several alternate concepts for the system that can meet mission objectives and requirements [26]. Through initial trades and analyses, possible constellation configurations, payload characteristics and launch vehicle options are identified.

Each concept is further explored and refined within a manual iterative process, best depicted by Figure 10. All of the subsystem experts are loosely coupled (independently perform analyses) and combined with the lack of structure in the process, applying an overall system optimization becomes

difficult. Few system-level trades are achieved as a result of the typically inefficient communications between the disciplines.

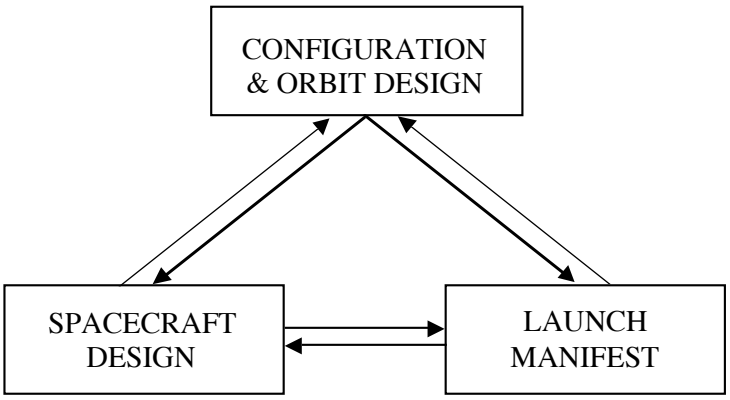

Figure 10. The satellite constellation design process used currently.

A new, emerging design process that is becoming more accepted is practiced at the Aerospace Corporation's Concept Design Center [24], [25]. The CDC was established in 1996 to provide a collaborative environment for the conceptual design of various space systems, including satellite constellations. Its facility, design process, and design team have brought great improvements in producing system-level designs and in performing system-level trades compared to the process shown in Figure 10 [24]. This type of approach has been shown to reduce the design cycle times by greater than 70% and the cost of the conceptual phase by two-thirds [20]. These improvements, however, are mainly products of greater efficiencies enabled by CDC's collaborative environment.

In the CDC, all of the disciplinary experts are assembled in the same room, interact through discussions, are interconnected by a networked set of computers, and concurrently participate in the design synthesis, also referred to as a session. Thus, the iterative process becomes collaborative and is typically allotted 2 to 4 four-hour sessions. The main objective of the session is to converge to a feasible design point with limited trades to consider improved alternatives. A flowchart describing this process as applied to the simplified constellation design problem is shown in Figure 11.

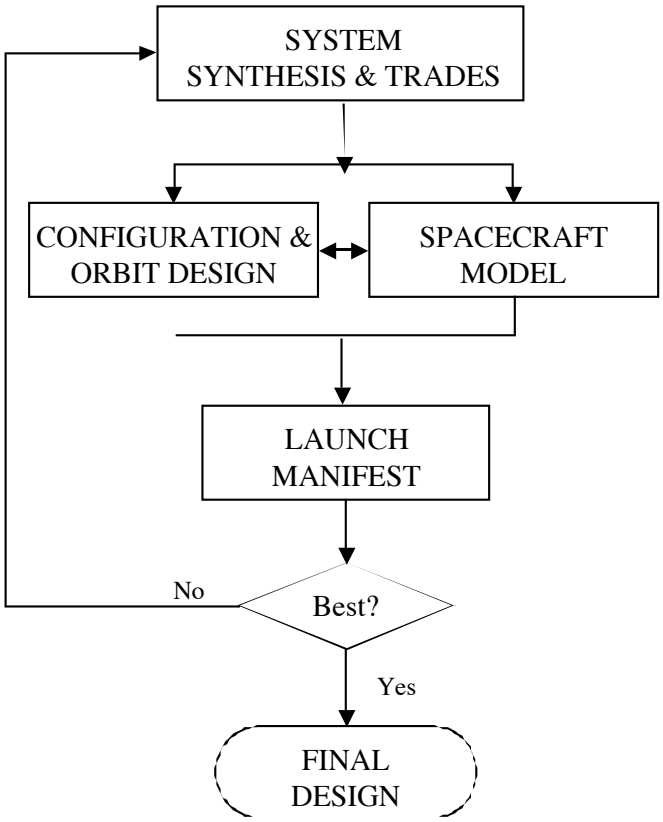

Figure 11. The CDC method for satellite constellation system synthesis.

System-level synthesis within this process is a series of key trade studies, usually involving mission orbit, coordinated by the systems engineer. The configuration and orbit design expert finds the smallest constellation to provide the required coverage, taking into account launch considerations. For example, a constellation of 12 satellites placed in 6 orbits is preferred over 11 total satellites in 11 orbits for the potential launch cost savings. The spacecraft designer finds the payload and the bus of minimum cost that satisfy the performance requirements at the mission orbit given by the systems engineer. Trades are required between the constellation configuration and spacecraft design modules to find the optimal elevation angle. Minimum-cost deployment of the constellation is then found once the configuration and the spacecraft mass are determined.

This process still lacks a structured, logical search method, which can be dangerous for any complex decision-making, especially if there are costly implications. With the subsystem optimizations, the potential exists for conflicting objectives, leading to sub-optimal solutions. Furthermore, the current process relies heavily on intuition and experience of the engineers involved during the integration and optimization session. Such expertise could be advantageous in reducing the design cycle times needed to arrive at a solution, especially if the system of interest is similar to existing ones. On the other hand, experience can introduce bias at this early stage of the design and may steer the solution away from the true, less intuitive optimum.

CHAPTER III

AN OVERVIEW OF THE MULTIDISCIPLINARY DESIGN OPTIMIZATION

Multidisciplinary Design Optimization (MDO) was established as a field of aerospace research when it was recognized that there exists a need for a systematic methodology in designing complex systems [18]. The overall goal is to improve design product and process with respect to system performance and/or cost, within the specified mission constraints. One way this is achieved is to apply optimization techniques in the conceptual phase that draw more knowledge about the system forward to the early stages of the design process and increase the level of design freedom therein. Figure 12 illustrates the role of MDO, shifting the level of design knowledge and design freedom towards the dashed lines. These optimization techniques allow analyses of system-level effects due to changes in design variables. The resulting systematic exploration and characterization of the design space will aid the design engineers in making better-informed decisions during the conceptual phase to significantly improve the final product.

Optimization has been shown to improve spacecraft design and deployment analyses in several studies [30], [31]. Applying optimization to the astrodynamics of the constellation design has also produced various improved configurations. Example problems are one which requires the fewest total satellites for a given coverage characteristics [32], [70] and one that meets best coverage and robustness criteria [71]. Optimization has further been applied to the constellation design at the system level, [33] and [34], accounting for payload and spacecraft bus sizing/selection and deployment strategies. The

contributions of MDO, however, lie not only in the application of optimization techniques. Design architectures are also important elements of MDO that can best address the organizational challenges it faces today [28], [30] by providing efficient team-oriented structures that are suitable to the multidisciplinary design groups found today. Thus, the research work presented in this thesis attempts to go a step further by adapting MDO into the satellite constellation design process.

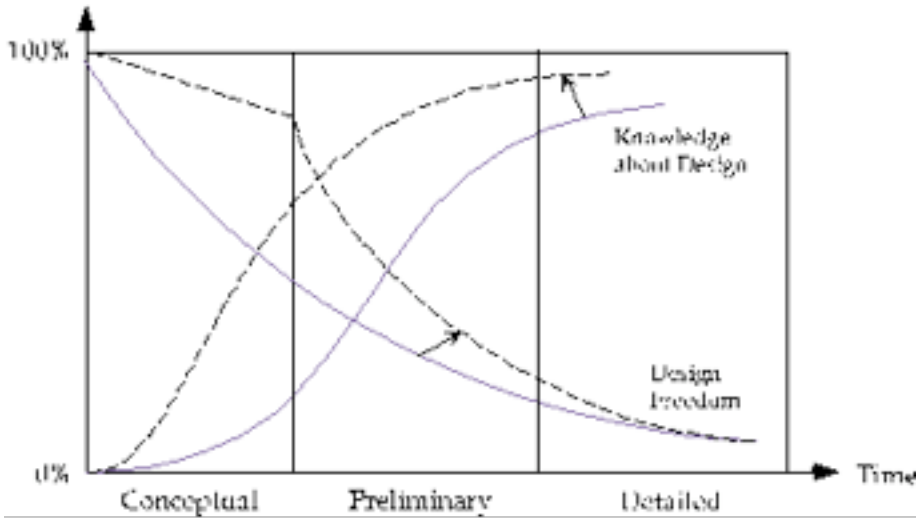

Figure 12. The role of MDO in the design process.

3.1 Distributed versus Integrated Analysis Architecture

Distributed analysis has become a key development in MDO [27], [38], [39]. It decomposes the overall system synthesis problem into smaller, usually discipline-oriented, tasks, coordinated at the system level. The CDC has utilized this type of architecture successfully, as proven by the resulting reduced design cycle times and costs. The alternative is to integrate (couple) the various analysis modules and to utilize a single optimizer to find a good solution, executing the subsystem analyses sequentially. This latter approach is not practical for complex large-scale multidisciplinary problems involving

many variables and constraints, such as most aerospace system designs including satellite constellations.

Compared to the integrated analysis approach, a distributed architecture, in general, provides clear organizational and computational advantages for large-scale complex design problems [39], leading to its selection for the new constellation design method. It more naturally fits into the multidisciplinary analysis environment of most design groups, where specialists are organized by their area of engineering expertise and where interdisciplinary interactions are fairly complex. The distributed analysis architecture provides the subsystems with flexibility with regards to computing platforms and programming environments. The independence provided to the disciplines further allows modularity, whereby each subsystem is free to modify its own analysis method, model, assumptions, etc., without requiring restatement of the overall problem or alterations in the other disciplines. This modularity also provides opportunities for parallel computations. Concurrent processing of the subsystems' analyses, perhaps even on heterogeneous platforms from remote sites, can lead to reduced design cycle times. Therefore, it was decided that the new approach to the conceptual design of satellite constellations was to comprise the distributed analysis architecture.

3.2 Collaborative Optimization Method

Several methodologies have been developed in the past decade to utilize the distributed architecture for solving large-scale problems [38], [39]. Some were motivated by the desire to give the disciplinary experts the most autonomy possible. One of these methodologies is Collaborative Optimization (CO [28]), a multi-level technique where a system optimizer orchestrates several optimization processes at the subspace level. The subsystems are given control over their design variables and responsibility for satisfying local constraints, allowing them opportunities to contribute to the overall design decision process.

Within CO, the system-level variables ($\bar{z} \in \Re^n$) consist of design parameters that affect the system objective and state variables that couple the subspaces. The system optimizer's task becomes twofold. First, it is responsible for coordinating the combined variables such that its overall objective ($F(\bar{z}): \Re^n \rightarrow \Re$ in Figure 13) is minimized (or maximized). Second, it sets values for the interdisciplinary (coupling) parameters and poses them as targets for the subsystems' optimizers to match. For example, $\bar{z}_i$ is a vector subset of $\bar{z}$ composed of all variables that affect subspace i. The subsystems have their own local versions of the same variables $\bar{y}_i$, and minimizing the discrepancies between these and the given targets become the objective of the subspace optimizers ($J_i = \left\| \bar{z}_i - \bar{y}_i \right\|^2$, where $J_i: \Re^{n_i} \rightarrow \Re \quad \forall i$). How well these targets are met by the subsystems, in turn, becomes compatibility constraints to guide the system-level optimizer. Thus, the final converged solution must ensure that $J_i = 0, \ \forall i$.

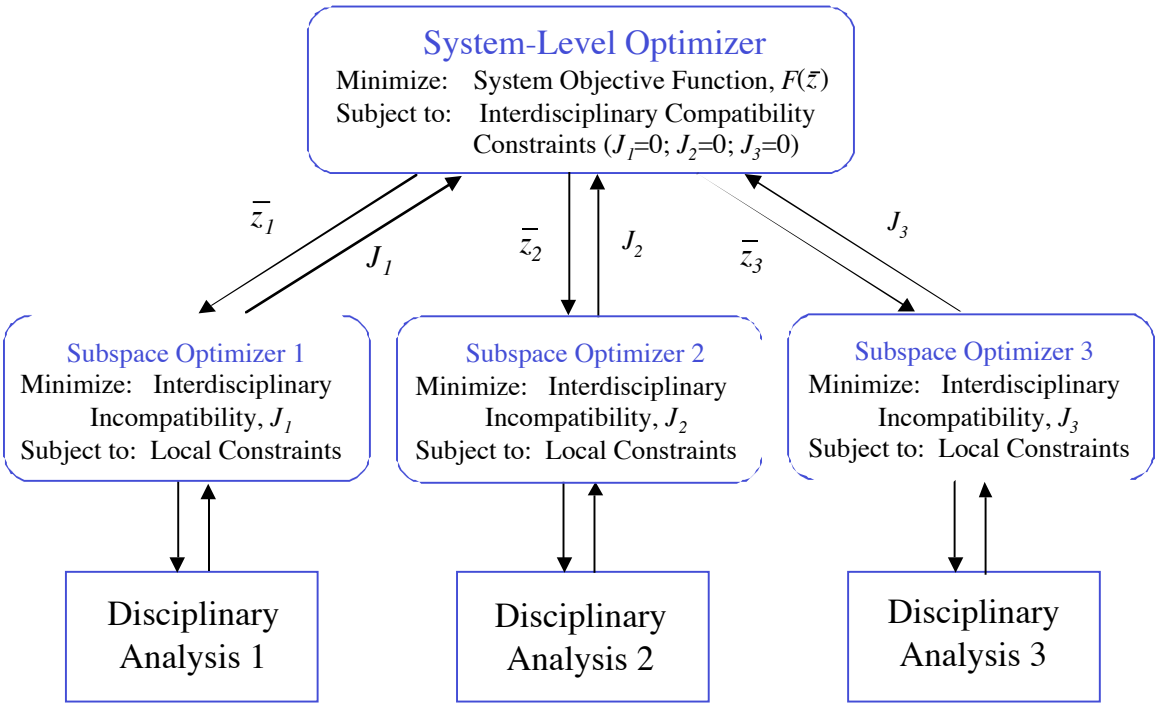

Figure 13. Collaborative optimization architecture.

This division of tasks from the overall problem is a characteristic of CO that can facilitate the solution-finding process and increase the scalability of the method. This is due mainly to the typical reduction in the number of variables and constraints involved in the system optimization problem. The subsystems can be trusted with local decision parameters and local constraints that do not explicitly affect the system objective or the evaluation of the other subsystems. Therefore, the problem growth is slowed and communication requirements between the system and the subspace analyses are easier with smaller demands on data exchange.

There are limits to these benefits, however. Problem sparseness is crucial to obtain these savings in computational costs. That is, in the worst case scenario where every variable affects every disciplinary analysis, CO will not provide significant advantage since each subspace would have to consider all of the system design variables. Thus, having comparatively few interdisciplinary couplings is key to CO's utility. Furthermore, the combined computational effort of the decomposed tasks in CO, even with the concurrent operations, can be fairly intensive. This is true especially since the subsystems are required to perform optimization, rather than the much simpler role of function evaluations.

Collaborative optimization has been successfully applied to large-scale multidisciplinary optimization problems related to aircraft and space vehicle design [28], [37]. The constellation design problem shares similar characteristics as these previously established applications. That is, the design and deployment of a satellite constellation is highly-constrained and is multidisciplinary in nature with a fair amount of interactions among the individual disciplines. The subsystems typically involve some type of optimization process. CO, unlike other approaches, allows these to be retained by employing an optimizer at the system-level to coordinate the overall process and circumvent the possibilities of having conflicting sub-level (disciplinary) objectives.

CO further offers all of the characteristics desired of the new approach to the constellation design problem. Namely, the distributed architecture offers subsystem flexibility and promises process efficiency by concurrent computations of the analyses. Application of a systematic search method ensures confidence on the "goodness" of the solution. Finally, CO provides scalability through decomposition of the overall problem.

CHAPTER IV

ANALYSIS MODELS

The three disciplinary analysis programs created to enable the demonstrations in support of this research study are explained in this chapter. The coverage analysis tool was written in Matlab and was executed on a Silicon Graphics platform to compute the regional or point coverage provided by a single spacecraft or a constellation of satellites using methods suggested in [44]. The spacecraft model was a MS Excel workbook that contained the estimating relationships to size and cost the payload and spacecraft bus. The launch manifest program consisted of an electronic database (also a MS Excel workbook) and LPSolve 2.3 (an integer problem optimizer written in C and compiled on a Sun workstation). The cost module in Figure 7 is an equation that forms the objective function of this problem. Therefore, it was combined with the system optimizer and will be explained in Chapter V.

4.1 Coverage Analysis I

There are numerous ways to configure the satellites in a constellation system. References [45] to [49] provide just a sampling of these different methods. The Walker delta pattern [45], which placed all of the spacecraft in circular orbits at the same altitude and inclination, is commonly used as a starting point in constellation designs (e.g., Globalstar [50] and GPS [71]). It offers many configurations that can provide global continuous single-fold coverage (at least one satellite is visible by all points of the Earth at all times), as required by the application example in this study. For the demonstrations in

this research, it was considered reasonable to limit the problem to only this pattern.

Walker constellations, often referred to using the shorthand notation $t_s/n_p/n_s$, are fully specified given the orbit (altitude and inclination), total number of spacecraft (t_s), number of planes (n_p), and relative spacing (n_s). These are the input parameters required by the coverage analysis tool. More detailed description of this constellation pattern and the meaning of these parameters can be found in Appendix A.

The new coverage analysis program written for this research treated each spacecraft as a point mass orbiting a spherical Earth. No atmospheric drag and solar radiation pressure calculations were included in the model. The propellant required for station-keeping throughout the life of the spacecraft was instead estimated to be 10% of the total dry mass (Section 4.2).

There was no capability to compute precession effects and third-body perturbations caused by the Moon and the Sun. The only force acting on the point masses was the Earth's gravity. These were reasonable assumptions since these perturbations caused the same nodal regressions and apsidal rotations on all of the satellites in a Walker constellation such that the pattern (or relative positioning of the satellites to one another) changed negligibly. These simplifications allowed for an analytical solution to the Kepler problem [43]. The propagation problem transformed into the following Euler's method formulation:

$$u_0(t+\Delta t) = u_0(t) + \left(\frac{du_0}{dt}\right)\cdot \Delta t \qquad \textbf{(4.01)}$$

u_0, a spacecraft's argument of latitude (the angle in the orbital plane measured from the line of ascending node to the satellite's current position) could

therefore be determined for any time t. $\left(\frac{du_0}{dt}\right)$ was constant, given the above assumptions, and related to the orbital period P:

$$\frac{du_0}{dt} = \frac{2\pi}{P} \qquad \textbf{(4.02)}$$

Since all of the spacecraft in the constellation had the same orbital period, the constellation pattern repeated at a frequency of $(1/P)$. Thus, it was sufficient to evaluate the coverage provided by the constellation over propagation duration of P.

The input required by the coverage analysis program consisted of the constellation configuration, orbital altitude and inclination, sensor capabilities (acquisition sensor nadir angle or field-of-view half-angle η), and the desired coverage characteristics (coverage region, overlap requirements, and surface altitudes). The coverage zone was specified by two geodetic latitude bounds $\left[\Gamma_{\min}, \Gamma_{\max}\right]$. The program then populated this region with grid points (targets) distributed between 180° W to 180° E longitude according to a given resolution r_Γ. The user specified r_0, which determines the grid sizes at the equator $(\Gamma = 0)$. At higher (or lower) latitudes $(|\Gamma| > 0)$, the east-west resolution was increased to ensure that the grid points represent approximately equal surface areas [44]:

$$r_\Gamma = \frac{r_0}{\cos\Gamma} \qquad \textbf{(4.03)}$$

These targets could also be given an altitude h_{BO} to compute coverage of an "atmospheric shell" above the Earth's surface. Finally, each point was propagated at the same rate as the planet's rotation.

The program produced several figures of merit, such as percent coverage, maximum gap, mean response time and shortest distance of approach between satellites. Percent coverage was the portion of the total specified area, at a

given instant, that was covered by one or more satellites. Maximum coverage gap was defined as the longest of the coverage gaps encountered for a particular point on Earth over the entire simulation. Mean response time was the average amount of time required for a point on Earth to come within view of any satellite, given a random request to observe it. Shortest approach distance would be useful for cross-linking (connectivity requirements for passing information) or collision avoidance.

The primary constraint in this study was zero maximum gap for single-fold global coverage (all grid points could be seen by at least one satellite at any instant of time) provided by the acquisition sensors (Chapter V). Although a global coverage region was specified, limiting the coverage zone to be between 0° and 90° was just as accurate, due to the symmetry of Walker constellations, and allowed savings in computation hours. A grid resolution r_0 of 6° was used throughout this study for reasonable computation efforts without compromising accuracy. SBIRS' requirement for detection of missiles up to their burnout altitude was handled by placing these grid points at the desired altitude above the Earth's surface. A minimum 150 km for the approach distance between satellites was also placed to ensure zero collisions.

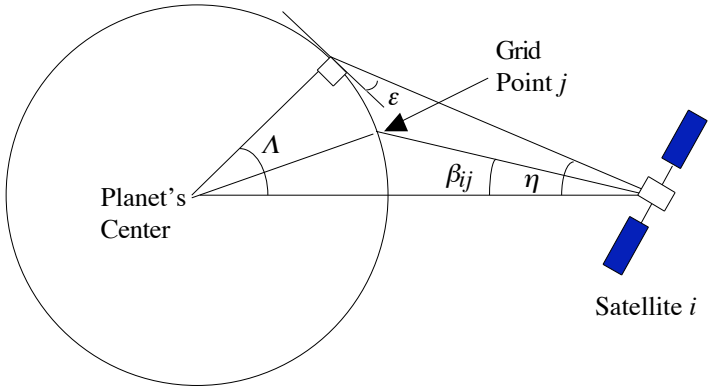

Figure 14. Geometric relationships for coverage analysis.

The coverage computations were solely based on geometric constraints (Figure 14). There was no capability to set lighting (i.e. to simulate eclipses) or

temporal (e.g. to simulate ground operation times) constraints. The satellites' sensors were assumed to have simple conic projections.

At each time step Δt, the program advanced all of the coverage grid points distributed over the specified coverage area and all of the spacecraft in the constellation. New subsatellite points (intersection points between the line joining the spacecraft to the Earth's center and the surface in which the grid points lie) were found and, after the appropriate coordinate transformations, spacecraft i's viewing angle of point j (β_{ij}) could be computed (Figure 14). In addition, the spacecraft's total field of regard depended on altitude, such that:

$$\eta_{\max} = \sin^{-1}\left(\frac{R_E + h_{BO}}{R_E + h_{BO} + h}\right) \qquad \textbf{(4.04)}$$

Thus, a surface point was visible to a satellite only if both of the following conditions were true:

$$\beta_{ij} \le \eta \qquad \textbf{(4.05)}$$

$$\beta_{ij} \le \eta_{\max} \qquad \textbf{(4.06)}$$

The elevation (grazing) angle ε, which was the angle measured from the surface point's local horizon to the Line of Sight (LOS), and the Earth central half-angle Λ were related geometrically to sensor beam size η and the spacecraft altitude as shown in Figure 14. With $\eta = \eta_{\max}$, elevation angle was zero and Λ was $\Lambda_{\max}$.

4.2 Spacecraft Model I

The equations used to size the payload and spacecraft bus were programmed into MS Excel. The mass and power calculations are given in kg and W, respectively. The values for angles are in radians. Based on spacecraft altitude, minimum elevation angle, ground resolution in km (x) and sensitivity

requirements, and finally, as in the case of SBIRS, burnout altitude, the angular resolution, α_{res}, were determined. Aperture diameters for the sensors (D) were found by iterations, allowing for angular blur (diffraction limit β_{DL} and spherical aberration β_{SA}, [48]) at the design wavelength λ:

$$\beta_{DL} = \frac{2.44\lambda}{D} \qquad \textbf{(4.07)}$$

$$\beta_{SA} = \frac{1}{128F^3} \qquad \textbf{(4.08)}$$

$$\beta_{DL}, \beta_{SA} < \alpha_{res} = x \diagup R_{\max} \qquad \textbf{(4.09)}$$

F was the F-stop (the ratio between sensor diameter and the effective focal length, f), which depended on the required ground resolution x (the minimum distance in which two target points could be resolved), and maximum range to target, $R_{\max}$ (distance to limb). The focal length was computed according to the focal plane array (FPA) design:

$$f = \frac{p_x \cdot p_p}{\alpha_{res}} \qquad \textbf{(4.10)}$$

p_x was pixel size (linear dimension of the detector element, which is assumed to be square) and p_p was pixel pitch (ratio of resolution image to number of pixels). The diffraction limit was based on Rayleigh criteria and ensured that at least 84% of the point source's total energy arrived at the focal plane. Spherical aberration resulted from light rays at the periphery of a spherical lens bending more strongly than those entering closer to its center.

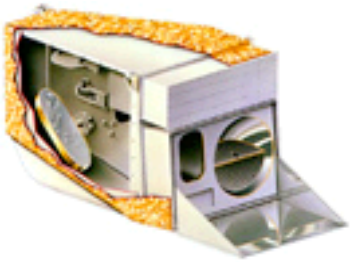

Figure 15. MODIS Instrument aboard *Terra.*

Once the aperture diameter was determined, payload mass and power could be computed by either scaling from an analogous existing system or by parametric estimating relationships. For this proof-of-concept work, the analogy approach was applied to size the acquisition sensor. The Moderate Resolution Imaging Spectroradiometer (MODIS [51]), a key instrument aboard *Terra* (a.k.a. *EOS AM-1* launched late in 1999), was the analogous system selected. It had 36 channels ranging in wavelength from 0.4 μm to 14.4 μm. A Pointing-Mirror assembly (PMA) allowed for a ±55° scanning pattern across track, providing approximately 2330 km swath. MODIS, with its 17.78 cm aperture diameter and ~38 cm effective focal length, had a mass of 250 kg and required an orbital average power of 225 W to perform its mission. The ground resolution capability for MODIS ranged between 0.25 and 1 km. The mass (M_{AS}) and power (P_{AS}) relationships were:

$$M_{AS} = \left(\frac{D_{AS}}{D_{MODIS}}\right)^2 \cdot \left(\frac{f_{AS}}{f_{MODIS}}\right) \cdot M_{MODIS} \qquad \textbf{(4.11)}$$

$$P_{AS} = \left(\frac{D_{AS}}{D_{MODIS}}\right)^4 \cdot P_{MODIS} \qquad \textbf{(4.12)}$$

The mass (M_{TS}) and power (P_{TS}) calculation for the tracking sensor utilized the parametric approach. A Mass Estimating Relationship (MER) for optical sensors was borrowed from Lomheim, et al [52]. Modification was made to

account for the slew-and-stare configuration and for the thermal control subsystem (to cool the focal planes).

$$m_{TS} = 0.8 \cdot \left(0.137 \frac{kg}{m^2} \cdot D_{TS}^2 + 0.586 \frac{kg}{m} \cdot D_{TS} + 17.8kg \right) \qquad \textbf{(4.13)}$$

With the support structure and the motors needed to point to the targets weighing approximately half the optical system, the total mass for the tracking sensor became:

$$M_{TS} = 1.5 \cdot m_{TS} \qquad \textbf{(4.14)}$$

The power calculation was based on first principles, recognizing that the major component was the power required by the motors to point the sensor assembly during the mission. The torque needed to point the LOS within the slew-and-target time (t_f) constraint was a function of mass moment of inertia of the optics assembly (I_{TS}) and the required angular acceleration of the LOS ($\ddot{\theta}_{LOS}$):

$$\tau_{TS} = I_{TS} \cdot \ddot{\theta}_{LOS} \qquad \textbf{(4.15)}$$

The mass moment of inertia was computed assuming a cylindrical assembly whose diameter and length were approximated by D_{TS} and f_{TS}, respectively:

$$I_{TS} = \frac{1}{12} \cdot m_{TS} \cdot \left(3 \cdot \left(\frac{D_{TS}}{2} \right)^2 + f_{TS}^2 \right) \qquad \textbf{(4.16)}$$

$\ddot{\theta}_{LOS}$ used the maximum angular acceleration encountered $\ddot{\theta}_{\max}$ as computed in Appendix B (with $\Delta\theta_{\max}$ and t_f specified):

$$\ddot{\theta}_{LOS} = \frac{6 \cdot \Delta\theta_{\max}}{t_f^2} \qquad \textbf{(4.17)}$$

The instantaneous power for the motor was directly proportional to the torque squared. Other than the two motors for slewing about two axes, power was also required for cooling the FPA. An estimate for the power requirement became:

$$P_{TS} = 2.1 \cdot \left(\frac{\tau_{TS}}{0.6\, N \cdot m / \sqrt{W}} \right)^2 \qquad \textbf{(4.18)}$$

The motor torque constant of 0.6 N m $W^{1/2}$ was also taken from Lomheim, et al [52].

The sensitivity equation was developed from fundamentals of radiometry [48]:

$$SNR = (MTF) \frac{\alpha_{res}}{f} \pi \left(\frac{D}{2} \right)^2 \sqrt{2 t_d}\, \Delta T \int \tau_a(\lambda) \tau_o(\lambda) D_\lambda^* \frac{\partial L_\lambda}{\partial T} d\lambda \qquad \textbf{(4.19)}$$

MTF was the modulation transfer function, whose value was assumed to be 0.7. ΔT was the change in temperature to be detected. The acquisition sensor was designed to detect missiles' hot plume during their boost phase. Thus, its SNR computations used ΔT of 800K. For the tracking sensor's sensitivity calculations, on the other hand, ΔT was set at 1K. τ_a and τ_o represented transmission losses due to the atmosphere and the optics, respectively. Both varied with wavelength. D_λ^* was the spectral specific detectivity, a property of the selected detector material that also depended on λ.

t_d in Equation (4.19) was the available detector dwell time. For the acquisition sensor, $t_{d,AS}$ was a function of the focal plane area (whose dimension was $n_{x,AS} n_{y,AS}$), the spacecraft orbit (altitude, h, and orbital period, P) and the swath width of twice the nadir angle (2η):

$$t_{d,AS} = \frac{n_{x,AS} n_{y,AS} \alpha_{res,AS}^2 h}{e_x e_y (2\eta)(2\pi R_e)} P \qquad \textbf{(4.20)}$$

e_x and e_y were scan overlap efficiencies. For the tracking sensor, $t_{d,TS}$ was computed by the number of targets n_t to be monitored within the response time available (the amount of time spent within an access area minus times for slewing, targeting and processing):

$$t_{d,TS} = \frac{1}{n_t} \cdot \left[\underbrace{\left(P \cdot \frac{2\Lambda}{2\pi} \right)}_{\text{time in access area}} - \underbrace{\left(n_t - 1 \right) \cdot t_f}_{\text{total slew-to-target time}} \right] - \underbrace{t_p}_{\text{signal processing time per target}} \qquad \textbf{(4.21)}$$

Λ was the Earth's central half-angle in Figure 14. To ensure that enough time was allotted for the detectors to receive the signals, these parameters were required to be greater than three times the detector's inherent time constant, τ_{det}:

$$t_{d,AS} > 3 \cdot \tau_{\text{det},AS} \qquad \textbf{(4.22)}$$

$$t_{d,TS} > 3 \cdot \tau_{\text{det},TS}$$

Finally, L_λ in Equation (4.19) was the blackbody spectral radiance obtained from Planck's Law:

$$E_\lambda = \frac{2\pi h_P c^2}{\lambda^5} \frac{1}{e^{ch_P / k_B T\lambda} - 1} \qquad \textbf{(4.23)}$$

E_λ was the spectral irradiance (energy per unit wavelength). h_P was Planck's constant (6.6261×10^{-34} W m^{-2} μm^{-1}), c was speed of light, k_B was Boltzmann's constant (1.381×10^{-23} W s K^{-1}) and T was the absolute temperature of the blackbody. L_λ was E_λ divided by the unit solid angle. With averaging of the integrated quantities, the sensitivity relationship simplified to [53]:

$$SNR = (MTF) \frac{\alpha_{res}}{f} \pi \left(\frac{D}{2} \right)^2 \sqrt{2t_d} \Delta T \tau_a(avg) \tau_o(avg) D_\lambda^*(avg) \frac{\Delta L}{\Delta T} \qquad \textbf{(4.24)}$$

For sizing the spacecraft bus to support the payload, a MER was developed based on data gathered on several existing spacecraft listed in Table 3. This curve-fit equation relates spacecraft bus dry mass to total payload mass and power:

$$M_{bus} = -90\,kg + 0.179 \cdot (M_{AS} + M_{TS}) + 1.757\,\frac{kg}{W} \cdot (P_{AS} + P_{TS}) \qquad \textbf{(4.25)}$$

Table 3. List of systems used to compute spacecraft bus MER.

SPACECRAFT	PAYLOAD MASS (kg)	PAYLOAD POWER (W)	SPACECRAFT BUS DRY MASS (kg)
NOAA 11	386	700	1166
ERS 2	710	800	1500
LM-900	500	300	462
SA-200S	200	60	80
SA-200B	100	75	80

Finally, the propellant mass required for station-keeping over the spacecraft's lifetime of 10 years at the range of altitudes considered was approximated by:

$$M_p = 0.1 \cdot (M_{AS} + M_{TS} + M_{bus}) \qquad \textbf{(4.26)}$$

This ignored the different drag effects with varying altitudes. The total mass of the spacecraft was therefore:

$$M_{s/c} = M_{AS} + M_{TS} + M_{bus} + M_p \qquad \textbf{(4.27)}$$

The RDT&E (R) and TFU (Theoretical First Unit, T) cost calculations were also based on aperture diameter for the sensors. For the spacecraft bus, dry mass was the important parameter. Cost Estimating Relationships (CER) published by Wong [53] were used, adjusted for FY99$M:

$$R_{sensor} = 1.249 \cdot \left(306.892 \cdot D^{0.562}\right) \quad \textbf{(4.28)}$$

$$T_{sensor} = 1.249 \cdot \left(122.758 \cdot D^{0.562}\right) \quad \textbf{(4.29)}$$

$$R_{bus} = 1.249 \cdot \left(16.253 + 0.11 \cdot M_{bus}\right) \quad \textbf{(4.30)}$$

$$T_{bus} = 1.249 \cdot \left(0.185 \cdot M_{bus}\right) \quad \textbf{(4.31)}$$

4.3 Launch Manifest

An electronic launch vehicle database was created in MS Excel. The payload capability of each vehicle for various altitudes and inclinations, launched from different sites, and for a variety of missions (e.g. circular LEO, sun-synchronous circular orbits, etc.) were obtained from their respective companies' publications (i.e., mission planner's guides [55] to [63]). The families of vehicles included were Atlas, Delta, LMLV, Pegasus, Proton and Taurus (Table 4).

The vehicles' payload capabilities were organized in tables as functions of altitude and inclination (Figure 16). Several Visual Basic for Applications (VBA) functions were coded to perform linear interpolation from the existing data points within a table. For example, given h and ϖ as the desired altitude and inclination, respectively, $s_i(h,\varpi)$, the carrying capability of vehicle i, was computed by:

$$s_i(h,\varpi_L) = s_i(h_L,\varpi_L) + \left(\frac{h-h_L}{h_U-h_L}\right)\left(s_i(h_L,\varpi_L) - s_i(h_U,\varpi_L)\right) \quad \textbf{(4.32)}$$

$$s_i(h,\varpi_U) = s_i(h_L,\varpi_U) + \left(\frac{h-h_L}{h_U-h_L}\right)\left(s_i(h_L,\varpi_U) - s_i(h_U,\varpi_U)\right)$$

$$s_i(h,\varpi) = s_i(h,\varpi_L) + \left(\frac{\varpi-\varpi_L}{\varpi_U-\varpi_L}\right)\left(s_i(h,\varpi_U) - s_i(h,\varpi_L)\right)$$

h_L, h_U, ϖ_L, and ϖ_U are the altitudes and inclinations of the data table such that:

$$h_L \le h \le h_U \qquad \textbf{(4.33)}$$

and

$$\varpi_L \le \varpi \le \varpi_U .$$

No extrapolations were allowed due to the inaccuracies that may result from projecting results beyond the range of available data.

Table 4. A listing of the launch vehicles in the database, their assumed launch prices, and samples of payload capabilities to a given orbit.

VEHICLE	PRICE PER LAUNCH (US$FY99M)	CAPABILITY (kg) TO 1600 km × 55°
Atlas IIA	85	5070
Atlas IIAS	105	6070
Atlas IIIA	90	6490
Atlas IIIB	105	7710
Delta II 7320	45	1630
Delta II 7920	55	2880
Delta III	90	5800
Delta IV DIV-M	90	6280
LMLV1 4-Tank	16	0
LMLV1 6-Tank	16	0
LMLV2 6-Tank	22	0
LMLV2B 6-Tank	26	0
Pegasus XL	14	0
Proton DM	85	4910
Taurus 4-Stage XLS	26	0
Taurus 4-Stage XL	24	0
Taurus 4-Stage Standard	22	0
Taurus 3-Stage XL	18	0

Publicly available cost data was compiled and averaged from various journals and reports [64], [65], [66]. For all of the computations presented in this thesis, it was assumed that up to eight of each type of vehicles were available to deploy the constellation within the given deployment schedule.

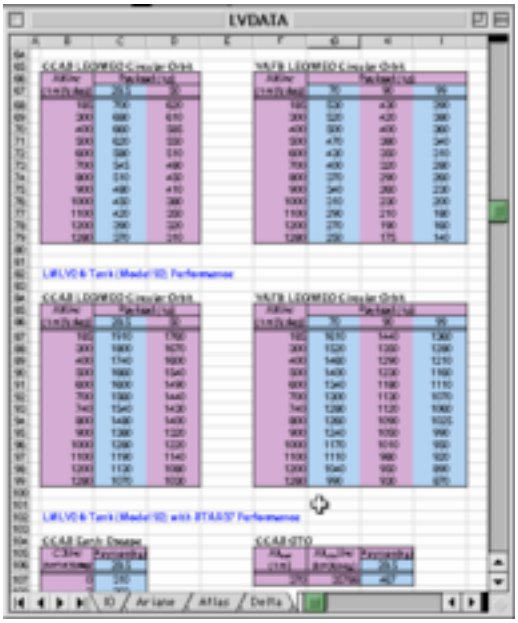

Figure 16. An example of payload capability tables in the launch vehicle database.

Assuming that spacecraft mass, mission orbit (i.e. altitude and inclination) and constellation configuration (i.e. number of planes and number of satellites per plane) were fixed, the problem could be formulated as an Integer Programming (IP) problem [67]:

$$Minimize: \qquad L = \sum_{i=1}^{m} c_i \cdot \sum_{j=1}^{n} \alpha_{ij} \qquad \textbf{(4.34)}$$

$$Subject\ to: \qquad \sum_{j=1}^{n} \alpha_{ij} \le A_i, \ for\ i = 1,...,m$$

$$\sum_{i=1}^{m} s_{ij} \cdot \alpha_{ij} \ge Z_j, \ for\ j = 1,...,n$$

$$\alpha_{ij} = \text{int}$$

α_{ij} was the flight rate for vehicle i to plane j. A_i was the number of available flights for vehicle i. s_{ij} was launch vehicle i's payload capability to plane j. Z_j was the required number of satellites to be deployed to plane j. Finally, the objective function, L, was total launch cost, which was a function of flight rates and c_i (price per flight for vehicle i).

This IP formulation for the launch manifest problem assumed that no vehicle was capable of multiple plane insertion on a single flight. Thus, each launch was designated to inject all of the satellites aboard into a single orbital plane. Publicly available software, LPSolve 2.3, was obtained and compiled on a Sun workstation to find the solution to the IP problem by branch-and-bound technique [68]. To create an interface between this C program and the database, a VBA procedure was written to create the input text file required by the solver and to read and parse the output file for the solution.

CHAPTER V

THE PRELIMINARY PROBLEM

Some proof-of-concept experiments for the design and deployment of a space-based infrared system were completed with promising results. At this preliminary stage, certain simplifications were allowed. The constellation configuration was fixed as a Walker delta pattern of four planes and seven satellites per plane with relative spacing of two (a 28/4/2 Walker constellation). This determines all of the spacecraft orbits to be circular, at a common altitude and inclination, and with their lines of nodes symmetrically positioned around the equator. One on-orbit, in-plane spare satellite resulted in a total of 8 satellites per plane, 32 units in all, to be deployed. Direct injections of the spacecraft by the launch vehicles were assumed.

The payload design concept (two sets of sensors per spacecraft similar to the current concept for SBIRS Low) was fixed. With these discrete parameters kept constant during each optimization process, the design problem is still sufficiently complex. The optimization objective was to find the mission orbit (altitude and inclination), the spacecraft design (sensor size and spacecraft mass), and launch strategy with the minimum cost through deployment, consisting of RDT&E (Research, Design, Testing and Development), production and launch costs.

The acquisition sensors were required to provide aggregately a continuous global coverage up to 30 km above the horizon with their cross-track whiskbroom imaging mode. The spatial (ground) resolution requirements (x), defined as the minimum distance within which two target points can be

resolved, were selected to be 0.4 km and 0.3 km at the limb for the acquisition and tracking sensors, respectively. Sensitivity is measured by the Signal-to-Noise ratio (SNR). For this type of mission, SNR of at least 10 dB is needed.

The CO implementation to this preliminary problem and the result found by this method is first discussed in this chapter, beginning with the formulation and optimization techniques for the subspace and system-level problems. Next, implementation of the All-at-Once method is explained and the converged solution is presented. Finally, a comparison of the results and processes is conducted.

5.1 Collaborative Optimization

The implementation details of the collaborative optimization method to the constellation design process are discussed in this section. Figure 17 illustrates the resulting multilevel architecture. The subsystems are shown separated into an optimizer and an analysis module. Each is independent of the others, allowing for parallel computations.

5.1.1 Configuration and Orbit Design Formulation and Approach

Some reformulation of the problem was required in implementing the collaborative optimization architecture. With the current process, the constellation design module was provided with information about the sensors' coverage capabilities (beam size). Using this input, it found the most efficient constellation configurations (i.e., one with the fewest satellites) and mission orbits that satisfied, or even maximized, some performance criteria, such as coverage [42], by a complex grid search.

Within CO, the constellation design module kept control over local versions of the n_1 coupling variables (altitude, inclination, and acquisition sensor's field-of-view half-angle). Each variable was normalized by the corresponding multiplier on Table 5 and became a component of the vector $\bar{y}_1 \ni \bar{y}_1 \in \Re^{n_1}$. For

this preliminary case, no other local variables were involved ($\bar{\psi}_1 \in \Re^0$). The system optimizer provided normalized target values $\bar{z}_1 \ni \bar{z}_1 \in \Re^{n_1}$ ($\bar{z}_1 \subset \bar{z}$, where $\bar{z}$ is the aggregate system-level variables of n-dimensions) for $\bar{y}_1$, which also formed the subspace objective function J_1. Thus, the task of the subspace optimizer was to minimize the differences between the target and the actual values of the local versions by varying the local variables $\bar{y}_1$:

$$\min_{\bar{y}_1}\{J_1\} = \min_{\bar{y}_1}\left\{\left\|\bar{y}_1 - \bar{z}_1\right\|^2\right\} \qquad \textbf{(5.01)}$$

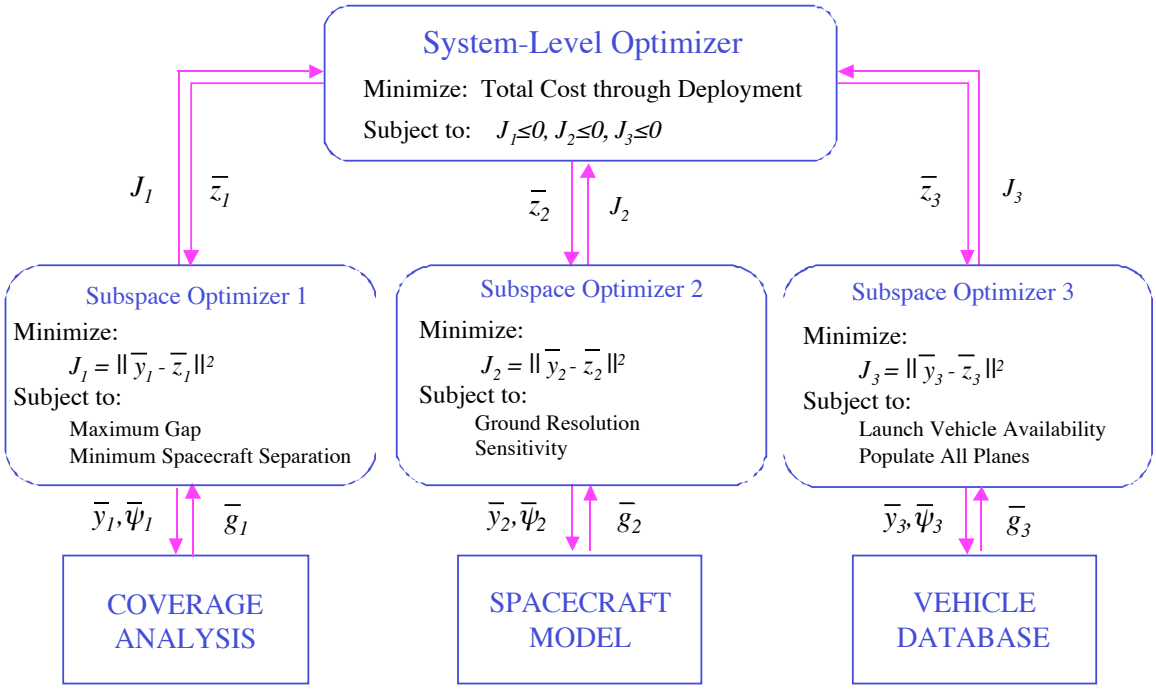

Figure 17. Details on the CO implementation to the demonstration example.

Maximum gap and minimum satellite approach distance were the local constraints. In this case, the requirement was a continuous one-fold global coverage at the 30 km burnout altitude. The minimum separation distance of 150 km was needed to ensure no collision and to prevent signal interference between satellites.

The built-in Matlab optimizer, which used Sequential Quadratic Programming (SQP) methods, failed at producing consistent solutions for this constellation design sub-problem. This was due to the complex nature of the problem. The surface plot in Figure 18 illustrated a border for the feasible design space for this particular Walker delta pattern. The combinations of altitude, inclination and beam angle that can satisfy the coverage requirements were those points located on or above this surface, whose shape was highly nonlinear. Furthermore, the minimum spacecraft approach distance added to the complexity of the problem as shown in Figure 19. The constraints, represented by the shaded areas, caused the design space to be non-convex.

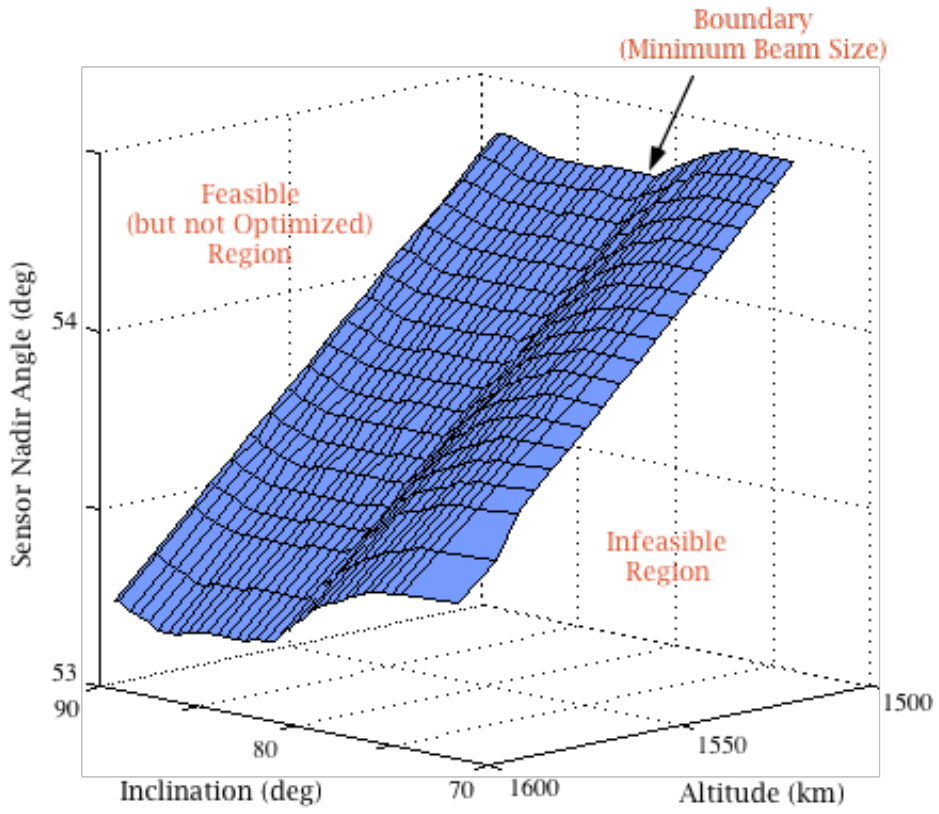

Figure 18. Surface plot of the minimum beam size required for continuous 1-fold coverage versus altitude and inclination.

Grid search [68] was chosen to be the subspace optimization method within the collaborative architecture. This is similar to the search method used in the

current process. Due to the computationally intensive nature of each run of the coverage analysis program, a set of heuristics was employed to help narrow down the search space and to guide the solution-finding process. For example, if the target beam size was lower than the minimum required for the given target altitude and inclination (Figure 18), then the rule of thumb was to stay on this minimum beam size constraint contour. Altitude and inclination were varied to find a combination that minimized J_1.

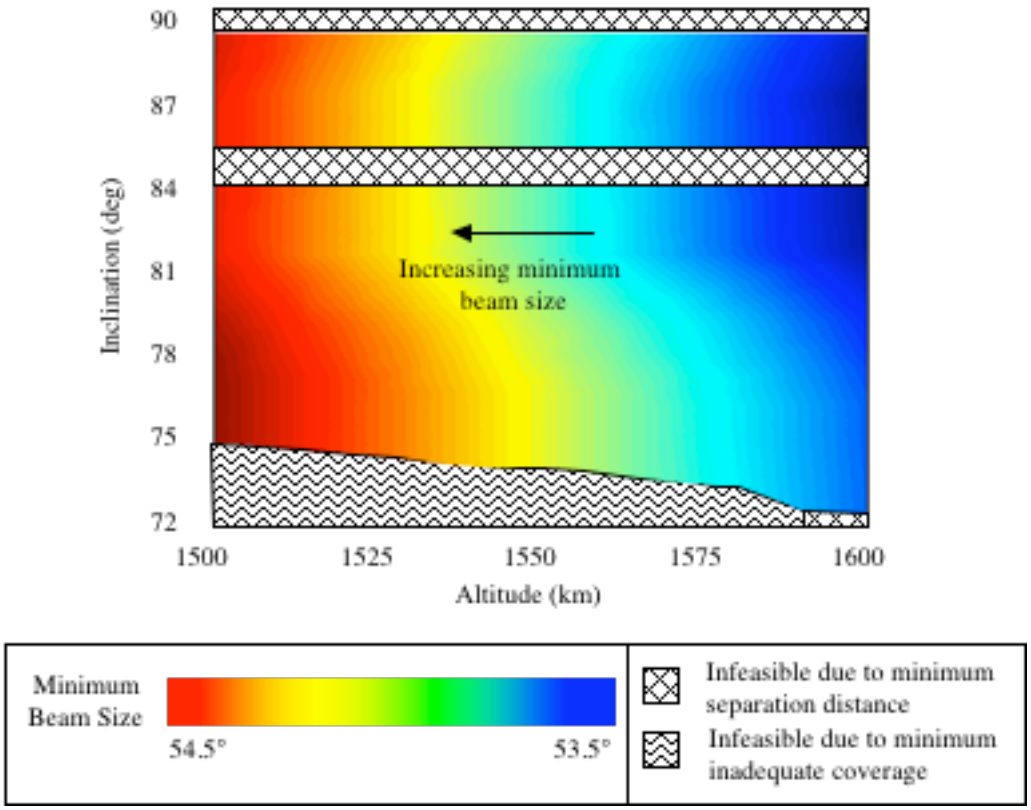

Figure 19. Minimum beam size contour superimposed with constraints.

5.1.2 *Spacecraft Design Formulation and Approach*

The spacecraft model sized the infrared payload and designed the bus to support these instruments for a specified mission orbit. Ordinarily, the subspace optimization here involved a trade-off between maximizing the sensors' performance parameters (resolution and/or sensitivity) without

demanding a spacecraft bus that is too large and costly. Within the collaborative environment, on the other hand, the module had the freedom to alter its mission orbit and retained control of its local variables $\overline{\psi}_2$ (e.g., pixel size, aperture diameter, etc.). It received from the system level a target for altitude, sensor size, spacecraft mass, and cost parameters (RDT&E and TFU), represented as the n_2-dimensional vector $\bar{z}_2$. Again, $\bar{z}_2$ was a subset of $\bar{z}$. Local versions for these variables were created, comprising the single vector $\bar{y}_2$. The subspace optimizer's task, then, was to meet the target values provided by the system optimizer as best as possible, by varying the local variables $\bar{y}_2 \cup \overline{\psi}_2$, while satisfying local constraints such as sensitivity and resolution requirements:

$$\min_{\bar{y}_2, \overline{\psi}_2} \{J_2\} = \min_{\bar{y}_2, \overline{\psi}_2} \left\{ \left\| \bar{y}_2 - \bar{z}_2 \right\|^2 \right\} \qquad \textbf{(5.02)}$$

subject to

$$g_{2,i}(\bar{y}_2, \overline{\psi}_2) \le 0, \quad i = 1, \ldots, m_2 \qquad \textbf{(5.03)}$$

The spacecraft design's optimization process employed a combination of Genetic Algorithm (GA [69]) and MS Excel's Solver to find a good solution. GA's advantage is in finding good solutions for a multi-modal problem, or one with intrinsic non-linearities and discontinuities. It had been applied (or proposed to be applied) to various problems, including constellation coverage-based "optimization" [70], [71], launch vehicle design [72], vehicle cost study [73], and spacecraft design [74], [75].

Evolver, a Windows-based GA add-in for MS Excel, was allowed to change the values for aperture diameters, minimum elevation angle (which determined sensor's field of view), and pixel sizes (dictated focal length f as shown in Equation (4.10)) to find a good value for J_2. The Solver's main task was to find

the local minimum with the same set of variables, given a good initial point found by GA.

For this proof of concept work, the acquisition sensor's aperture diameter was designed to give the specified resolution at 4 μm. Its detector array was fixed to be a 256 by 256 pixels of PbSe (Lead Selenide) with pixel pitch p_p of 1.5, leaving pixel size p_x as the main variable for changing the focal plane design. The time constant, τ_{det}, of the detector material of choice was 25 μs and required an operating temperature of 193K. At a wavelength of 4 μm, the average specific detectivity D_λ^* was 2.25 cm $\text{Hz}^{1/2}\,\text{W}^{-1}$. The tracking system was designed for the far infrared wavelength of 11 μm. It used a 512 x 512 detector array. The detector material selected was HgCdTe (Mercury Cadmium Telluride) cooled to 77K with τ_{det} of 0.5 μs and D_λ^* of 4 cm $\text{Hz}^{1/2}\,\text{W}^{-1}$.

5.1.3 Launch Manifest Formulation and Approach

The launch manifest problem was to find the strategy with the minimum total launch cost. In the typical constellation design process, the launch manifest subsystem was given the spacecraft mass, mission orbit, and constellation configuration (number of planes and number of satellites per plane). The problem could thus be formulated as an Integer Programming (IP) problem as explained in Chapter V. In CO, however, the subspace optimizer was allowed to vary the local versions of these parameters. The optimization problem became a minimization of the discrepancies between the target and local values for these interdisciplinary coupling variables (mission orbit and spacecraft unit mass for this preliminary work) and the total launch cost:

$$\min_{\bar{y}_3,\bar{\psi}_3}\left\{J_3\right\} = \min_{\bar{y}_3,\bar{\psi}_3}\left\{\left\|\bar{y}_3 - \bar{\bar{z}}_3\right\|^2\right\},\ (\bar{\bar{z}}_3 \subset \bar{\bar{z}}) \qquad \textbf{(5.04)}$$

This reformulation caused the problem to be no longer linear, more challenging, and unsolvable by IP alone. Launch rates α_{ij} comprised the local

variable vector ($\overline{\psi}_3$), and launch vehicle availability and capabilities formed the local constraints. A two-step hybrid scheme was developed as the subspace optimization technique. First, IP was used to find the best launch strategy using the target values $\overline{z}_3 \in \Re^{n_3}$. Next, a search through the candidate vehicles determined whether or not alternative strategies existed that could result in lower total launch cost (and therefore improved J_3) allowing some deviations in $\overline{y}_3$ from their target values. If other options existed, a univariate search was performed to reduce altitude, inclination, and/or satellite mass to gain better J_3 by possibly fitting the constellation into smaller but less expensive vehicles.

5.1.4 System Optimization Formulation and Approach

At the system level, an optimizer coordinated the overall process by selecting target values for all the interdisciplinary variables $\overline{z} \in \Re^n$. The allowable ranges for these variables (side constraints) are summarized in Table 5, along with their initial values and the constant multipliers used to normalize them. Additionally, the system optimizer was required to satisfy the compatibility constraints, such that J_1, J_2, and J_3 had zero values in the final solution. The objective function, $F(\overline{z})$, was the total cost through deployment:

$$F(\overline{z}) = L_0 + R_0 + T_0\left(\sum_{i=0}^{\gamma}(2g)^i + \mathrm{K}g^{\gamma+1}\right), (L_0, R_0, T_0 \in \overline{z}) \qquad \textbf{(5.05)}$$

L_0, R_0, and T_0 were target values chosen by the system optimizer for total launch cost, RDT&E and TFU spacecraft costs, respectively. The last term in Equation 5.05 was the total production cost, where given N total number of units produced (in this case, $N = 32$, including 4 spares) and a learning rate effect g ($g = 0.9$ was used throughout this study), γ was an integer constant such that:

$$\sum_{j=0}^{\gamma} 2^j < N \leq \sum_{j=0}^{\gamma+1} 2^j \qquad \textbf{(5.06)}$$

and

$$\mathrm{K} = N - \sum_{j=0}^{\gamma} 2^j . \qquad \textbf{(5.07)}$$

An exterior penalty function strategy was chosen to handle the compatibility constraints. This indirect method allowed a constrained optimization problem to be treated as if unconstrained by penalizing the objective function for any violations:

$$\min_{\bar{z}} \left\{ \Phi_k \right\} = \min_{\bar{z}} \left\{ F(\bar{z}) + r_k \left(J_1(\bar{z}) + J_2(\bar{z}) + J_3(\bar{z}) \right) \right\} \qquad \textbf{(5.08)}$$

With this technique, the transformed problem Φ was sequentially minimized over several system-level iterations indicated by k. Within each system-level iteration, r_k was held constant. As k was increased, however, so did r_k, penalizing more heavily for violated constraints (i.e., non-zero J_i):

$$r_{k+1} = C_r \cdot r_k , \; C_r > 1.0 \qquad \textbf{(5.09)}$$

For this study, the value used for C_r was 5.0.

Powell's method with three point quadratic approximation along each line search [68], [76] was used to minimize the Φ function at each system-level iteration, k. This was a zero-order optimization technique, and therefore required no gradient information. Powell's method was also fairly easy to implement, but may require many function evaluations to converge. It first searched for improved solutions in the n orthogonal directions, corresponding to the n variables involved, and updated $\bar{z}$. A conjugate direction, formed by connecting the starting and final design points, became a new search direction. This process was continued until convergence was found for iteration k.

Quadratic approximation is a one-dimensional optimization technique used to find the minimum at each search direction in Powell's method. It required function evaluations at three points and fitted a quadratic polynomial to these known points. The minimum of this fitted function was analytically found, and was considered a good approximation of the true minimum.

Table 5. Summary of the system-level variables for the CO implementation in the preliminary problem.

VARIABLES	RANGE OF VALUES	INITIAL VALUES	NORMALIZING MULTIPLIERS
Orbit Altitude	1400 km - 1700 km	1600 km	0.001
Orbit Inclination	50° - 90°	55°	0.017453
Spacecraft Unit Mass	500 kg – 1500 kg	700 kg	0.001
Sensor Field of View	50° - 55°	55°	0.017453
Total Launch Cost*	$100M - $1000M	$100M	1.25×10^{-7}
Spacecraft RDT&E Cost*	$200M - $500M	$200M	1.25×10^{-7}
Spacecraft TFU Cost*	$100M - $500M	$100M	1.25×10^{-7}

*US Fiscal Year 1999 Dollars

Table 6. Summary of CO's implementation to the preliminary problem.

DESIGN MODULE	VARIABLES	CONSTRAINTS	OBJECTIVE FUNCTION	OPTIMIZATION SCHEME
Configuration & Orbit Design	Altitude Inclination Sensor FOV	Global Continuous One-Fold Coverage Closest Approach Distance > 150 km	J_1	Grid Search + Heuristics
Spacecraft Design	Altitude Sensor FOV Minimum Elevation Aperture Diameter Pixel Size	SNR > 10 dB Angular Blur < Required Resolution Dwell Times > $3\tau_{det}$ (detector's time constant)	J_2	Genetic Algorithm + Solver
Launch Manifest	Altitude Inclination Spacecraft Unit Mass Flight Rates	Launch Vehicle Availability Complete Population of Specified Constellation	J_3	Integer Programming + Heuristics
System Design	Altitude Inclination Sensor FOV Spacecraft Unit Mass Total Launch Cost Spacecraft RDTE Cost Spacecraft TFU Cost	$J_1 = 0$ $J_2 = 0$ $J_3 = 0$	Total Cost through Deployment (F)	Penalty Function using Powell's Method with Quadratic Approximation

5.1.5 Collaborative Optimization Preliminary Results

The converged design for the 28/4/2 constellation configuration using collaborative optimization was obtained after 9 system-level iterations. Each of these consisted of several Powell's method sub-iterations of $n+1$ search directions, which changed the system target values. A single system-level iteration was considered complete when the convergence criteria for the unconstrained problem were met (i.e., when changes in the variables and objective function were less than the set tolerances). The overall optimization process adopted similar convergence criteria.

The given initial condition was found to be infeasible by all three design modules. The coverage requirement was not satisfied with the given configuration and mission orbit. Furthermore, the spacecraft design and launch manifest modules were unable to meet the cost targets.

Figure 20 through Figure 23 plot the progression of the system-level variables, depicting the negotiations occurring between the disciplines. Altitude was the only variable involved in all three sub-problems. For this particular example, the launch manifest module well matched the target altitude, inclination and mass given by the system optimizer throughout the process. The constellation design module, on the other hand, preferred higher altitude and drove the inclination and sensor view angles up to satisfy the coverage requirements.

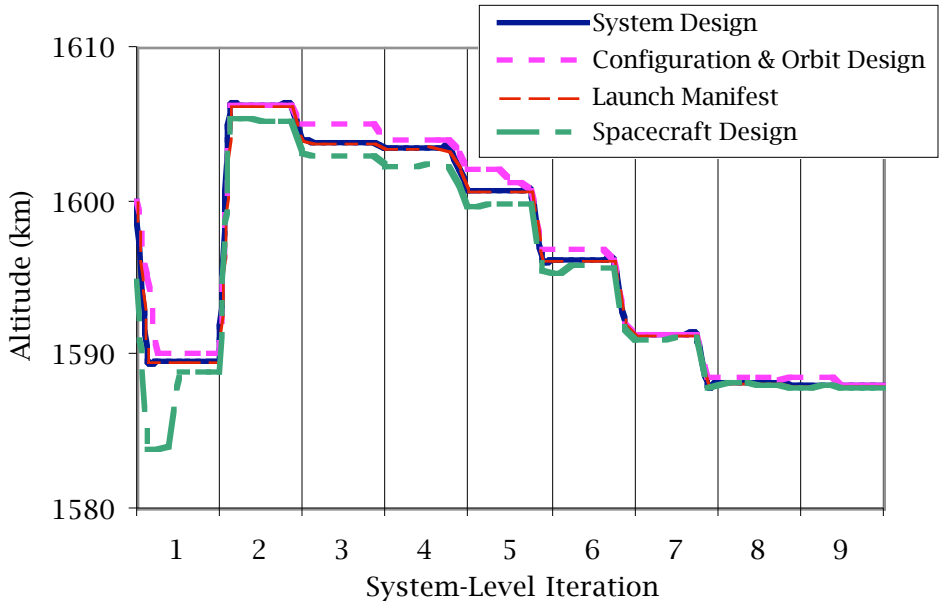

Figure 20. Progression of altitude within the collaborative architecture.

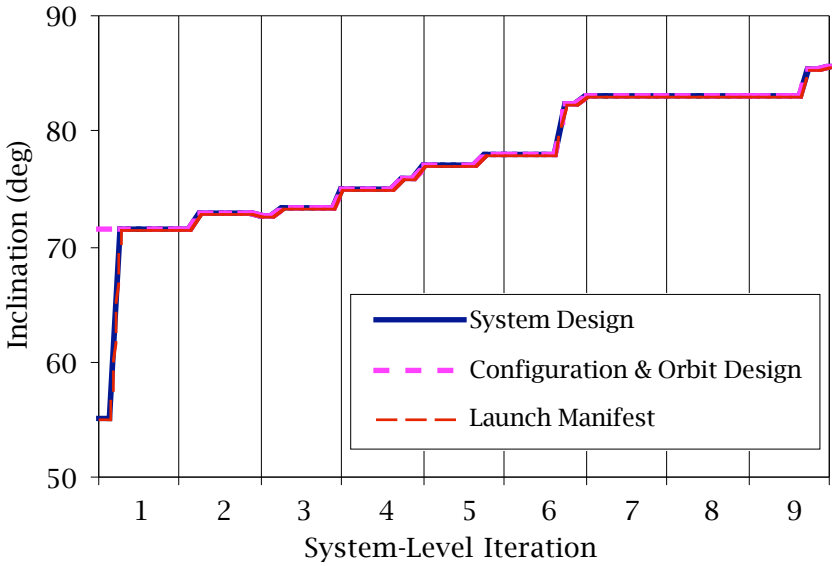

Figure 21. Progression of inclination angle within the collaborative architecture.

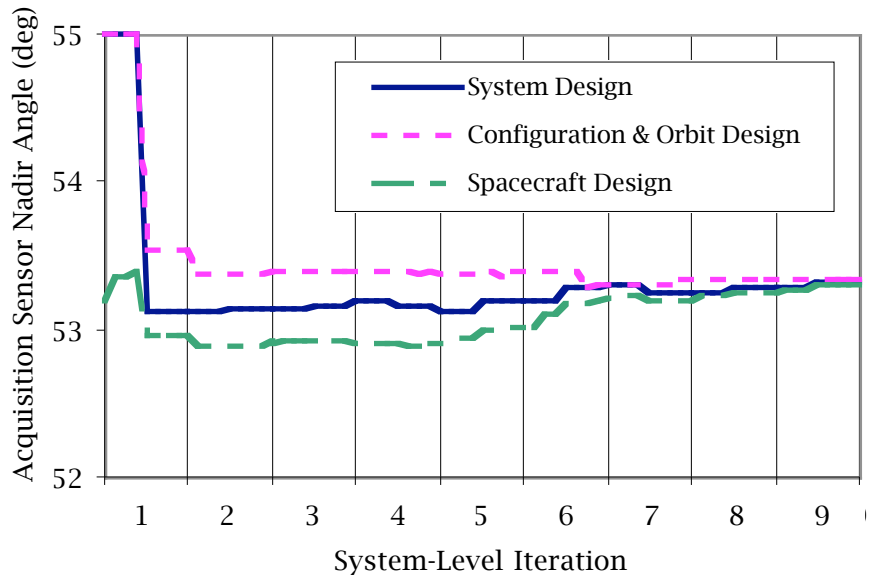

Figure 22. Progression of nadir angle (swath width) for acquisition sensor within the collaborative architecture.

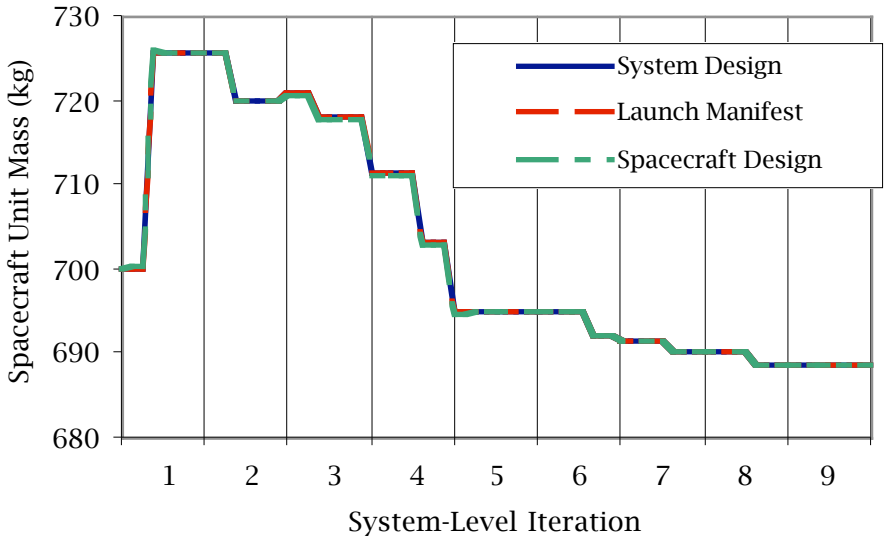

Figure 23. Progression of spacecraft unit mass within the collaborative architecture.

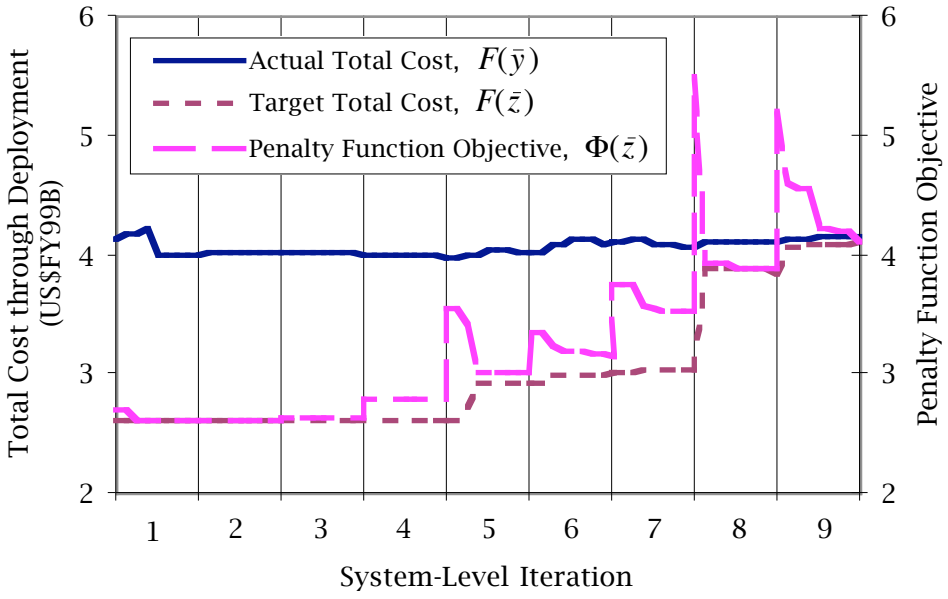

Figure 24. Progression of the total cost through deployment and the penalty function objective Φ within the collaborative architecture.

The cost targets stayed level until iteration 4, at which time, the penalty function multiplier r_k had finally become large enough to allow the compatibility constraints greater influence on the direction of the optimization process (note the jumps in the values of Φ in Figure 24 due to increased r_k at the beginning of each system-level iteration). Previous to this point, the quadratic approximation tried to drive the cost variables R_0, L_0, and T_0 to negative values, activating the side constraints.

In the converged design, the target total cost finally arrived within 1% of the actual cost computed by the individual analysis modules (Figure 24). The discrepancies between the local versions of the coupling variables also fell below 1% for the final solution. These tolerances are considered appropriate given the level of fidelity of the analysis programs used.

5.2 All-At-Once Method

5.2.1 Problem Formulation

An alternative method using the All-At-Once (AAO) formulation of the preliminary problem was implemented as a distributed analysis architecture. Unlike CO (a distributed *optimization* architecture), AAO eliminated the subspace optimization problems. The subsystems were simply required to produce analyses as dictated by the system optimizer. Thus, all of the variables and constraints of the problem became the responsibility of the system optimizer. However, parallel execution of the analyses was still possible with this technique.

Table 7 presented a list of all the variables for this AAO problem along with their bounds and initial values. As shown, a larger more complex system-level optimization problem involving a mixture of continuous and integer variables resulted. Unlike CO, to maintain a manageable problem, some elimination of the launch options was needed prior to the AAO optimization, leaving only the five vehicles listed in Table 7. The preliminary problem to be solved remained nonlinear, and using AAO method became:

$$\min_{\bar{x}} \left\{ F(\bar{x}) \right\} \tag{5.10}$$

subject to

$$h(\bar{x}) = 0 \tag{5.11}$$

$$g_i(\bar{x}) \leq 0, \quad i = 1, \ldots, m \tag{5.12}$$

$$\bar{x} = \begin{bmatrix} x_1 \\ \vdots \\ x_n \end{bmatrix} = \begin{bmatrix} \bar{x}^c \\ \bar{x}^d \end{bmatrix} \tag{5.13}$$

Table 7. Summary of system-level variables for All-At-Once formulation of the preliminary problem.

NAME	TYPE	LOWER BOUND	UPPER BOUND	INITIAL VALUE
Orbit Altitude (km)	Continuous	1400	1700	1600
Orbit Inclination (deg)	Continuous	50	90	86
AS Field of View (deg)	Continuous	50	55	53.29
AS Aperture Diameter (m)	Continuous	0.06	0.15	0.11
TS Aperture Diameter (m)	Continuous	0.30	0.50	0.42
AS Pixel Size (μm)	Continuous	30	200	31
TS Pixel Size (μm)	Continuous	30	200	92
No. Atlas IIA for Plane 1	Discrete	0	2	0
No. Atlas IIA for Plane 2	Discrete	0	2	0
No. Atlas IIA for Plane 3	Discrete	0	2	0
No. Atlas IIA for Plane 4	Discrete	0	2	0
No. Atlas IIIA for Plane 1	Discrete	0	2	0
No. Atlas IIIA for Plane 2	Discrete	0	2	0
No. Atlas IIIA for Plane 3	Discrete	0	2	0
No. Atlas IIIA for Plane 4	Discrete	0	2	0
No. Atlas IIIB for Plane 1	Discrete	0	2	1
No. Atlas IIIB for Plane 2	Discrete	0	2	1
No. Atlas IIIB for Plane 3	Discrete	0	2	1
No. Atlas IIIB for Plane 4	Discrete	0	2	1
No. Delta 7920 for Plane 1	Discrete	0	2	1
No. Delta 7920 for Plane 2	Discrete	0	2	1
No. Delta 7920 for Plane 3	Discrete	0	2	1
No. Delta 7920 for Plane 4	Discrete	0	2	1
No. Proton-DM for Plane 1	Discrete	0	2	0
No. Proton-DM for Plane 2	Discrete	0	2	0
No. Proton-DM for Plane 3	Discrete	0	2	0
No. Proton-DM for Plane 4	Discrete	0	2	0

Table 8. Summary of the constraints involved in the AAO problem.

NAME		FORMULATION
Maximum Coverage Gap	=	0.0
Closest Approach Distance	≥	150 km
AS Sensitivity	≥	10.0 dB
TS Sensitivity	≥	10.0 dB
AS Diffraction Limit	≥	AS Angular Resolution
TS Diffraction Limit	≥	TS Angular Resolution
AS Spherical Aberration	≥	AS Angular Resolution
TS Spherical Aberration	≥	TS Angular Resolution
AS Dwell Time	≥	AS Detector's Limit
TS Dwell Time	≥	TS Detector's Limit
AS F#	≤	10.0
TS F#	≤	10.0
AS Pixel Size	≥	30 μm
Total No. Atlas IIA Launches	≤	8
Total No. Atlas IIIA Launches	≤	8
Total No. Atlas IIIB Launches	≤	8
Total No. Delta 7920 Launches	≤	8
Total No. Proton-DM Launches	≤	8
No. of Satellites Deployed in Plane 1	≥	8
No. of Satellites Deployed in Plane 2	≥	8
No. of Satellites Deployed in Plane 3	≥	8
No. of Satellites Deployed in Plane 4	≥	8

$F(\bar{x})$ was the original objective function, which was total cost through deployment. $\bar{x}$ was the independent variable vector, consisting of n_c continuous ($\bar{x}^c \in \Re^{n_c}$) and n_d discrete ($\bar{x}^d \in \Omega_d^{n_d} \in \Re^{n_d}$) components. These were listed in Table 7 along with their corresponding limit values. $h(\bar{x})$ was the equality constraint for zero maximum gap. $g_i(\bar{x})$ consisted of all m inequality

constraints, such as sensitivity, angular blur, and launch vehicles availability. Table 8 listed these constraints in more detail.

Several methods had been proposed for solving nonlinear mixed-integer programming problems [68], but none could guarantee global optimality. Gisvold and Moe modified the interior penalty function by treating the discrete decision parameters as continuous and attaching a penalty term if these variables had non-integer values [78]. As a result, standard continuous optimization techniques could be used for solving mixed integer problems. This approach was chosen as the AAO optimization scheme. The transformed problem, which included the original $F(\bar{x})$, became:

$$\min_{\bar{x}} \left\{\Phi_k(\bar{x})\right\} = \min_{\bar{x}} \left\{F(\bar{x}) + q_k h(\bar{x}) + r_k I_k(g_i(\bar{x})) + s_k Q_k(\bar{x}^d)\right\} \qquad \textbf{(5.14)}$$

q_k provided the weighting factor for the equality constraint penalty function, $h(\bar{x})$. k indexed the system-level iterations. $I_k(g_i(\bar{x}))$ was a scalar equation composed of the inequality constraints:

$$I_k(g_i(\bar{x})) = \sum_{i=1}^{m} \frac{1}{g_i(\bar{x})} \qquad \textbf{(5.15)}$$

r_k was the multiplier for this inequality constraint penalty function. Finally, s_k was the weighting factor for the discretization penalty term, $Q_k(\bar{x}^d)$, which had the property that:

$$Q_k(\bar{x}^d) = \begin{cases} 0, \; if \; \bar{x}^d \in \Omega_d^{n_d} \\ b > 0, if \; \bar{x}^d \notin \Omega_d^{n_d} \end{cases} \qquad \textbf{(5.16)}$$

Following [78], the function used for this problem was:

$$Q_k(\bar{x}^d) = \sum_{j=1}^{n_d} \left\{ 4\left(\frac{x_j^d - \sigma_j^L}{\sigma_j^U - \sigma_j^L}\right)\left(1 - \frac{x_j^d - \sigma_j^L}{\sigma_j^U - \sigma_j^L}\right)\right\}^{\xi_k} \qquad \textbf{(5.17)}$$

where σ_j^L and σ_j^U were the neighboring discrete points for $x_j^d \in \bar{x}^d$:

$$\left\{\sigma_j^L \le x_j^d \le \sigma_j^U ; \sigma_j^L, \sigma_j^U \in \Omega_d^{n_d}\right\} \qquad \textbf{(5.18)}$$

$Q_k(\bar{x}^d)$ in Equation (5.16) was a normalized (maximum value of 1.0), symmetrical Beta-function integrand and is illustrated in Figure 25 for several values of ξ_k $(\sigma_j^L = 0, \sigma_j^U = 1)$. For this function to be continuous in its first derivative, ξ_k ought to be greater than 1.0. As $k \to \infty$, ξ_k was decreased such that:

$$\xi_{k+1} = C_\xi \cdot \xi_k, C_\xi < 1.0 \qquad \textbf{(5.19)}$$

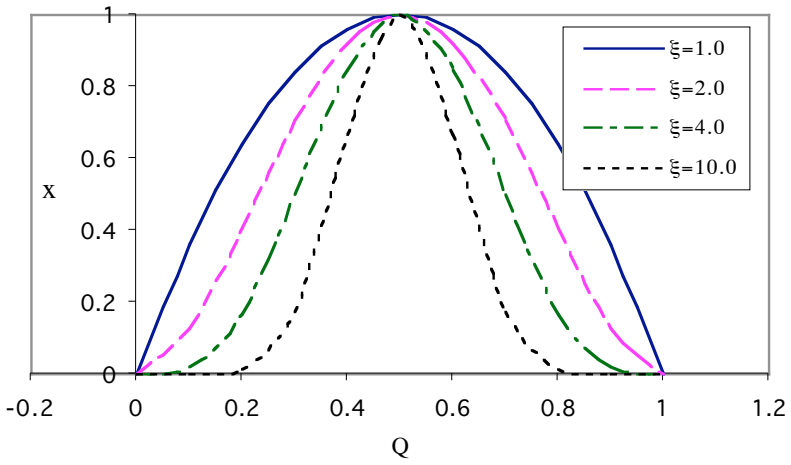

Figure 25. Single-variable Beta function for several values of ξ parameter.

Similar to the exterior penalty function method described previously, the transformed objective function $\Phi_k(\bar{x})$, was minimized at each iteration k, within which the weighting factors q_k, r_k, and s_k and the parameter ξ_k were held constant. Powell's method with quadratic approximation was again chosen as the system optimization technique. As $k \to \infty$, r_k and ξ_k were sequentially reduced, while q_k and s_k had increasing values. That is,

$$q_{k+1} = C_q \cdot q_k, C_q > 1.0 \quad \textbf{(5.20)}$$

$$r_{k+1} = C_r \cdot r_k, C_r < 1.0$$

$$s_{k+1} = C_s \cdot s_k, C_s > 1.0$$

The guidelines provided in [68] and [78] for selecting initial values for these weighting factors were followed, along with suggested values for the constant multipliers C_ξ, C_r, and C_s. That is, C_ξ, C_r, and C_s were given the values 0.9, 0.3, and 4.5, respectively. Since no equality constraints were treated in previous studies, C_q was obtained empirically to keep the solution at each iteration from straying too far into the infeasible region due to insufficient penalty on the equality constraint $h(\bar{x})$. The relation used for determining C_q was:

$$C_q = \frac{14 - 2k}{\sqrt{r_{k+1}}} \quad \textbf{(5.21)}$$

5.2.2 All-At-Once Preliminary Results

Figure 26 through Figure 31 illustrated the progression of the system-level variables. Plots of the output variables were given in Figure 32 through Figure 36, where a smooth progression to a constellation of smaller and less expensive spacecraft was observed. Convergence using the All-At-Once formulation was found after 8 system-level iterations. As shown, however, past the fifth iteration most of the changes occurred in the spacecraft instrument level, refining the optics and focal plane designs. Similar to the collaborative case, the iteration process was stopped when the variables and the objective function showed negligible improvements.

The interior penalty function method required that the initial design was feasible with respect to the inequality constraints $g_i(\bar{x})$ and drove the solution away from these constraint boundaries in the first few iterations. The coverage

gap requirement was relaxed until the fourth iteration where the weighting factor for its penalty term overcame that of the inequality constraints (i.e., $q_k h(\bar{x}) > r_k I_k(g_i(\bar{x}))$). The constraint boundaries were gradually approached, as was most evident, for example, in Figure 30 where the detector pixel size neared the minimum value of 30 μm (Table 8) in the final iterations.

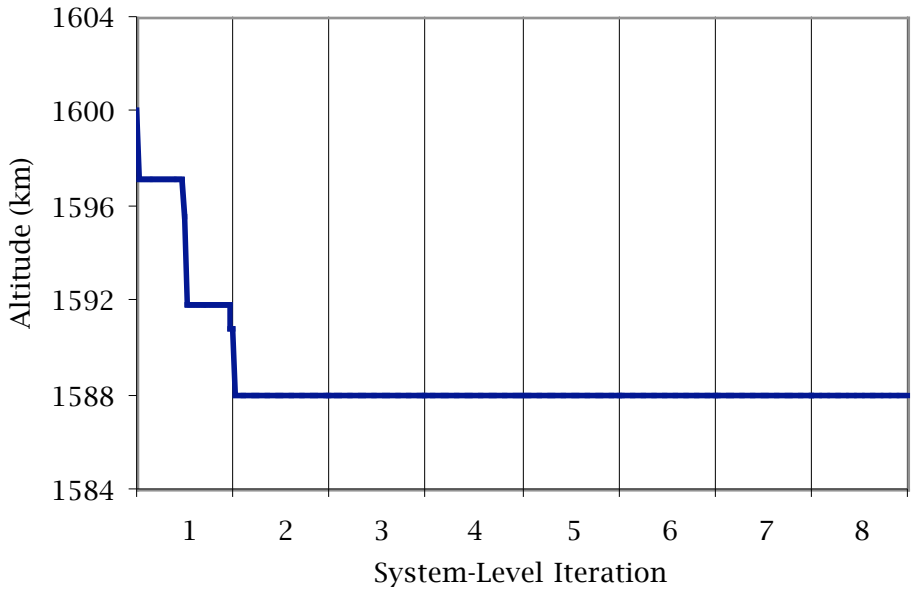

Figure 26. Progression of altitude, with All-At-Once method.

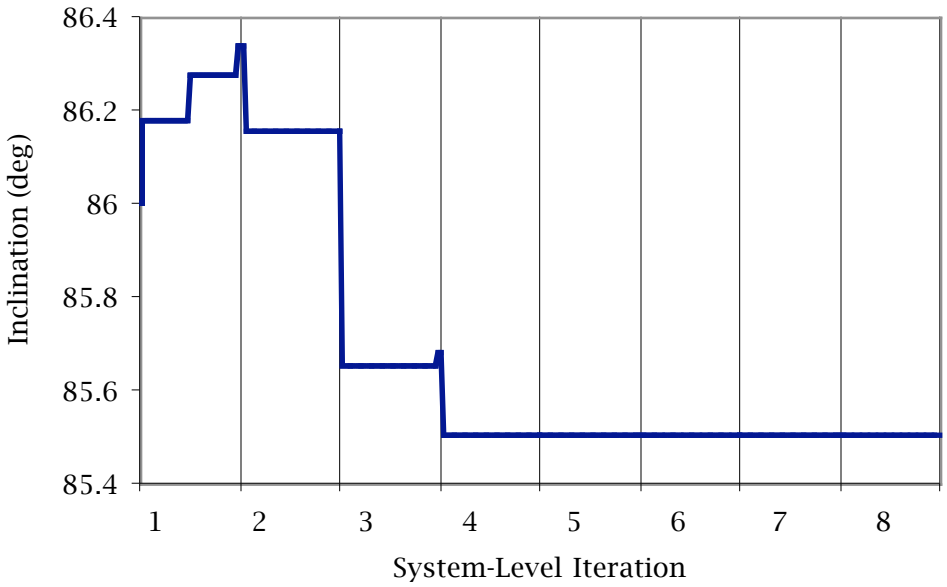

Figure 27. Progression of inclination, with All-At-Once method.

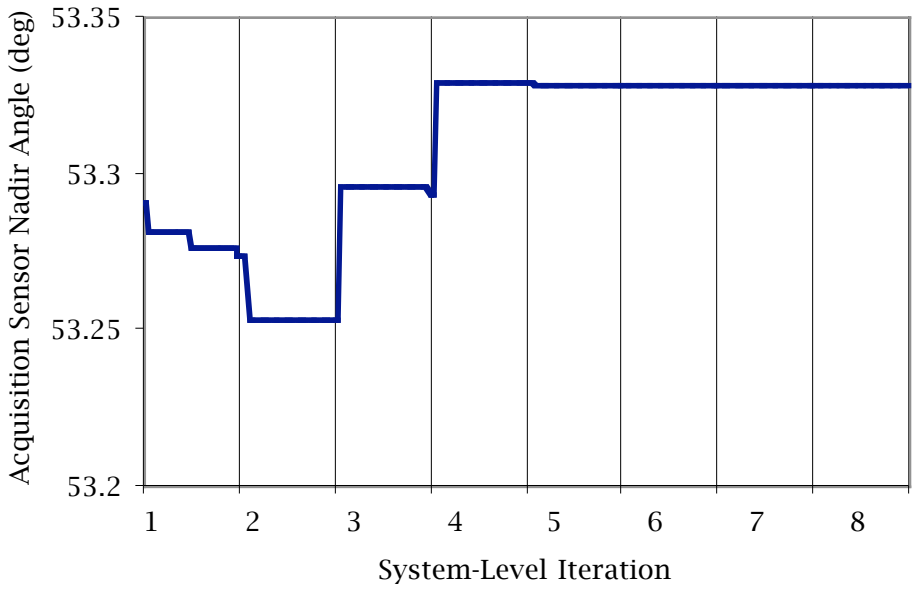

Figure 28. Progression of nadir angle for the acquisition sensor, with All-at-Once method.

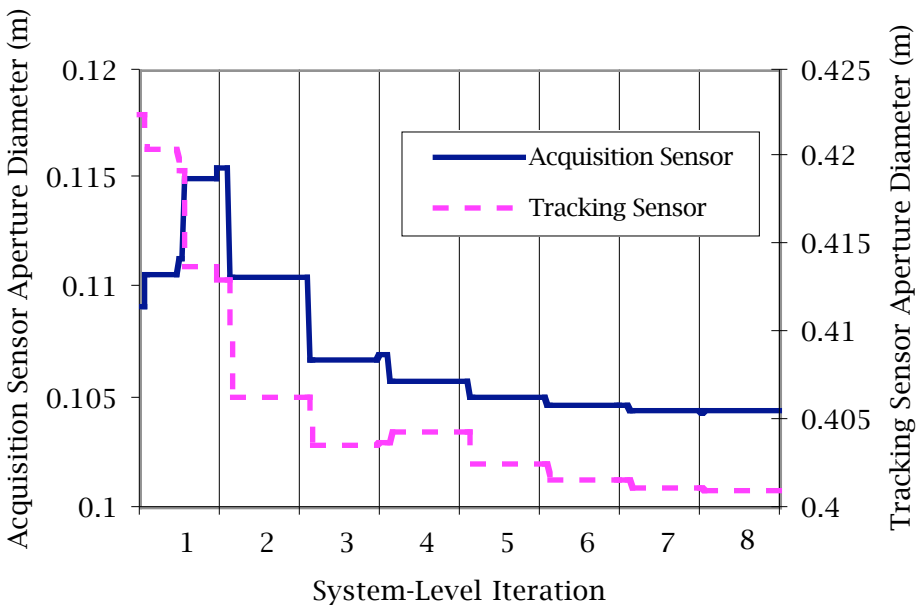

Figure 29. Progression of sensor aperture diameters, with All-At-Once method.

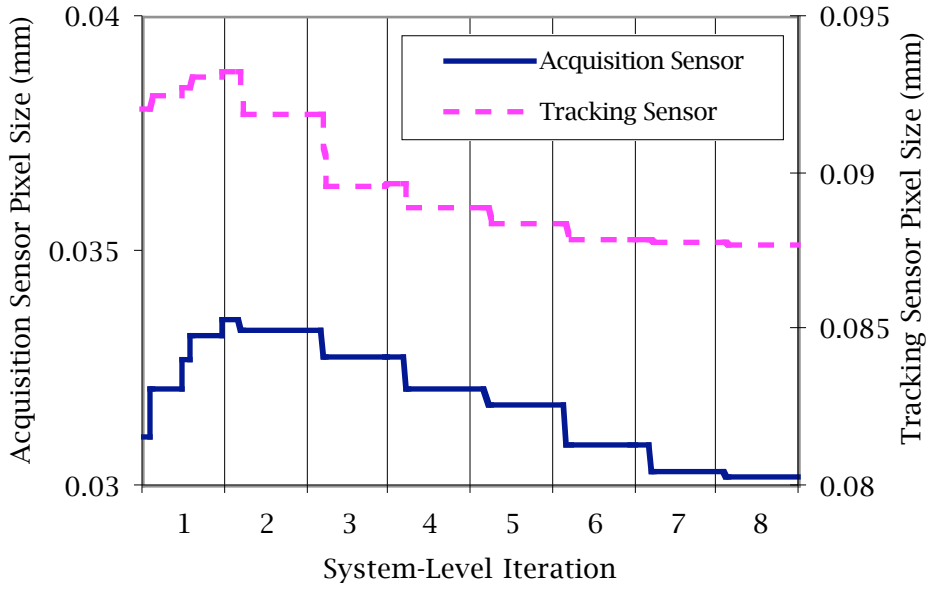

Figure 30. Progression of detector size, with All-At-Once method.

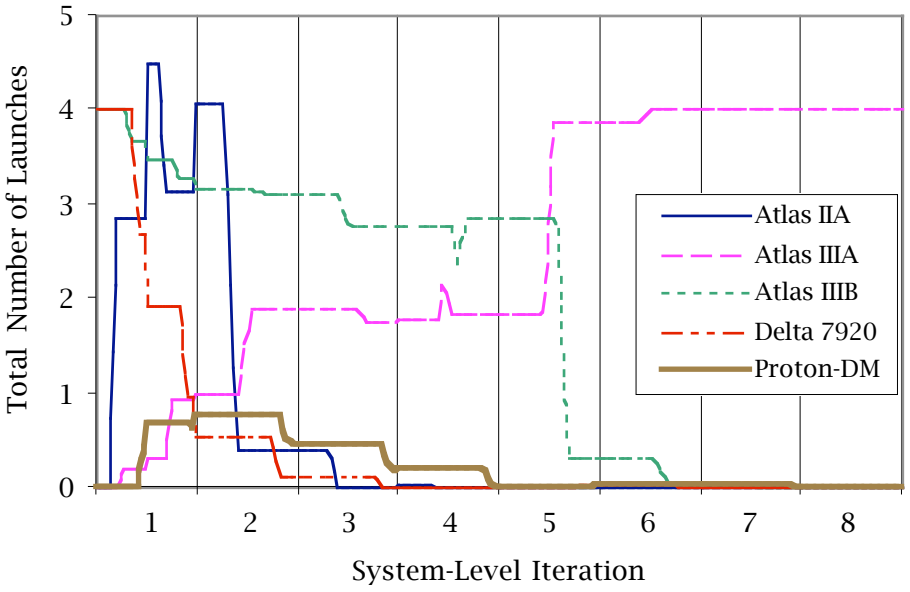

Figure 31. Progression of launch rates, with All-At-Once method.

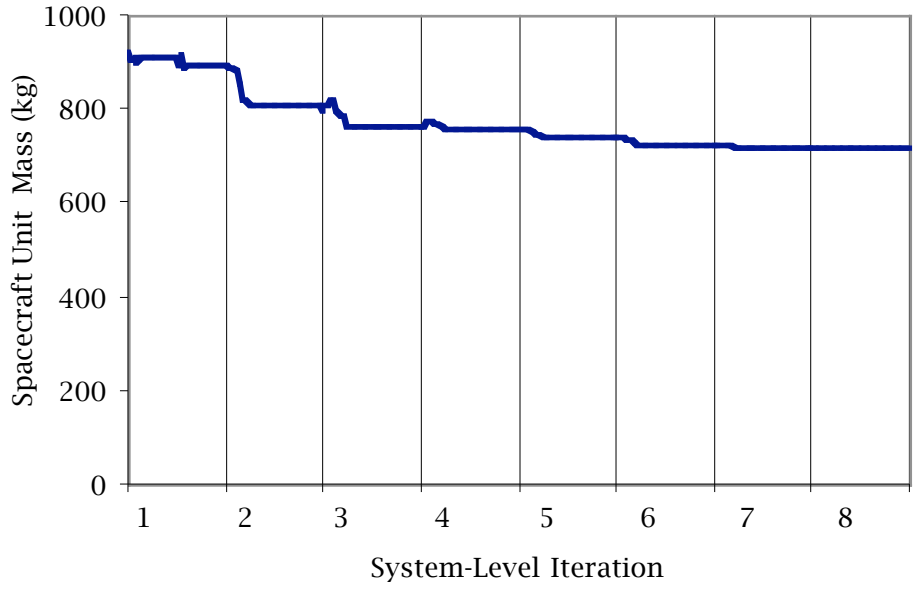

Figure 32. Spacecraft unit mass history, with All-At-Once method.

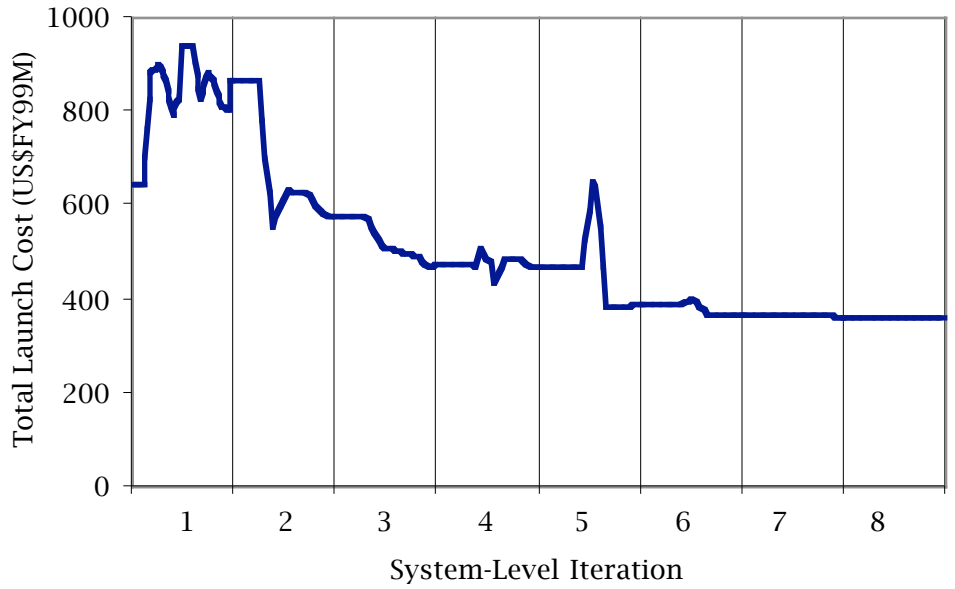

Figure 33. Total launch cost history, with All-At-Once method.

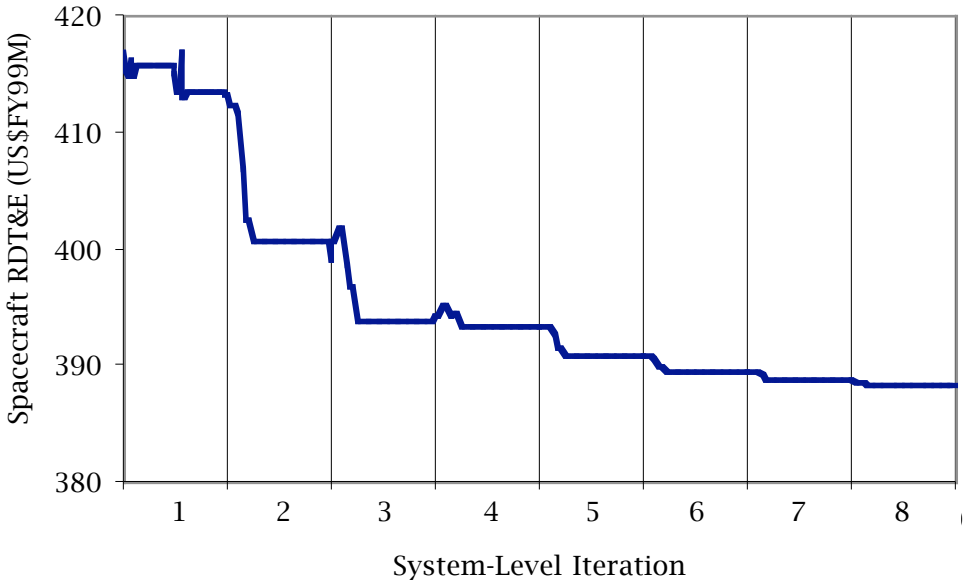

Figure 34. Spacecraft RDT&E cost history, with All-At-Once method.

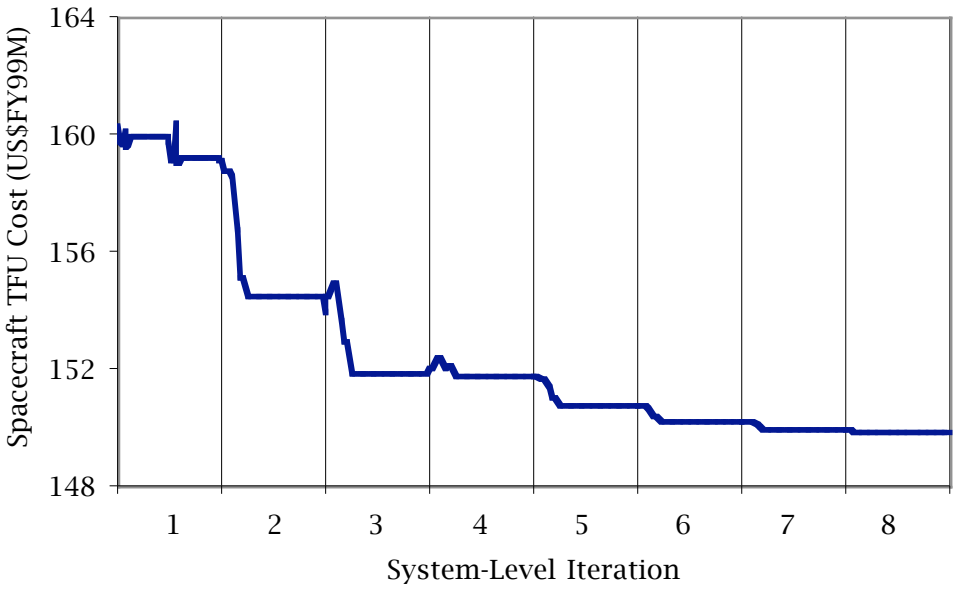

Figure 35. Spacecraft TFU cost history, with All-At-Once method.

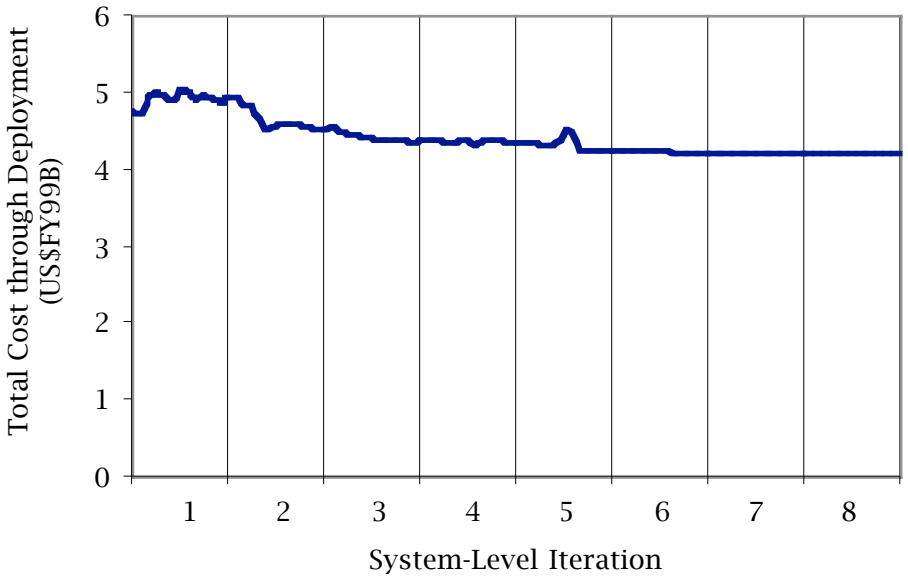

Figure 36. History of total cost through deployment, with All-At-Once method.

5.3 Preliminary Results Comparisons

Table 9 presents the preliminary results from the two approaches to the design and deployment problem of a space-based infrared constellation system. The results presented for CO are the system target values (rather than local variable values). As expected, the solutions produced by the two methods were the same (discrepancies were less than 2%), providing verification for the CO method.

Table 9. Summary of the preliminary results.

	CO	AAO
Number of Planes	4	4
Number of Satellites/Plane	7	7
Relative Spacing	2	2
Orbit Altitude (km)	1588	1588
Orbit Inclination (deg)	85.6	85.5
Spacecraft Unit Mass (kg)	690	710
Acquisition Sensor Nadir Angle (deg)	53.32	53.33
Acquisition Sensor Minimum Elevation Angle (deg)	4.47	4.37
Total Launch Cost ($M)	360	360
Spacecraft RDT&E ($M)	384.2	388.3
Spacecraft TFU ($M)	148.2	149.8
Total Production Cost ($M)	3403.3	3439.1
Average Unit Production Cost ($M)	106.4	107.5
Total Cost through Deployment ($M)	4147.6	4187.4

*US Fiscal Year 1999 Dollars

The small differences between the converged designs were mainly due to the inherent differences between exterior and interior penalty function methods used by CO and AAO, respectively. The exterior penalty method approached the final solution from the infeasible region. Thus, theoretically, the true constrained optimum was found as $k \to \infty$. In this problem, although the compatibility constraints in the final solution of the collaborative case were

within the set tolerances (10^{-6}), they were still not exactly zeros. For example, with the target values given in Table 9, the constellation design module used an acquisition sensor nadir angle of 53.33° to meet the coverage requirements, resulting in $J_1 = 6.7 \times 10^{-7}$. The spacecraft design module, at the same time, minimized J_2 to 4.6×10^{-7} with 53.3° swath width and a slightly lower altitude than the target value to give smaller sensors. The interior penalty function method was more conservative in comparison. Therefore, with the same tolerances, AAO was expected to yield a slightly more expensive (a more conservative) solution.

Both CO and AAO selected four Atlas IIIA to deploy the constellation (one vehicle to populate each plane), for a total launch cost of $360M. Each Atlas was capable of carrying the 8 satellites required per plane (including one on-orbit spare per plane). A breakdown of the total cost through deployment is given in Figure 37, where production cost formed the largest percentage. Figure 38 through Figure 40 further illustrate the dry mass and cost contributions for the spacecraft. The tracking sensor dominated in all three categories.

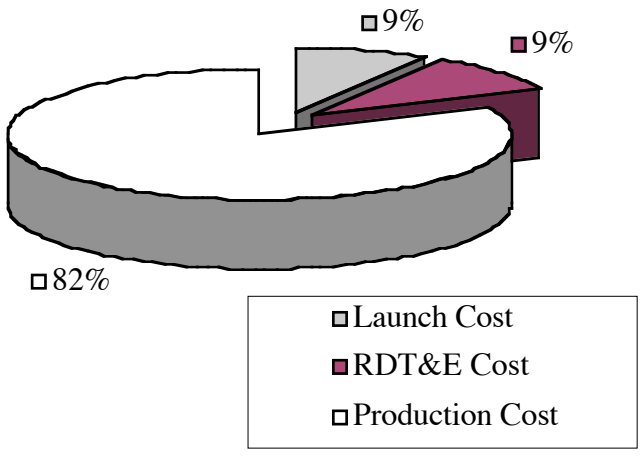

Figure 37. Percentage breakdown of total cost through deployment.

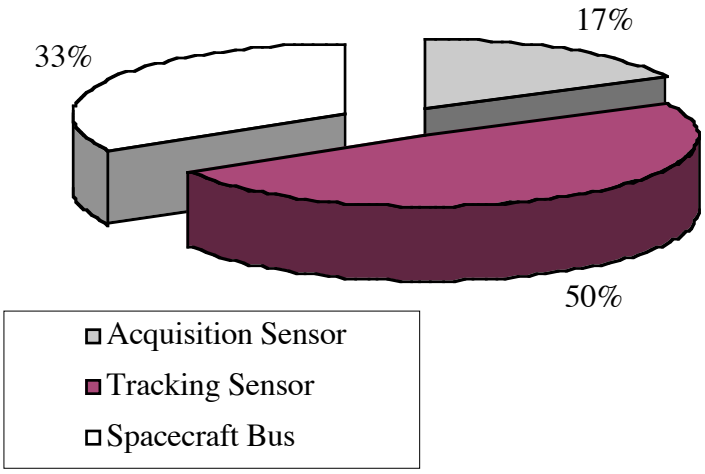

Figure 38. Dry mass contributions for the converged spacecraft design.

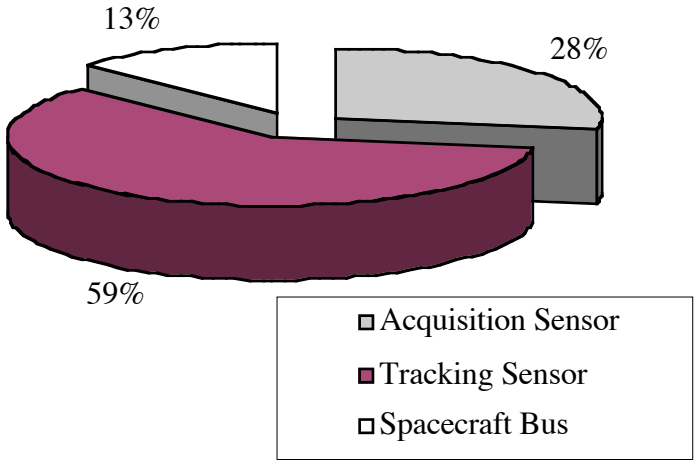

Figure 39. RDT&E cost contributions for the converged spacecraft design.

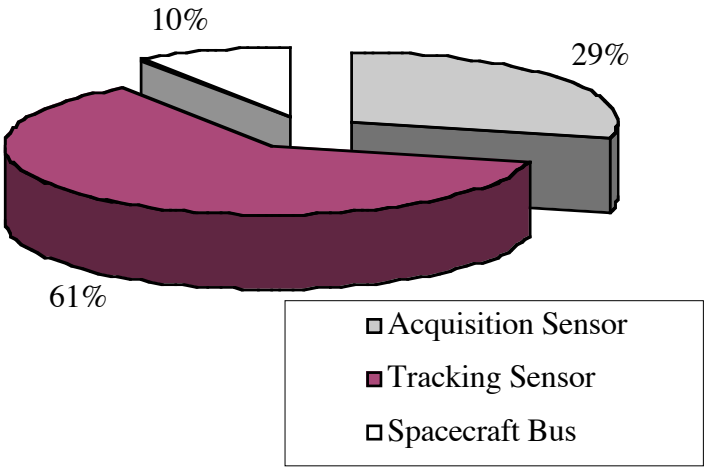

Figure 40. TFU cost contributions for the converged spacecraft design.

5.4 Preliminary Methods Comparisons

Table 10 summarizes the problem characteristics and approximate computational requirements of the two methods applied in the preliminary study. The CPU times given for the system design of both methods was obtained by averaging the CPU requirements of the individual subsystems, accounting for their parallel processing. The CO method required optimizers at both system and disciplinary levels. A considerable amount of effort and time was spent formulating these optimization problem and sub-problems and implementing the appropriate techniques to solve them. The integration and optimization process of CO further demanded a significant amount of CPU time, due to not only the difficult coordination problem at the system level, but also the subspace optimization involved at each function call. The approximate total CPU time in Table 10 of 195.7 hours for the overall system design took into account the concurrent processing capability allowed by CO.

Table 10. Summary of preliminary problem characteristics and computational comparisons.

DESIGN METHODS	DESIGN MODULE	Number of Variables	Number of Constraints	Average CPU per Call (min)	Number of Calls	Total CPU time (hrs)
Collaborative Optimization	Configuration & Orbit Design	3 [C]	2	40	181	120.7
	Spacecraft Design	6 [C]	11	30	271	135.5
	Launch Manifest	3 [C] 20 [D]	9	10	226	37.7
	System Design	7 [C]	3	32.52	361	**195.7**
All-at-Once	Configuration & Orbit Design	—	—	10	325	54.2
	Spacecraft Design	—	—	4	568	37.9
	Launch Manifest	—	—	4	1864	124.3
	System Design	7 [C] 20 [D]	22	4.86	2268	**183.7**

AAO, on the other hand, had simpler subsystem setups, since each disciplinary module was only required to perform analyses (no subspace optimization). A single optimizer controlled all of the variables (even those that did not directly affect other subsystems) and dealt with all of the constraints. A significantly larger and more complex system-level optimization problem resulted, requiring several restarts to converge, even after the reduction of the launch options. Thus, a larger number of function calls was needed compared to the CO method. However, as shown in Table 10, AAO still had a slight advantage over CO in terms of total CPU time for the overall problem due to the simpler subsystem tasks and their concurrent computations.

Although from the preliminary computations AAO seemed to be the better method, CO was preferred for scalability and organizational reasons. AAO would be the correct choice for certain problems. In this case, however, AAO is

more easily affected by the "curse of dimensionality." As more details or greater scope was considered (e.g., more launch vehicle options, detector and spacecraft bus materials, etc), the size, and therefore the complexity, of the system optimization problem with AAO would grow much faster than with CO. This scalability feature of CO was mainly a result of the decomposition of the system problem allowed in CO. Furthermore, collaborative optimization was organizationally more suited to the structure and culture found in most multidisciplinary design groups. Providing disciplinary experts with autonomy, more control and responsibilities, and more opportunities to contribute to the overall system integration and optimization, CO was a more acceptable approach. Therefore, since CO offered these characteristics that were closer to the desired methodology stated in Chapter I, it was selected as the method to be further pursued in the final problem.

CHAPTER VI

MODIFIED ANALYSIS MODELS

Solving the preliminary problem provided not only useful knowledge and experience about the constellation design process, but also evaluation of the analysis tools. These lessons-learned would improve the solution-finding process of the complete problem required for this thesis work and the quality of the solution itself. Modifications were implemented to both the coverage analysis code and the spacecraft model, while the launch manifest module remained intact. Some of these changes were aimed to further increase the generalities of these tools. This chapter presents an overview of these improvements.

6.1 Coverage Analysis II

Matlab as an interpreted language is easy to code, but lacked in computational speed. Due to the large number of runs anticipated, the coverage analysis was reprogrammed in C++ language for faster execution times. Other improvements were aimed to make the code as flexible as possible. 5^{th}-order Runge-Kutta-Fehlberg (RKF56) integration method with adaptive time step τ [79] was implemented to allow propagation of orbits of any sizes and shapes. This technique determined from six function evaluations the values of the state vector at the next time step, as explained in Appendix C.

The capability to add non-spherical gravity potential model to the problem was also offered by the new coverage analysis program [43]. The equation of motion used for propagating spacecraft i became:

$$\ddot{\bar{r}}_i = \nabla\phi_i \qquad \textbf{(6.01)}$$

$\ddot{\bar{r}}_i$ was the spacecraft i's acceleration vector and ϕ_i was its gravity potential function, which was also elaborated in further details in Appendix C along with relations for its derivative components. However, due to research schedule constraints, the Earth's oblateness continued to be neglected in the subsequent analyses for this study.

The coverage grid point evaluations also underwent several changes, basing its computations on elevation angle instead of sensor beam size. The coverage analysis code computed $\bar{\rho}_{ji}$, the position vector of the satellite i with respect to the grid point j:

$$\bar{\rho}_{ji} = \bar{r}_i - \bar{R}_j \qquad \textbf{(6.02)}$$

$\bar{R}_j$ was the position vector of the grid point j measured from the Earth's center. Figure 41 illustrates these relationships.

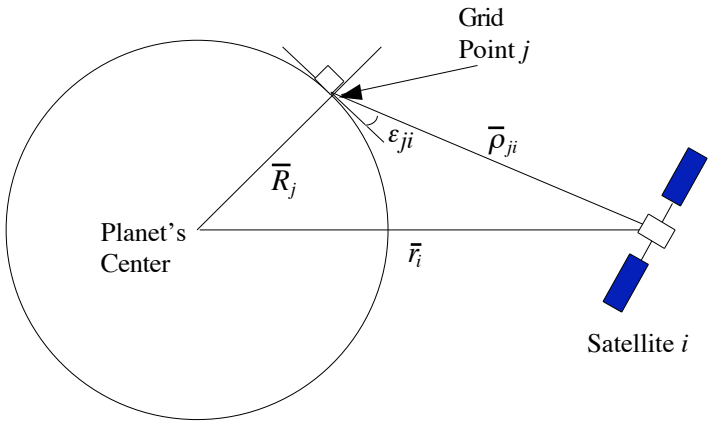

Figure 41. Geometric diagram for new coverage analysis.

After the appropriate coordinate transformation, the elevation angles ε_{ji}, which could have values between -90° and +90°, was found from the local z-component of $\bar{\rho}_{ji}$ and its magnitude:

$$\varepsilon_{ji} = \sin^{-1}\left(\frac{\rho_{ji,z}}{\rho_{ji}}\right) \qquad \textbf{(6.03)}$$

If ε_{ji} was greater than or equal to the specified $\varepsilon_{\min}$, then coverage of point j was provided by satellite i.

6.2 Spacecraft Model II

The spacecraft model was modified for improved analyses. In addition to diffraction limit and spherical aberration, optics imperfections caused by coma aberration β_{CA} (dispersion of off-axis parts of the image) and astigmatism β_{AA} (aberration where image is blurred due to rays converging to different foci) were also computed:

$$\beta_{CA} = \frac{\alpha_{res} n_x}{16F^2} \qquad \textbf{(6.04)}$$

$$\beta_{AA} = \frac{(\alpha_{res} n_x)^2}{2F} \qquad \textbf{(6.05)}$$

These equations can be used as constraints to ensure that the optics design sufficiently allowed for these distortions:

$$\beta_{CA}, \beta_{AA} < \alpha_{res} = x / R_{\max} \qquad \textbf{(6.06)}$$

Limiting aberrations from these sources (diffraction limit, spherical, coma and astigmatism) was achieved by increasing F-stop (i.e., by increasing aperture diameter to focal length ratio). The acquisition sensor required a reasonable F-stop, which enabled the use of a simple spherical mirror as its optical system. The tracking sensor, on the other hand, demands F-stop at such high speed as to be impractical. Thus to satisfy the coma aberration and astigmatism constraints, uncorrected Schmidt, a spherical mirror with the stop at the center of the curvature and with no corrector, sufficiently compensated for these third-

order aberrations and was a possible suitable optical system [80]. More detailed analysis on optical configurations, essential in later phases of the design process required complex ray-tracing, but was considered beyond the scope of the present study.

Mass and power estimation by scaling from existing system, though relatively simple to implement, only works well if the two systems compared are truly similar in performance and complexity. The analogous instrument selected in the preliminary problem (MODIS) had a much more challenging mission requirements than the acquisition sensor. The results showed that throughout the iterations, the aperture diameter ratios between the two instruments $\left(\frac{D_{AS}}{D_{MODIS}}\right)$ fell ~0.55, while this mass/power estimation approach demanded values in the proximity of 1.0 for best accuracy.

A method found in [31] was adopted with some modifications. The first step was to approximate the volume of the acquisition sensor:

$$V_{AS} = (1.25 \cdot D_{AS})^2 \cdot (1.25 \cdot f_{AS}) \qquad \textbf{(6.07)}$$

The instrument's mass was then found by assuming a density of 3000 kg/cm^3:

$$M_{AS} = 3000 \frac{kg}{m^3} \cdot V_{AS} \qquad \textbf{(6.08)}$$

The relationship to obtain an estimate for payload power requirement was:

$$P_{AS} = 2000 \frac{W}{m^3} \cdot V_{AS} \qquad \textbf{(6.09)}$$

These Design Estimating Relationships (DER) were not accurate for the tracking sensor, which included motors and additional structures to support the slew-and-stare configuration. The same approach explained in Chapter IV was used, modified such that the mass estimation was less conservative:

$$M_{TS} = 1.1 \cdot (0.75 \cdot (0.137 \frac{kg}{m^2} \cdot D_{TS}^2 + 0.586 \frac{kg}{m} \cdot D_{TS} + 17.8kg)) \quad \textbf{(6.10)}$$

The moment of inertia equation was also slightly altered, resulting in higher calculated power requirements:

$$I_{TS} = \frac{1}{12} \cdot m_{TS} \cdot \left(3 \cdot \left(\frac{1.25 \cdot D_{TS}}{2} \right)^2 + \left(1.25 \cdot f_{TS} \right)^2 \right) \quad \textbf{(6.11)}$$

Table 11. List of systems used to compute a new spacecraft bus MER.

SPACECRAFT	PAYLOAD MASS (kg)	PAYLOAD POWER (W)	SPACECRAFT BUS DRY MASS (kg)
NOAA 11	386	700	1166
ERS 2	710	800	1500
LM-900	200	60	80
Starbus	200	555	558
Envisat 1	2145	1900	5700
RS2000	1000	5000	500

The selected set of spacecraft used to obtain a new MER curve-fit for spacecraft bus included three additional spacecraft beyond those listed in Table 3. The new list consisted of support buses designed for LEO missions that were zero momentum three-axis stabilized, constituted of aluminum and composite structures, had deployable arrays, and were capable of highly accurate pointing control and knowledge ($< 0.1^{\circ}$) using combinations of chemical thrusters and either reaction wheels or magnetic torquers. Table 11 presents these selected systems in greater detail. The new equation for the spacecraft bus dry mass was:

$$M_{bus} = 2.0684 \cdot M_{payload} + 0.4889 \frac{kg}{W} \cdot P_{payload} \quad \textbf{(6.12)}$$

CHAPTER VII

OPTIMIZATION PROCESS

Most of the system-level and subspace optimization strategies adopted for the final constellation design and deployment problem were similar to those used in the collaborative optimization proof-of-concept stage and explained in Section 5.1. The addition of two system-level discrete variables (the number of orbital planes and the number of spacecraft within each plane) called for changes in some of the optimization techniques. These modifications are discussed in this chapter. The overall process was automated to improve computational efficiency. All of the programs were compiled and executed on a Power Mac G4. Macintosh AppleScript was used for communications between modules. Table 12 summarized the subspace and system optimization problems.

7.1 Configuration and Orbit Design Optimization Approach

Grid search was still considered the most appropriate optimization technique for this subsystem due to the discrete nature of the problem (i.e., existence of several integer variables and the discrete time steps used in the simulations). Knowledge of the feasible design space, relating altitude, inclination, and minimum elevation angle, was found to be beneficial in the preliminary studies. Thus, prior to initiating the system optimization process, a coarse grid search of the maximum ε required to achieve global continuous single-fold coverage (corresponding to minimum beam size η search in Chapter V) for different combinations of altitude and inclination and for several Walker delta patterns, was executed. This effort generated coordinates for the points

such that surfaces could be formed for the different constellation configurations. Again, as shown in Figure 18 for a 28/4/2 Walker pattern, these surfaces bordered the feasible (areas on and below the surface) and the infeasible design space.

This surface information, organized in a spreadsheet format, further became useful in narrowing down the search region for the subspace optimizer within the collaborative environment, yielding savings in computation times. By calculating the differences between the target and all the data points, which are in essence possible J_1's, the configurations with surface points closest to the target could be determined. These configurations were further investigated using a finer grid search. Again, as described in Section 5.1, heuristics programmed in C++ played an important role to ensure a "smart" search.

7.2 Spacecraft Design Optimization Approach

Since constellation configuration had no effects on the spacecraft design module, this subspace optimization problem was similar to that of the proof-of-concept study described in Chapter V. That is, the final subspace problem involved mostly the same target variables $\bar{z}_2$ (altitude, minimum elevation angle replacing sensor beam size, spacecraft mass and RDT&E and TFU costs) and local variables (local versions of the target variables $\bar{y}_2$, along with sensors' aperture diameters and pixel sizes $\overline{\psi}_2$). The subspace objective function (minimize J_2) remained unchanged, but extra constraints were added to the problem (resolution accounting for aberrations, besides the sensitivity requirements and detector material limits).

The utilization of genetic algorithm was found necessary in the preliminary case due to the difficulties encountered by MS Excel's built-in Solver in finding the solution to the nonlinear problem. It was observed, however, that if altitude and minimum elevation are eliminated from the variable list (i.e., if their values are held constant), Solver had little trouble finding the solution. This was

perhaps due to high degree of dependence of the other variables on these two parameters, via constraints. Altitude and minimum elevation angle were the only truly independent variables, limited only by the bounds given on their values. Furthermore, the problem of minimizing J_2 was basically a trade-off between error contributions of the various components of $\bar{y}_2$. For example, if altitude and minimum elevation angle were perturbed farther from their target values, would a smaller combined error from the resulting mass and cost variables gained a better J_2? These discoveries led to a new approach to the spacecraft design optimization for the final design problem, employing an iterative scheme shown in Figure 42.

An univariate search, which in effect replaced GA, performed a one-variable-at-a-time optimization with altitude and minimum elevation as its variables. Its function evaluation consisted of launching Solver whose task was, given a fixed altitude and minimum elevation angle, to find the best combination of aperture diameters and pixel sizes that minimized J_2 while satisfying all of the spacecraft constraints. Based on the best solution found by Solver, the unidirectional optimization, again using quadratic approximation, determined the next set of values for its variables that could possibly improve J_2 and the process continued until the solution could not be further improved. This iterative method proved to be robust and more efficient than the technique employed in the preliminary problem. Automation of the subsystem optimization was implemented in VBA.

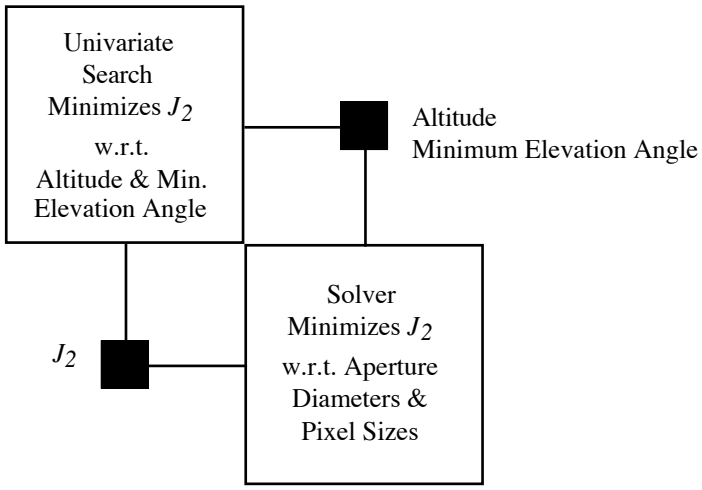

Figure 42. DSM of the two-level scheme used for spacecraft design subspace optimization.

7.3 Launch Manifest Optimization Approach

The launch manifest subspace optimization involved three steps. A combination of VBA and AppleScript was used. First, the IP solver was used to find the lowest cost deployment strategy with constellation configuration, mission orbit, and spacecraft unit mass kept at their target values. This gave an initial J_3, which consisted of only the error difference between the target and the actual launch costs, since the other coupling variables were kept at their system input values. If the launch cost obtained by IP was higher than the target value, an expert system called CLIPS (C Language Integrated Production System [81]) was needed as a second step to automate heuristics similar to those used in the proof-of-concept stage, which did not lend themselves easily to algorithmic programming.

The rules coded into CLIPS were aimed at improving the initial J_3 obtained from the IP results mainly by reducing the number of planes, the number of spacecraft per plane, and the spacecraft unit mass in search of lower launch cost solutions, and ultimately lower J_3. If an option with reduced mass (actual mass lower than the target value) was selected by CLIPS as the one with the

best J_3, then a third step involving an univariate search was necessary. Retaining the constellation configuration and the launch vehicles opted by CLIPS, the trade-off was between reducing altitude and inclination such that the vehicles' higher payload-carrying capabilities allowed sufficient increase in spacecraft mass, closer to its target value, while keeping altitude and inclination error contributions to J_3 from becoming too large.

7.4 System Optimization Approach

With the introduction of the two discrete variables, namely number of planes and number of satellites per plane, the system-level optimization problem became a nonlinear mixed-integer programming (NLMIP) problem. The penalty function method used for AAO optimization scheme in the preliminary problem (Chapter V) was deemed suitable as the system optimization technique for this final constellation design and deployment problem. Powell's method with quadratic approximation was again the unconstrained optimization technique selected.

Table 12. Summary of CO's implementation to the final problem.

DESIGN MODULE	VARIABLES	CONSTRAINTS	OBJECTIVE FUNCTION	OPTIMIZATION SCHEME
Configuration & Orbit Design	# Planes # Sats/Plane Relative Phasing Altitude Inclination Sensor FOV	Global Continuous One-Fold Coverage Closest Approach Distance > 150 km	J_1	Grid Search + Heuristics
Spacecraft Design	Altitude Minimum Elevation Aperture Diameter Pixel Size	SNR > 10 dB Angular Blur < Required Resolution Dwell Times > $3\tau_{det}$ (detector's time constant)	J_2	Univariate Search + Solver
Launch Manifest	# Planes # Sats/Plane Altitude Inclination Spacecraft Unit Mass Flight Rates	Launch Vehicle Availability Complete Population of Specified Constellation	J_3	Integer Programming + Heuristics + Univariate Search
System Design	# Planes # Sats/Plane Altitude Inclination Sensor FOV Spacecraft Unit Mass Total Launch Cost Spacecraft RDT&E Cost Spacecraft TFU Cost	$J_1 = 0$ $J_2 = 0$ $J_3 = 0$	Total Cost through Deployment (F)	Penalty Function using Powell's Method with Quadratic Approximation

CHAPTER VIII

FINAL RESULTS

The system-level variables involved in the final design problem are summarized in Table 13. Note that there are two additional discrete variables added to the preliminary problem setup. The ranges of allowable values are also given, along with the initial condition at the start of the collaborative process. The upper and lower bounds for this problem were kept the same as those used in the preliminary study.

The coordination for the system-level variables within the collaborative architecture is illustrated in Figure 43 through Figure 48. As in the preliminary study, successful convergence was achieved after 9 iterations at the system level. The final optimized configuration is summarized in Table 14.

The 28/4/3 Walker pattern was the chosen configuration that minimized the total cost through deployment phase. The launch strategy involved one Atlas IIIA and one Delta 7920 to serve each plane, resulting in a total launch cost of $580M. An Atlas IIIA is capable of carrying 6 satellites weighing 930 kg each to the determined orbit. The Delta 7920 can deploy 2 more, for a total of 8 spacecraft per plane (including one spare). The increase in satellite mass from the previous studies was due to the modified satellite design model.

Table 13. Summary of the system-level variables for the collaborative architecture.

VARIABLES	RANGE OF VALUES	INITIAL VALUES	NORMALIZING MULTIPLIERS
Number of Planes	2 – 7	5	0.02
Number of Satellites per Plane	3 – 8	5	0.02
Orbit Altitude	1400 km – 1700 km	1700	0.001
Orbit Inclination	50° - 90°	60	0.017453
Spacecraft Unit Mass	500 kg – 1500 kg	800	0.001
Minimum Elevation Angle	0° - 10°	0	0.017453
Total Launch Cost	$100M - $1000M	100	1.25×10^{-7}
Spacecraft RDT&E Cost	$200M - $500M	200	1.25×10^{-7}
Spacecraft TFU Cost	$100M - $500M	100	1.25×10^{-7}

*US Fiscal Year 1999 Dollars

Table 14. Summary of the final result for the collaborative architecture.

	OPTIMIZED VALUES
Number of Planes	4
Number of Satellites/Plane	7
Relative Spacing	3
Orbit Altitude (km)	1585
Orbit Inclination (deg)	83.6
Spacecraft Unit Mass (kg)	930
Acquisition Sensor Nadir Angle (deg)	53.33
Acquisition Sensor Minimum Elevation Angle (deg)	4.57
Total Launch Cost (US$FY99M)	580
Spacecraft RDT&E (US$FY99M)	440.6
Spacecraft TFU (US$FY99M)	164.9
Total Production Cost (US$FY99M)	3786.4
Average Unit Production Cost (US$FY99M)	118.3
Total Cost through Deployment (US$FY99M)	4807

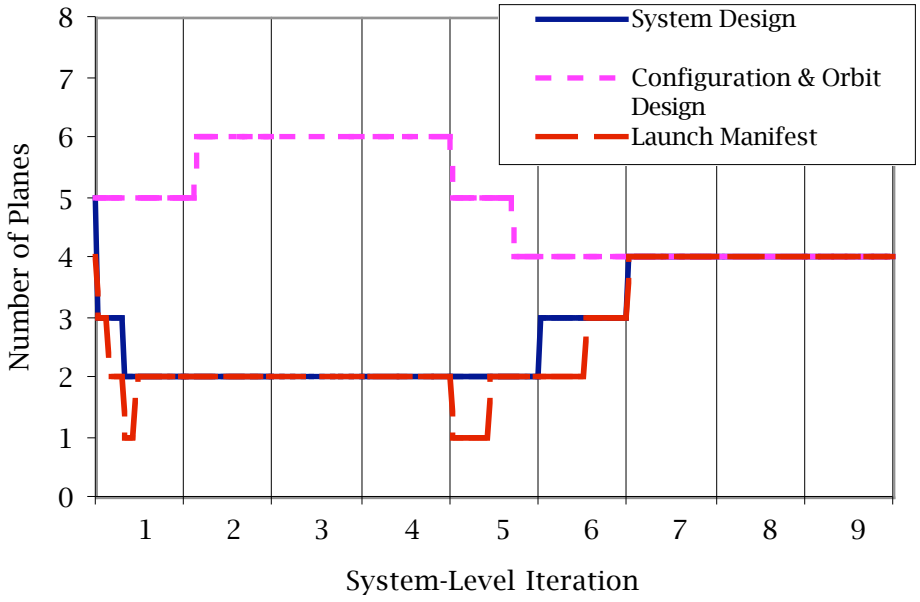

Figure 43. Progression of number of planes within the collaborative architecture.

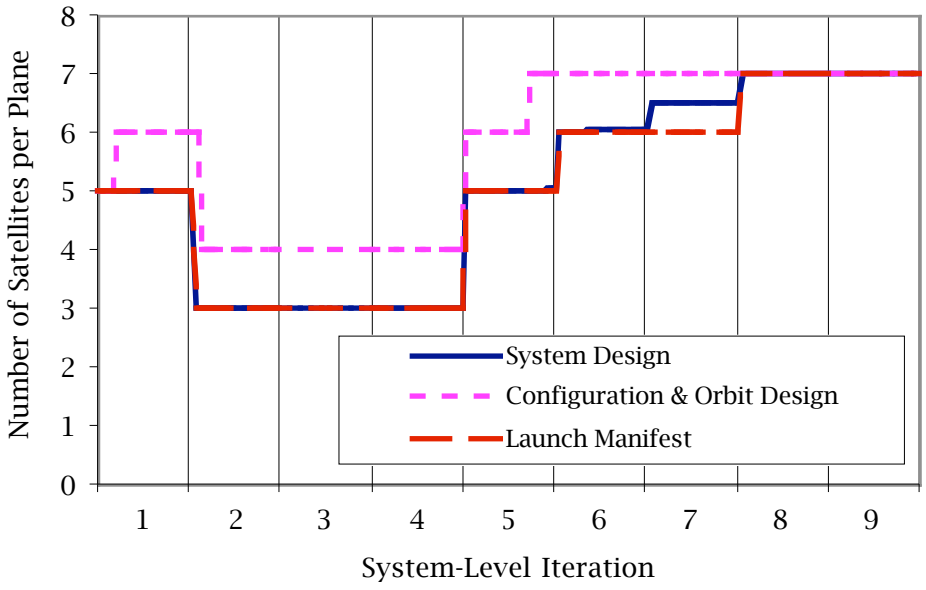

Figure 44. Progression of number of spacecraft per plane within the collaborative architecture.

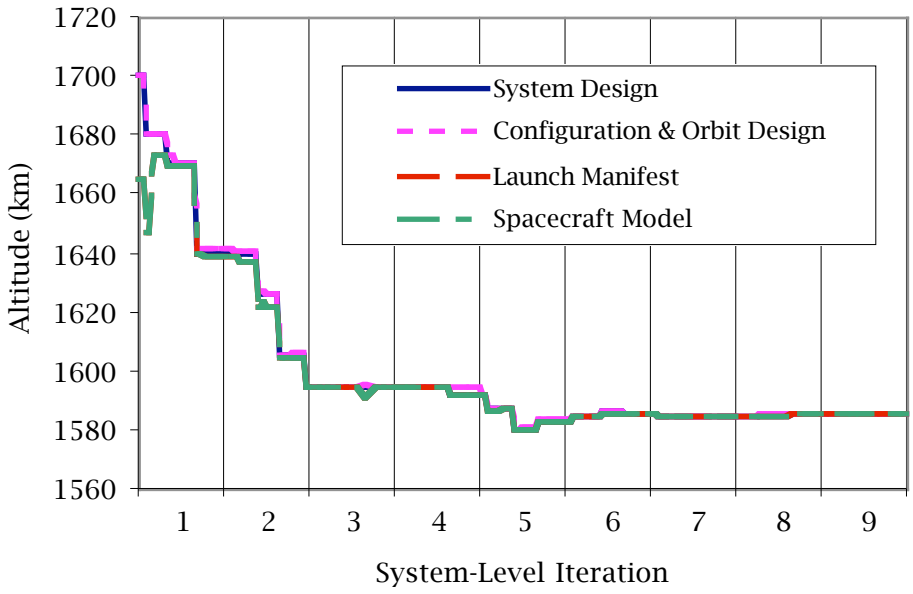

Figure 45. Progression of altitude within the collaborative architecture.

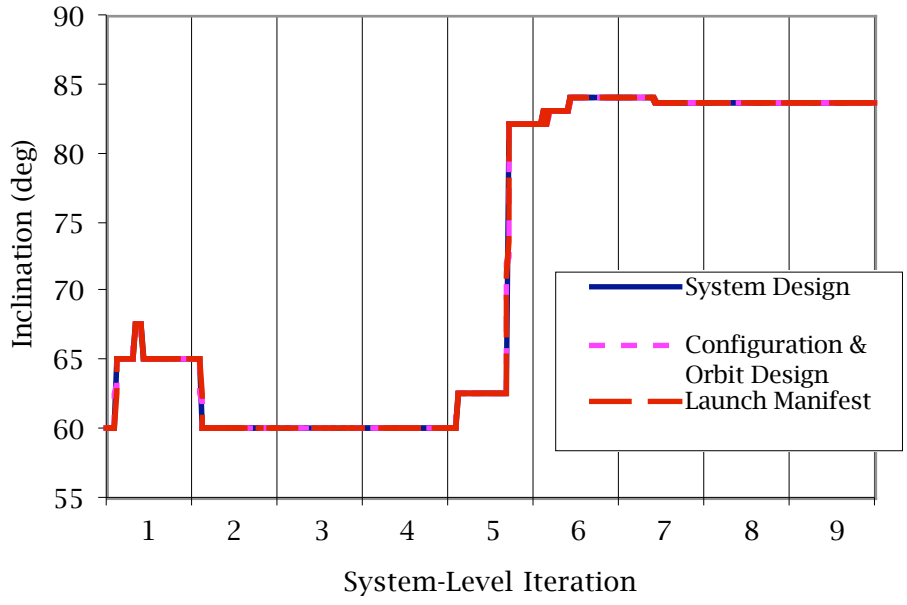

Figure 46. Progression of inclination within the collaborative architecture.

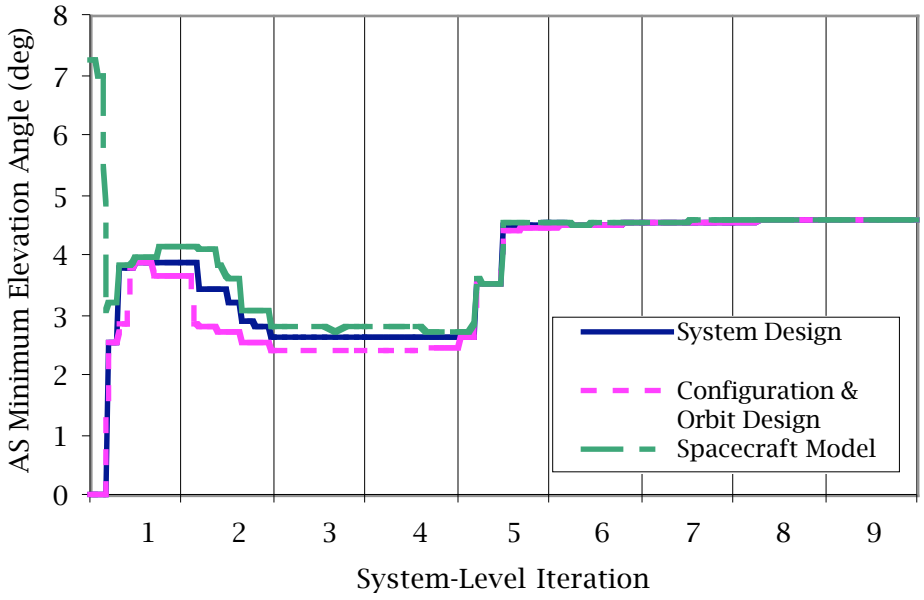

Figure 47. Progression of minimum elevation angle for acquisition sensor within the collaborative architecture.

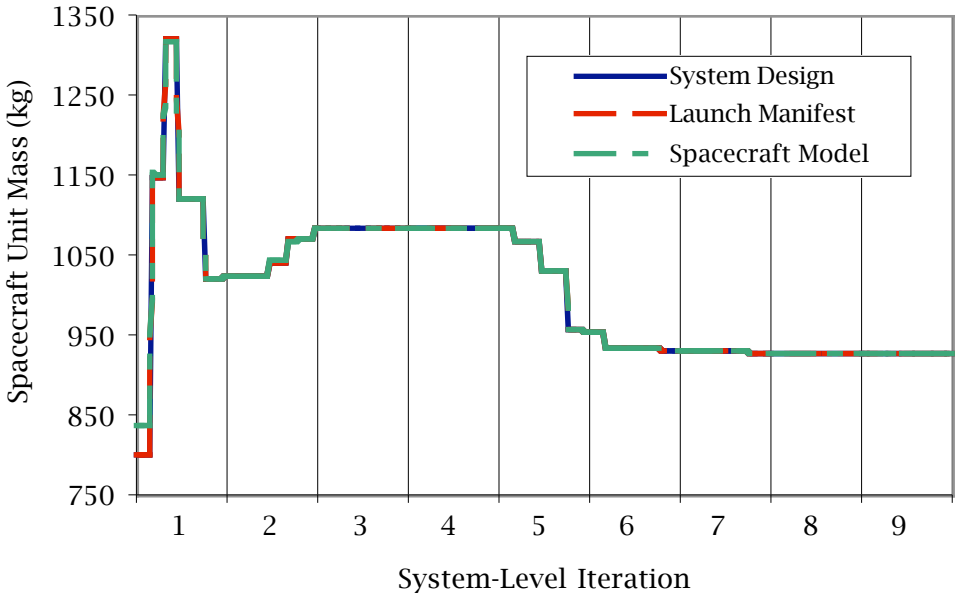

Figure 48. Progression of spacecraft unit mass within the collaborative architecture.

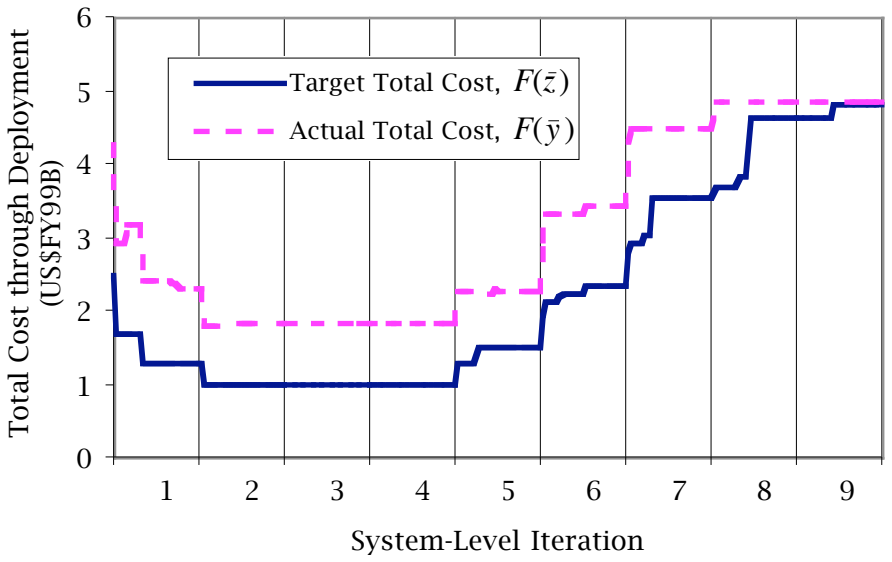

Figure 49. Progression of the total cost through deployment within the collaborative architecture

Again, the behavior of the system-level variables and the local versions controlled by the subspace optimizers revealed the dynamics that made this problem both interesting and challenging. The configuration and orbit design module always preferred larger constellations (more planes and greater number of satellites per plane), higher altitude, and lower minimum elevation angle. The spacecraft model, to come as close as possible to the low cost targets set by the system optimizer, would bid for lower altitude and increased minimum elevation angle (equivalent to smaller sensor nadir angle). Finally, the launch manifest module favored fewer planes to keep launch cost down.

Figure 49 presents the behavior of the resulting total cost through deployment. The lowest point was achieved at the second iteration and maintained until the beginning of the fifth iteration. This resulted from the system optimizer's selection of the smallest allowable constellation size (2 planes with 3 satellites per plane). At iteration 5, the penalty function

multiplier for the compatibility constraints gained sufficient weights to drive the design towards the feasible region.

Figure 50 is a graphical representation of the percentage contributions in cost. Similar to the findings from the preliminary studies, the production of the spacecraft still costs the most up to the deployment phase of the constellation system. Figure 51 presents the approximate percentage breakdown in spacecraft dry mass. With the modified spacecraft model, the supporting bus has the largest fraction of the total dry mass. However, it contributes the least to the spacecraft total RDT&E and TFU cost (Figure 52 and Figure 53).

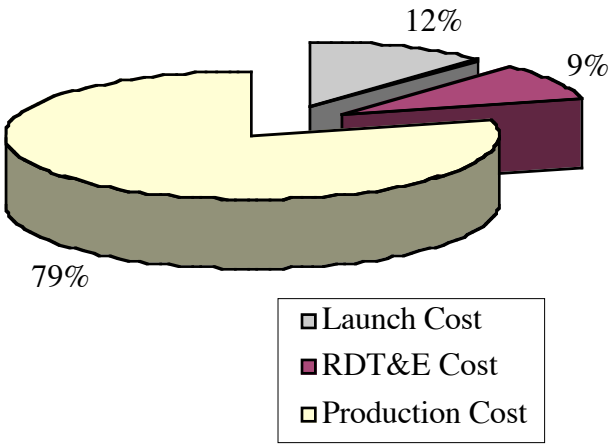

Figure 50. Percentage breakdown of total cost through deployment.

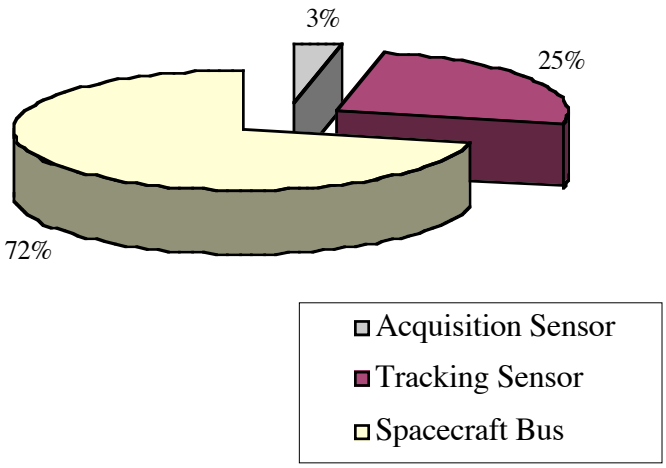

Figure 51. Dry mass contributions for the converged spacecraft design.

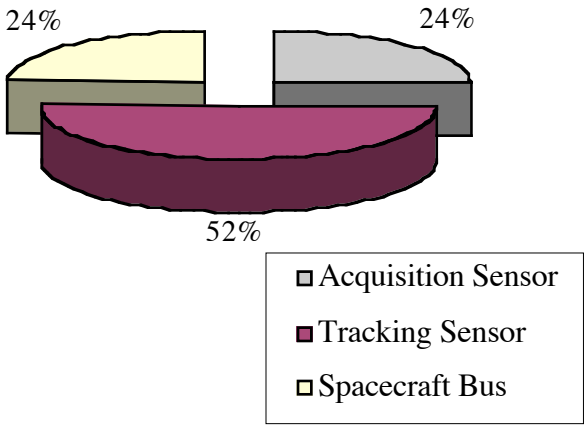

Figure 52. Percentage breakdown of spacecraft RDT&E cost.

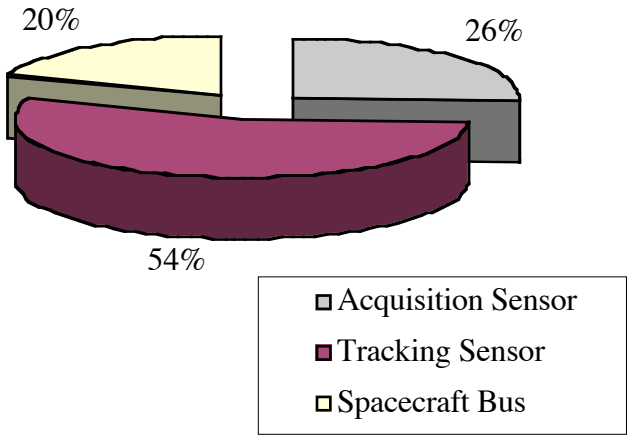

Figure 53. Percentage breakdown of spacecraft TFU cost.

CHAPTER IX

CONCLUSION

Recognizing the need for a systematic, multivariable, multidisciplinary method, the research presented in this thesis introduced a new approach for the integration and optimization of a satellite constellation system, including designs of the orbit and configuration, the individual spacecraft, and the deployment. The application example selected was to design and deploy a space-based infrared constellation system placed at near-Earth orbits for ballistic missile defense. Mission objectives and requirements were determined specifically for this application.

One objective of this thesis was that this new approach provided the subspaces with as much flexibility as possible during the overall optimization process. Implementation of the distributed analysis architecture was the first step to attaining this goal. Within this type of architecture, each individual discipline was allowed complete control over its analysis, with freedom to use any computing platforms and programming environments. This reflected a team-oriented (e.g., prime and sub-contractor) arrangement. The preliminary studies of thesis work verified this subsystem flexibility, utilizing programs running on SGI, PC, and MacIntosh, written in C language, Matlab, and VBA on MS Excel.

Two optimization methods (i.e., collaborative optimization and All-at-Once) utilizing the distributed architecture were further implemented on the preliminary problem, which fixed the constellation configuration. These optimization procedures were aimed to give better confidence on the solution

obtained by this new approach to constellation designs. Both CO and AAO, as expected, yielded the same design (within the specified numerical tolerance). Computationally, the optimization processes with the two methods were comparably difficult, requiring approximately the same CPU times. CO's system optimization problem was much simpler than AAO's (fewer variables and constraints), but at the cost of more difficult subspace tasks (subsystem optimization versus analysis). Thus, CO demanded more effort and time to setup the subsystem problems.

Organizationally, on the other hand, CO had an advantage over AAO, giving the disciplines an influence over the overall system optimization. Local variables were controlled by the individual subsystems, allowing them some design freedom. Each discipline also provided guidance to the system optimizer through the negotiation processes to satisfy the local constraints. This feature of CO also led to better scalability of the method with increased problem complexity, another desired characteristic of the proposed approach.

CO was further implemented in a final more complex problem where the configuration of the constellation was allowed to vary. Successful convergence of this problem further justified the feasibility of CO for the multi-satellite system design. The CO problem formulation and computational requirements are presented in Table 15.

The already collaborative environment of Aerospace Corporation's CDC has been shown to work very efficiently in integrating constellation systems and performing system-level trades, improving the standard practice used currently. However, design schedule constraints, and often preferences of the engineers involved, necessitate the manual unstructured process used currently. Compared to these processes, the advantages of the CO approach lie in the systematic multivariable, multidisciplinary method to extensively explore the design space. This is an important characteristic of the conceptual design for

high-cost systems especially in this day when *more knowledge earlier* is emphasized.

This benefit does not come freely. The intensive computational requirement of this approach to solve the final problem (Table 15), even with automation and concurrent executions of subsystem processes, may not be acceptable in today's design environment. Perhaps with further technological advances in computing power, this approach would become more practical in the future.

Table 15. Summary of final problem characteristic and computational requirement for the collaborative approach.

DESIGN MODULE	Number of Variables	Number of Constraints	Average CPU per Call (min)	Number of Calls	Total CPU (hrs)
Configuration & Orbit Design	3 [C] 3 [D]	2	40	397	264.7
Spacecraft Design	6 [C]	13	10	397	66.2
Launch Manifest	3 [C] 100 [D]	21	10	463	77.2
System Design	7 [C] 2 [D]	3	28	661	**308.5**

Beyond demonstrating the applicability of CO to satellite constellation designs, this thesis also further extended the current state of collaborative optimization. First, successful convergence of all the test cases proved the feasibility of using non-gradient-based optimization techniques within the CO architecture at both system and subsystem levels. Second, this research had also extended the domain of applicability of CO to mixed-integer multidisciplinary design problems by demonstrating stability in the system optimization process, leading to convergence.

9.1 Recommendations

Several areas for future extensions of this work have been identified. The recommendations related to different areas to improve the utilization of collaborative optimization for the conceptual design of satellite constellations.

9.1.1 Application-Specifics

For military missions similar to the SBIRS Low, performance criteria other than coverage include probabilities of detection of false alarm, mean time to detection, and mean time between false alarms [82]. These are important considerations that may place additional limits on the constellation design.

9.1.2 Problem Characteristics

An even more complete representation of the constellation design problem can include non-Walker configurations. Variants on the sensor beam shapes are important for SBR applications. Other factors include ground station accesses, eclipse duration, on-orbit drag, radiation effects, spacecraft configuration, and maximum *g*-loading and volume constraints due to launch vehicle selection.

9.1.3 Modeling Tools

Increasing the fidelity of the individual analyses can lead to improvements in the quality of the solution. The spacecraft model can be better-defined using a bottom-up approach, where mass and cost estimates of the spacecraft subsystems are obtained parametrically [30] or calculated based on first principles [31]. More data for the launch vehicles database would be beneficial, along with *g*-loading and payload fairing volume information.

9.1.4 Optimization Methods

It may be advantageous to investigate other optimization techniques at the system level. Few algorithms using classical search techniques exist that can

handle mixed-integer problems, apart from the one based on penalty function used in this thesis. These include branch-and-bound and cutting plane methods [68]. Investigations of combinatorial optimization techniques using meta-heuristics (e.g., genetic algorithm and tabu search) to solve this complex problem may be an interesting extension of this research.

9.1.5 System Studies

A demonstration of system-level sensitivity studies or "what-if" scenarios using the collaborative approach presented in this thesis can further support the benefits of this method. For example, this distributed design architecture can be used to assess the impact of a new spacecraft bus material from the overall constellation system's perspective such that decisions can be made as to whether or not investment should be made on that particular technology.

REFERENCES

[1] Clarke, A. C., "Extra-terrestrial Relays," *Wireless World*, pp. 305-308, October 1945.

[2] http://samadhi.jpl.nasa.gov/msl/Programs/dmsp.html

[3] http://www.af.mil/news/factsheets/Defense_Satellite_Communicati.html

[4] http://www.spacecom.af.mil/hqafspc/library/facts/dsp.html

[5] http://www.af.mil/news/factsheets/NAVSTAR_Global_Positioning_Sy.html

[6] http://www.wired.com/wired/archive/6.10/satellite.html

[7] http://www.ee.surrey.ac.uk/Personal/L.Wood/constellations/

[8] Canan, J. W., "Setting a Date for Missile Defense," *Aerospace America*, pp. 35-41, May 2000.

[9] http://sun00781.dn.net/spp/military/program/warning/smts.htm

[10] Ferster, W., "NRO Eyes Smaller Spacecraft for Eavesdropping," *Space News*, Sept. 29-Oct. 5, 1997.

[11] Kobel, C. J., Johannsen, D. C., *Optimal Constellations for Space Based Laser Coverage, Evaluated Parametrically with Range*, Aerospace Report No. TOR-96(1019)-3, June 10, 1996.

[12] Tollefson, M. V., Preiss, B. K., "Space Based Radar Constellation Optimization," *1998 IEEE Aerospace Conference Proceedings*, vol. 3, pp. 379-388, March 1998.

[13] Andreas, N. S., "Space-Based Infrared System (SBIRS) System of Systems," *1997 IEEE Aerospace Conference Proceedings*, vol. 4, pp. 429-438, Aspen, CO, February 1997.

[14] Pierce, J. R., "Orbital Radio Relays," *Jet Propulsion*, vol. 25, pp. 153-157, April 1955.

[15] Garrison, T. P., Ince, M., Pizzicaroli, J., Swan, P. A., "Systems Engineering Trades for the IRIDIUM Constellation," *Journal of Spacecraft and Rockets*, vol. 34, no. 5, pp. 675-680, September-October 1997.

[16] Federal Aviation Administration's Associate Administrator for Commercial Space Transportation (AST), *Commercial Space Transportation: 1999 Year in Review*, Washington D. C., January 2000.

[17] Wertz, J. R., Larson, W. J., "The Space Mission Analysis and Design Process," *Space Mission Analysis and Design*, Second Edition, pp. 1-17, edited by Larson, W. J., and Wertz. J. R., jointly published by Microcosm, Inc., Torrance, and Kluwer Academic Publishers, Boston, 1992.

[18] AIAA Technical Committee for MDO, "Current State of the Art of Multidisciplinary Design optimization," AIAA White Paper, approved by AIAA Technical Activities Committee, Washington, D. C., September 1991.

[19] Steward, D. V., *Systems Analysis and Management: Structure, Strategy and Design,* Petrocelli Books, Inc., New York, NY, 1981.

[20] Smith, J. L., "Concurrent Engineering," *Aerospace Engineering*, pp. 32-35, August 1998.

[21] Rawlings, M. R., Balling, R. J., "Collaborative Optimization with Disciplinary Conceptual Design," AIAA-98-4919, 7th AIAA/USAF/ NASA/ISSMO Symposium on Multidisciplinary Analysis and Optimization, St. Louis, Mo., Sept 2-4, 1998.

[22] Lang, T. J., Adams, W. S., "A Comparison of Satellite Constellations for Continuous Global Coverage," IAF Conference on Mission Design and Implementation of Satellite Constellations, Toulouse, France, November 1997.

[23] Cornara, S., Beech, T. W., Bello-Mora, M., Martinez de Aragon, A., "Satellite Constellation Launch, Deployment, Replacement and End-of-Life Strategies," SSC99-X-1, 13th Annual AIAA/USU Conference on Small Satellites, Logan, UT, 1999.

[24] Neff, J., Presley, S. P., "Implementing a Collaborative Conceptual Design System," 13.0101, IEEE 2000 Aerospace Conference, Big Sky, MT, March 2000.

[25] Aguilar, J. A., Dawdy, A., "Scope vs. Detail: The Teams of the Concept Design Center," 13.0402, IEEE 2000 Aerospace Conference, Big Sky, MT, March 2000.

[26] Reinert, R. P., Wertz, J. R., "Mission Characterization," *Space Mission Analysis and Design*, Second Edition, pp. 19-46, edited by Larson, W. J., and Wertz. J. R., jointly published by Microcosm, Inc., Torrance, and Kluwer Academic Publishers, Boston, MA, 1992.

[27] Logan, T. R., "Strategy for Multilevel Optimization of Aircraft," *Journal of Aircraft*, vol. 27, no. 12, pp. 1068-1072, December 1990.

[28] Braun, R. D., *Collaborative Architecture for Large-Scale Distributed Design*, Ph.D. Thesis, Stanford University, June 1996.

[29] Lillie, C. F., Wehner, M. J., Fitzgerald, T., "Multidiscipline Design as Applied to Space," 7th AIAA/USAF/NASA/ISSMO Symposium on Multidisciplinary Analysis and Optimization, St. Louis, MO, September 2-4, 1998.

[30] Mosher, T. J., *Improving Spacecraft Design Using a Multidisciplinary Design Optimization Methodology*, Ph.D. Thesis, University of Colorado at Boulder, April 2000.

[31] Riddle-Taylor, E., *Evaluation of Multidisciplinary Design Optimization Techniques as Applied to the Spacecraft Design Process*, Ph.D. Thesis, University of Colorado at Boulder, December 1999.

[32] Ely, T. A., Crossley, W. A., and Williams, E. A., "Satellite Constellation Design for Zonal Coverage Using Genetic Algorithms," AAS paper 98-128, AAS/AIAA Space Flight Mechanics Meeting, Monterey, CA, Feb. 1998.

[33] Jilla, C. D., Miller, D. W., Sedwick, R. J., "Application of Multidisciplinary Design Optimization Techniques to Distributed Satellite Systems," *Journal of Spacecraft and Rockets*, vol. 37, no. 4, July-August 2000.

[34] Matossian, M. G., *Configuration Design Optimization of Multi-Satellite Distributed Task Constellations*, Ph.D. Thesis, University of Colorado at Boulder, December 1995.

[35] Braun, R. D., Moore, A. A., "Collaborative Approach to Launch Vehicle Design," *Journal of Spacecraft and Rockets*, vol. 34, no. 4, July-August 1997.

[36] Sobieski, I., Kroo, I., "Aircraft Design Using Collaborative Optimization," AIAA 96-0715, 34th Aerospace Sciences Meeting & Exhibit, Reno, NV, January 15-18, 1996.

[37] Ledsinger, L., *Solutions to Decomposed Branching Trajectories with Powered Flyback Using Multidisciplinary Design Optimization*, Ph.D. Thesis, Georgia Institute of Technology, July 2000.

[38] Sobieszczanski-Sobieski, J., Agte, J. S., Sandusky, R. R., Jr., "Bilevel Integrated System Synthesis," *AIAA Journal*, vol. 38, no. 1, pp. 164-172, January 2000.

[39] Sobieszczanski-Sobieski, J., Haftka, R. T., "Multidisciplinary Aerospace Design Optimization: Survey of Recent Developments," *Structural Optimization*, vol. 14, no. 1, pp. 1-23, August 1997.

[40] Kroo, I., Altus, S., Braun, R., Gage, P., Sobieski, I., "Multidisciplinary Optimization Methods for Aircraft Preliminary Design," AIAA 94-4325, September 1994.

[41] Hoult, C. P., Wright, R. P., "Space Surveillance Catalog Growth During SBIRS Low Deployment," *1999 IEEE Aerospace Conference Proceedings*, vol. 4, pp. 209-224, Aspen, CO, March 1999.

[42] Lang, T. J., "Symmetric Circular Orbit Satellite Constellation for Continuous Global Coverage," AAS 87-499, AAS/AIAA Astrodynamics Specialist Conference, Kalispell, MT, August 10-13, 1987.

[43] Bate, R. R., Mueller, D. D., White, J. E., *Fundamentals of Astrodynamics*, Dover Publications, Inc., NY, 1971.

[44] Wertz, J. R., "Orbit and Constellation Design," *Space Mission Analysis and Design*, Second Edition, pp. 157-195, edited by Larson, W. J., and Wertz. J. R., jointly published by Microcosm, Inc., Torrance, and Kluwer Academic Publishers, Boston, 1992.

[45] Walker, J. G., "Some Circular Patterns Providing Continuous Whole Earth Coverage," *Journal of the British Interplanetary Society*, vol. 24, pp. 369-384, 1971.

[46] Draim, J. E., "A Common-Period Four-Satellite Continuous Global Coverage Constellation," *Journal of Guidance, Control, and Dynamics*, vol. 10, no. 5, pp. 492-499, September-October 1987.

[47] Rider, L., "Optimized Polar Orbit Constellations for Redundant Earth Coverage," *Journal of the Astronautical Sciences*, vol. 33, no. 2, pp. 147-161, April-June 1985.

[48] Riedl, M. J., *Optical Design Fundamentals for Infrared Systems*, Tutorial Texts in Optical Engineering, edited by O'Shea, D. C., vol. TT20, SPIE Optical Engineering Press, Bellingham, WA, 1995.

[49] Ulybyshev, Y., "Near-Polar Satellite Constellations for Continuous Global Coverage," *Journal of Spacecraft and Rockets*, vol. 36, no. 1, pp. 91-99, January-February 1999.

[50] Monte, P. A., Turner, A. E., "Constellation Selection for Globalstar™, A Global Mobile Communication System," AIAA 14th Communication Satellite Systems Conference, AIAA-92-1987-CP, 1992.

[51] http://ltpwww.gsfc.nasa.gov/MODIS/MODIS.html

[52] Lomheim, T. S., Milne, E. L., Kwok, J. D., Tsuda, A., "Performance/Sizing Relationships for a Short-wave/Mid-wave Infrared Scanning Point-Source Detection Space Sensor," *1999 IEEE Aerospace Conference Proceedings*, vol. 4, pp. 113-138, Aspen, CO, March 1999.

[53] Wong, R., "Cost Modeling," *Space Mission Analysis and Design*, Second Edition, pp. 715-740, edited by W. J. Larson and J. R. Wertz, jointly published by Microcosm, Inc., Torrance, and Kluwer Academic Publishers, Boston, 1992.

[54] Brodsky, R. F., "Defining and Sizing Space Payloads," *Space Mission Analysis and Design*, Second Edition, pp. 229-284, edited by W. J. Larson and J. R. Wertz, jointly published by Microcosm, Inc., Torrance, and Kluwer Academic Publishers, Boston, 1992.

[55] *Atlas Launch System Mission Planner's Guide,* Revision 6, Lockheed Martin Corporation, February 1997.

[56] *Delta II Payload Planners Guide,* The Boeing Company, April 1996.

[57] *Delta III Payload Planners Guide*, The Boeing Company, March 1997.

[58] *Delta IV Payload Planners Guide,* The Boeing Company, September 1998.

[59] *LMLV Mission Planner's Guide*, Initial Release, Lockheed Martin Corporation, September 1997.

[60] *Pegasus Vehicle Description Document*, Release 3.5, Orbital Sciences Corporation, July 3 1997.

[61] http://www.orbital.com/Prods_n_Servs/Products/LaunchSystems/Pegasus/index.html

[62] *Proton Launch System User's Guide*, Revision 3, Issue 1, International Launch Services, February 1997.

[63] *Commercial Taurus Launch Vehicle User's Guide,* Release 2.0, Orbital Sciences Corporation, April 18, 1996.

[64] "Launchers of the World," *International Space Industry Report*, Launchspace Publications, Inc., pp. 22-23, McLean, VA, October 26, 1998.

[65] *Quarterly Launch Report*, Commercial Space Transportation, Washington, D.C., 1999.

[66] *US Expendable Launch Vehicle Data for Planetary Missions*, http://www.jsc.nasa.gov/bu2/ELV_US.html.

[67] Hillier, F. S., Lieberman, G. J., *Introduction to Operations Research*, Fifth Edition, McGraw-Hill, Inc., NY, 1990.

[68] Rao, S. S., *Engineering Optimization: Theory and Practice*, Third Edition, John Wiley & Sons, Inc., NY, 1996.

[69] Goldberg, D., Genetic Algorithms in Search, Optimization and Machine Learning, Addison-Wesley, Reading, MA, 1989.

[70] George, E., "Optimization of Satellite Constellations for Discontinuous Global Coverage via Genetic Algorithms," AAS 97-621, AAS/AIAA Astrodynamics Specialist Conference, Sun Valley, ID, August 4-7, 1997.

[71] Lansard, E., Frayssinhes, E., Palmade, J., "Global Design of Satellite Constellations: A Multi-Criteria Performance Comparison of Classical Walker Patterns and New Design Patterns," *Acta Astronautica*, vol. 42, no. 9, pp. 555-564, 1998.

[72] Way, D.W., Olds, J. R., "Sirius: A New Launch Vehicle Option for Mega-LEO Constellation Deployment," AIAA 97-3122, 33rd AIAA/ASME/SAE/ASEE Joint Propulsion Conference and Exhibit, Seattle, WA, July 1997.

[73] Olds, J. R., Steadman, K. B., "Cross-Platform Computational Techniques for Analysis Code Integration and Optimization," AIAA 98-4743, 7th AIAA/USAF/NASA/ISSMO Symposium on Multidisciplinary Analysis and Optimization, St. Louis, MO, September 2-4, 1998.

[74] Mosher, T. J., "Conceptual Spacecraft Design Using a Genetic Algorithm Trade Selection Process," *Journal of Aircraft*, vol. 36, no. 1, pp. 200-208, January-February 1999.

[75] Fukunaga, A. S., et al, "Automating the Process of Optimization in Spacecraft Design," *1997 IEEE Aerospace Conference Proceedings,* vol. 4, pp. 411-427, Aspen, CO, February 1997.

[76] Vanderplaats, G. N., *Numerical Optimization Techniques for Engineering Design: with Applications*, McGraw-Hill Publishing Co., NY, 1984.

[77] Manning, V., Ph.D. Thesis, Stanford University, 1999.

[78] Gisvold, K. M., Moe, J., "A Method for Nonlinear Mixed-Integer Programming and its Application to Design Problems," *Journal of Engineering for Industry*, pp. 353-363, May 1972.

[79] Cheney W., Kincaid D., *Numerical Mathematics and Computing*, Second Edition, Brooks/Cole Publishing, CA, 1985.

[80] Wolfe, W. L., *Introduction to Infrared System Design,* Tutorial Texts in Optical Engineering, edited by O'Shea, D. C., vol. TT24, SPIE Optical Engineering Press, Bellingham, WA, 1996.

[81] Giarratano, J.C., Riley, G. D., *Expert Systems: Principles and Programming*, Third Edition, PWS Publishing Company, Boston, 1998.

[82] Wickert, D. P., Shaw, G. B., Hastings, D., "Impact of a Distributed Architecture for Space-Based Radar," *Journal of Spacecraft and Rockets*, vol. 35, no. 5, pp. 703- 713, September-October 1998.

APPENDIX A – AN OVERVIEW OF WALKER CONSTELLATIONS

Walker delta patterns are symmetric with t_s total number of spacecraft divided evenly in n_p planes. The spacing between satellites in the same plane is therefore given as:

$$\Delta\upsilon = \frac{360^\circ}{t_s} \cdot n_p. \qquad \textbf{(A.01)}$$

All of the orbital planes are at the same inclination and their ascending nodes are distributed evenly around the equator. Relative spacing (n_s), which defines the inter-plane phasing of the satellites $\Delta\phi$, is the final piece of information needed to fully specify the configuration:

$$\Delta\phi = \frac{360^\circ}{t_s} \cdot n_s \qquad \textbf{(A.02)}$$

$\Delta\phi$, as shown in Figure A 1, is the angle of a satellite to its ascending node, if the closest satellite in the next most westerly plane is at its ascending node. To ensure the same relationship for all the orbit planes, n_s must be an integer between 0 and $n_p - 1$. The notation $t_s/n_p/n_s$ is commonly used to refer to a specific Walker delta pattern.

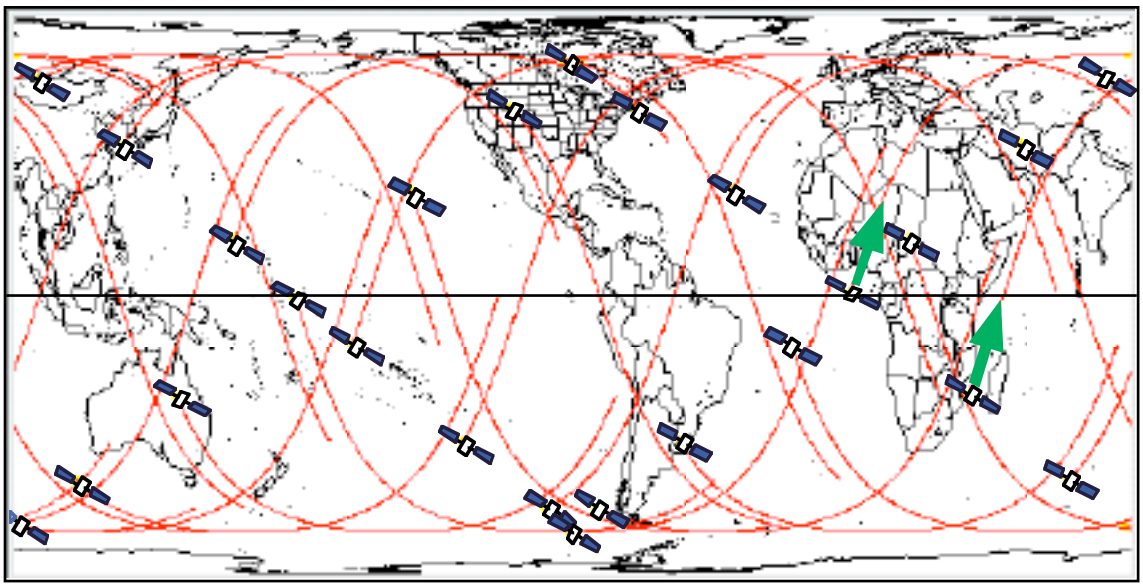

Figure A 1. An illustration for relative phasing $(\Delta\phi)$.

APPENDIX B – CALCULATIONS FOR TRACKING SENSOR'S ANGULAR ACCELERATION

With the slew-and-target time t_f for the tracking sensor given as a parameter, the maximum angular acceleration experienced can be computed. First, assuming angular acceleration is a linear function of time,

$$\ddot{\theta}(t) = b - ct \qquad \textbf{(B.01)}$$

the angular velocity is simply its integral with respect to time:

$$\dot{\theta}(t) = a_1 + bt - \tfrac{1}{2}ct^2, \qquad \textbf{(B.02)}$$

where a_1 is basically $\dot{\theta}(t_0)$. One more integration yields a relationship for angular distance:

$$\theta(t) = a_0 + a_1 t + \tfrac{1}{2}bt^2 - \tfrac{1}{6}ct^3 \qquad \textbf{(B.03)}$$

Again, a_0 is essentially $\theta(t_0)$. With the following initial and final conditions:

$$\dot{\theta}(t_0 = 0) = 0 \qquad \textbf{(B.04)}$$

and

$$\dot{\theta}(t_f) = 0, \qquad \textbf{(B.05)}$$

b can be expressed as a function of c,

$$b = \tfrac{1}{2}ct_f \qquad \textbf{(B.06)}$$

Substituting (B.06) into equation (B.03) then becomes:

$$\theta(t) = \theta(t_0) + c \cdot \left(\tfrac{1}{4} t_f t^2 - \tfrac{1}{6} t^3 \right) \qquad \textbf{(B.07)}$$

At $t = t_f$,

$$\theta(t_f) - \theta(t_0) = \Delta\theta_{\max} = \tfrac{1}{12} c t_f^3, \qquad \textbf{(B.08)}$$

where $\Delta\theta_{\max}$ is also a design parameter.

For the preliminary study, t_f was fixed at 5 seconds and $\Delta\theta_{\max}$ was specified to be $\frac{\pi}{12}$ (or 15°). Figure B 1 through Figure B 3 present plots for these settings. As shown, b is the maximum angular acceleration $\ddot{\theta}_{\max}$ encountered.

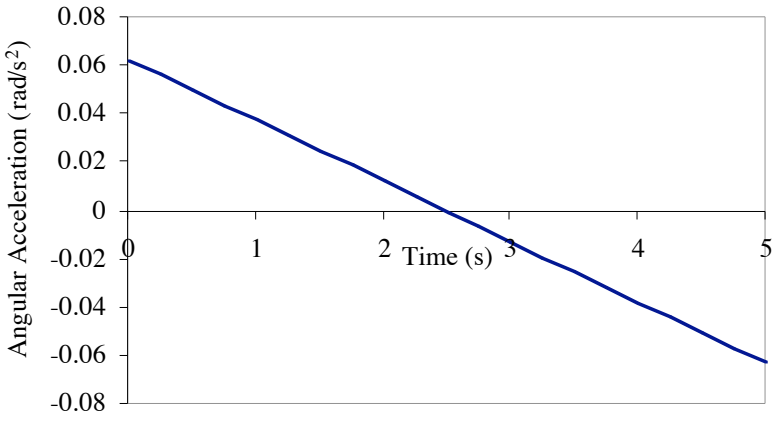

Figure B 1. Angular acceleration function with $(t_f = 5, \Delta\theta_{\max} = \frac{\pi}{12})$.

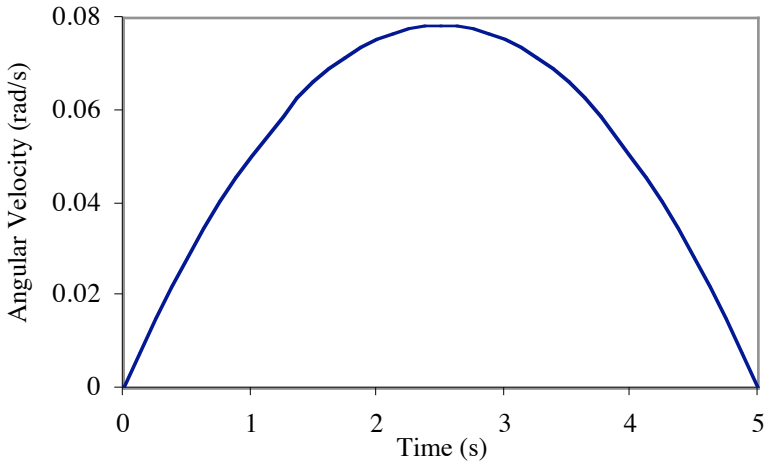

Figure B 2. Angular velocity function with $(t_f = 5, \Delta\theta_{\max} = \frac{\pi}{12})$.

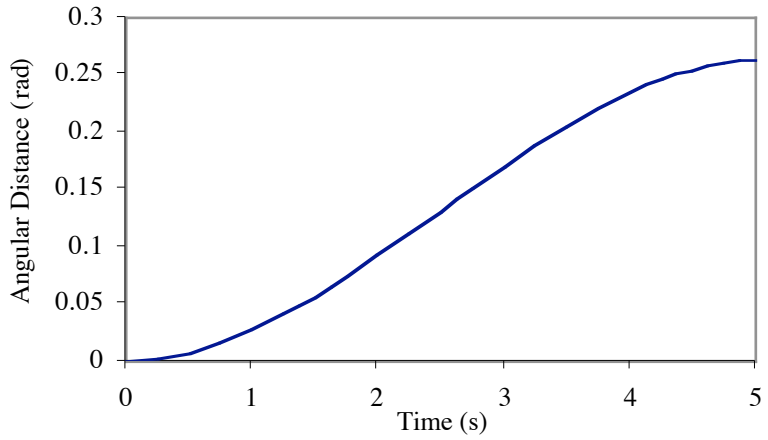

Figure B 3. Angular distance function with $(t_f = 5, \Delta\theta_{\max} = \frac{\pi}{12})$.

APPENDIX C – A REVIEW OF RUNGE-KUTTA-FEHLBERG METHOD

5th-order Runge-Kutta-Fehlberg (RKF56) integration method with adaptive time step τ determines from six function evaluations ($\bar{f} = \overline{\vartheta}'(t)$) the values of the state vector at the next time step, $\overline{\vartheta}(t+\tau)$:

$$\overline{\vartheta}(t+\tau) = \overline{\vartheta}(t) + \tfrac{47}{450}\overline{F}_1 + \tfrac{12}{25}\overline{F}_3 + \tfrac{32}{225}\overline{F}_4 + \tfrac{1}{30}\overline{F}_5 + \tfrac{6}{25}\overline{F}_6 \qquad \textbf{(C.01)}$$

$$\overline{F}_1 = \tau \cdot \bar{f}(\overline{\vartheta}(t), t) \qquad \textbf{(C.02)}$$

$$\overline{F}_2 = \tau \cdot \bar{f}(\overline{\vartheta}(t) + \tfrac{2}{9}\overline{F}_1, t + \tfrac{2}{9}\tau) \qquad \textbf{(C.03)}$$

$$\overline{F}_3 = \tau \cdot \bar{f}(\overline{\vartheta}(t) + \tfrac{1}{12}\overline{F}_1 + \tfrac{1}{4}\overline{F}_2, t + \tfrac{1}{3}\tau) \qquad \textbf{(C.04)}$$

$$\overline{F}_4 = \tau \cdot \bar{f}(\overline{\vartheta}(t) + \tfrac{69}{128}\overline{F}_1 - \tfrac{243}{128}\overline{F}_2 + \tfrac{135}{64}\overline{F}_3, t + \tfrac{3}{4}\tau) \qquad \textbf{(C.05)}$$

$$\overline{F}_5 = \tau \cdot \bar{f}(\overline{\vartheta}(t) - \tfrac{17}{12}\overline{F}_1 + \tfrac{27}{4}\overline{F}_2 - \tfrac{27}{5}\overline{F}_3 + \tfrac{16}{15}\overline{F}_4, t + \tau) \qquad \textbf{(C.06)}$$

$$\overline{F}_6 = \tau \cdot \bar{f}(\overline{\vartheta}(t) + \tfrac{65}{432}\overline{F}_1 - \tfrac{5}{16}\overline{F}_2 + \tfrac{13}{16}\overline{F}_3 + \tfrac{4}{27}\overline{F}_4 + \tfrac{5}{144}\overline{F}_5, t + \tfrac{5}{6}\tau) \qquad \textbf{(C.07)}$$

This leads to an estimate of the local truncation error:

$$\overline{E} = \left| -\tfrac{1}{150}\overline{F}_1 + \tfrac{3}{100}\overline{F}_2 - \tfrac{16}{75}\overline{F}_4 - \tfrac{1}{20}\overline{F}_5 + \tfrac{6}{25}\overline{F}_6 \right| \qquad \textbf{(C.08)}$$

The component of this error vector with the maximum value is used to determine the new time step. If $(10^{-16} \le E_{\max} \le 10^{-10})$, keep the current τ; if $(E_{\max} < 10^{-16})$, the current time step is doubled; if $(E_{\max} > 10^{-10})$, the error is too large and the current τ is halved. Maximum and minimum time steps are

specified, however, such that τ is not allowed to be outside the interval $(10^{-12}, 0.1)$.

For a spacecraft's coverage analysis, the state vector consists of the components of the satellite's position and velocity vectors, $\bar{r} = (r_x, r_y, r_z)$ and $\bar{v} = (v_x, v_y, v_z)$ respectively:

$$\vartheta(t) = \begin{bmatrix} r_x \\ r_y \\ r_z \\ v_x \\ v_y \\ v_z \end{bmatrix} \qquad \textbf{(C.09)}$$

The function used to compute $F_1, F_2, F_3, F_4, F_5, F_6$ is the governing equation of motion with a non-spherical gravity model for the Earth:

$$f(\bar{\vartheta}(t), t) = \dot{\bar{\vartheta}}(t) = \begin{bmatrix} v_x \\ v_y \\ v_z \\ \frac{\delta\phi}{\delta r_x} \\ \frac{\delta\phi}{\delta r_y} \\ \frac{\delta\phi}{\delta r_z} \end{bmatrix} \qquad \textbf{(C.10)}$$

ϕ is the gravity potential:

$$\phi = \frac{\mu}{r}\left[1 - \sum_{n=2}^{\infty} J_n \left(\frac{R_E}{r}\right)^n P_n \sin\Gamma'\right] \qquad \textbf{(C.11)}$$

r is the magnitude of the position vector $\bar{r}$. μ is the Earth's gravitational parameter, J_n is the coefficients available from experimental observations, R_E is the radius of the Earth, P_n is the Legendre polynomials, and Γ' is the satellite's

geocentric latitude $\left(\sin\Gamma' = \frac{r_z}{r}\right)$. The equations to compute $\nabla\phi$ components with up to J6 effect:

$$\frac{\delta\phi}{\delta r_x} = -\frac{\mu r_x}{r^3}\left[1 - J_2\frac{3}{2}\frac{R_e^2}{r^2}\left(5\frac{r_z^2}{r^2}-1\right) + J_3\frac{5}{2}\frac{R_e^3}{r^3}\left(3\frac{r_z}{r}-7\frac{r_z^3}{r^3}\right)\right.$$

$$-J_4\frac{5}{8}\frac{R_e^4}{r^4}\left(3-42\frac{r_z^2}{r^2}+63\frac{r_z^4}{r^4}\right)$$

$$-J_5\frac{3}{8}\frac{R_e^5}{r^5}\left(35\frac{r_z}{r}-210\frac{r_z^3}{r^3}+231\frac{r_z^5}{r^5}\right) \qquad \textbf{(C.12)}$$

$$\left.+J_6\frac{1}{16}\frac{R_e^6}{r^6}\left(35-945\frac{r_z^2}{r^2}+3465\frac{r_z^4}{r^4}-3003\frac{r_z^6}{r^6}\right)\right]$$

$$\frac{\delta\phi}{\delta r_y} = -\frac{\mu r_y}{r^3}\left[1 - J_2\frac{3}{2}\frac{R_e^2}{r^2}\left(5\frac{r_z^2}{r^2}-1\right) + J_3\frac{5}{2}\frac{R_e^3}{r^3}\left(3\frac{r_z}{r}-7\frac{r_z^3}{r^3}\right)\right.$$

$$-J_4\frac{5}{8}\frac{R_e^4}{r^4}\left(3-42\frac{r_z^2}{r^2}+63\frac{r_z^4}{r^4}\right)$$

$$-J_5\frac{3}{8}\frac{R_e^5}{r^5}\left(35\frac{r_z}{r}-210\frac{r_z^3}{r^3}+231\frac{r_z^5}{r^5}\right) \qquad \textbf{(C.13)}$$

$$\left.+J_6\frac{1}{16}\frac{R_e^6}{r^6}\left(35-945\frac{r_z^2}{r^2}+3465\frac{r_z^4}{r^4}-3003\frac{r_z^6}{r^6}\right)\right]$$

VITA

Irene Arianti Budianto was born on October 4, 1971 in Magelang, Central Java, Indonesia. On June 1984, she moved to Arcadia, CA, with her family. She graduated from Arcadia High School with honors in 1989 and started her career in Aerospace Engineering at the University of California at Los Angeles, where she made the Dean's List during her time there. In the fall of 1991, she transferred to Massachusetts Institute of Technology to continue her studies in the school of Aeronautics/Astronautics. She earned her Bachelor of Science degree in May 1993.

Upon graduation, Irene took part in the MIT-Japan program. Sponsored by the Starr Fellowship, she studied reentry aerodynamics and stability analysis of a single stage to orbit vehicle at the Institute of Space and Astronautical Science in Sagamihara, Kanagawa prefecture, Japan.

Irene began her graduate studies at Georgia Institute of Technology in the fall of 1995 under the U. S. Air Force Palace Knight program. She received her Masters of Science in Aerospace Engineering in October 1996. She spent one year working at the U. S. Air Force Phillips Laboratory at Kirtland AFB, NM, where at the Satellite Assessment Center she programmed a model translator and conducted numerical simulations and analyses. She then returned to Georgia Tech in the fall of 1997 to pursue a Ph.D., as a member of the Space Systems Design Laboratory. Both Masters and Ph.D. degrees were earned under the advisement of Dr. John R. Olds. Her thesis was entitled, *A Collaborative Optimization Approach to Improve the Design and Deployment of Satellite Constellations*, which was successfully defended in September 2000.